

**University of Alberta**

**Molecular Dynamics Simulation Study of Chain Molecules  
at Surfaces and Interfaces**

by

**Chunli Li**



A thesis submitted to the Faculty of Graduate Studies and Research  
in partial fulfillment of the requirements for the degree of

**Doctor of Philosophy**

in

**Chemical Engineering**

**Department of Chemical and Materials Engineering**

**Edmonton, Alberta, Canada**

**Spring 2008**



Library and  
Archives Canada

Bibliothèque et  
Archives Canada

Published Heritage  
Branch

Direction du  
Patrimoine de l'édition

395 Wellington Street  
Ottawa ON K1A 0N4  
Canada

395, rue Wellington  
Ottawa ON K1A 0N4  
Canada

*Your file* *Votre référence*

*ISBN: 978-0-494-45553-1*

*Our file* *Notre référence*

*ISBN: 978-0-494-45553-1*

**NOTICE:**

The author has granted a non-exclusive license allowing Library and Archives Canada to reproduce, publish, archive, preserve, conserve, communicate to the public by telecommunication or on the Internet, loan, distribute and sell theses worldwide, for commercial or non-commercial purposes, in microform, paper, electronic and/or any other formats.

The author retains copyright ownership and moral rights in this thesis. Neither the thesis nor substantial extracts from it may be printed or otherwise reproduced without the author's permission.

**AVIS:**

L'auteur a accordé une licence non exclusive permettant à la Bibliothèque et Archives Canada de reproduire, publier, archiver, sauvegarder, conserver, transmettre au public par télécommunication ou par l'Internet, prêter, distribuer et vendre des thèses partout dans le monde, à des fins commerciales ou autres, sur support microforme, papier, électronique et/ou autres formats.

L'auteur conserve la propriété du droit d'auteur et des droits moraux qui protègent cette thèse. Ni la thèse ni des extraits substantiels de celle-ci ne doivent être imprimés ou autrement reproduits sans son autorisation.

---

In compliance with the Canadian Privacy Act some supporting forms may have been removed from this thesis.

Conformément à la loi canadienne sur la protection de la vie privée, quelques formulaires secondaires ont été enlevés de cette thèse.

While these forms may be included in the document page count, their removal does not represent any loss of content from the thesis.

Bien que ces formulaires aient inclus dans la pagination, il n'y aura aucun contenu manquant.

  
**Canada**

# University of Alberta

## Library Release Form

**Name of Author:** Chunli Li

**Title of Thesis:** Molecular Dynamics Simulation Study of Chain Molecules at Surfaces and Interfaces

**Degree:** Doctor of Philosophy

**Year this Degree Granted:** 2008

Permission is hereby granted to the University of Alberta to reproduce single copies of this thesis and to lend or sell such copies for private, scholarly, or scientific research purposes only.

This author reserves all other publication and other rights in association with the copyright in the thesis, and except as hereinbefore provided, neither the thesis nor any substantial portion thereof may be printed or otherwise reproduced in any material form whatever without the author's prior written permission.

Chunli Li  
307, 10720-83 Ave.  
Edmonton  
Alberta, T6E 2E4  
Canada

Date: \_\_\_\_\_

*Dec 10, 2007*

## Abstract

The objective of this thesis is to apply molecular dynamics (MD) simulation techniques to study the behavior of chain like molecules at surfaces and interfaces.

Firstly, surface tensions ( $\gamma$ ) of normal alkanes and methyl methacrylate (MMA) oligomers at various molecular weights were computed using a newly proposed MD strategy. Our simulation reproduced the experimentally observed molecular weight dependence of  $\gamma$  (i.e.,  $\gamma \propto M_n^{-2/3}$ , where  $M_n$  is the number average molecular weight) for both series of oligomers. Analysis of the data reveals that solvent accessible surface area, one of the key input variables used for the calculation of  $\gamma$ , exhibits an  $M_n^{2/3}$  dependence. The reason for such dependence is that solvent accessible surface area formed by the chain like small molecules depends, to a larger extent, on their orientations rather than their sizes.

On the other hand, adsorption behavior of two normal alkanes ( $C_{11}$  and  $C_{200}$ ) on a relaxed  $\alpha - Al_2O_3$  (0001) surface was studied using density functional theory (DFT) and classical MD simulation techniques. The computed adsorption energy agrees well with those obtained from inverse gas chromatography measurements. The present work suggests that both the orientation and adsorption energy of normal alkanes on the alumina (0001) surface depends on whether the surface is relaxed or not.

Another major focus of this thesis is to study the relative growth rates of five commonly emerged crystal faces of  $\alpha - Al_2O_3$  in the presence of 1, 4-butanediol. Simulation results show that the corresponding adsorption energy values could be

compared as:  $E_{ads}(012) > E_{ads}(001) > E_{ads}(102) > E_{ads}(113) > E_{ads}(110)$ . The growth rates of the five crystal faces are in the reverse order. Our results also show that the growth habits are also influenced by the mobility of 1, 4-butanediol near the crystal growth faces.

Finally, stability of water/toluene interfaces saturated with adsorbed naphthenic acids was also studied. In direct comparison with our recent results on similar systems involving *n*-heptane as the oil phase, it has been found that toluene significantly enhances the stability of water/oil interface. However, the naphthenic acid size dependence of interface stability is much more pronounced for the water/toluene than the water/*n*-heptane interface.

## Acknowledgements

Firstly, I would like to take this opportunity to thank my supervisor Dr. Phillip Choi for his expert guidance and extreme patience in my graduate study at the University of Alberta. His infectious enthusiasm and unlimited zeal to science have been the major driving forces for me to finish this thesis and keep exploring in the wonderful world of science.

I would also like to express my gratitude to my previous research group members: Dr. Liyan Zhao, Dr. Mingzong Zhang, Ms. Zhiying Li for their generous help and valuable discussions in finishing this thesis.

The financial supports provided by the University of Alberta and the Natural Science and Engineering Research Council of Canada are gratefully acknowledged. Thanks also go to Westgrid computing resources.

Thank my friends Lao Xiansheng, Zhiying Li, Xiaozhen Niu, Lichun Zhang, Chunfen Han, Ling Yang, Xu Wang, Yun Bai, Jing Hu and Hong Guo for all the happiest time we have spent together and their understanding, respect and love.

Thank my beloved grandparents, parents and brothers. I love them and am always proud of them.

# Table of Contents

## Chapter 1 Introduction

1.1 Chain molecules in the melt.....	1
1.2 Chain molecules at surfaces and interfaces.....	2
1.3 Computer modeling of chain molecules.....	6
1.4 Scope of the thesis.....	8

## Chapter 2 Molecular Dynamics Simulation

2.1 Fundamentals of molecular dynamics.....	11
2.2 Force field.....	11
2.2.1 Force field.....	11
2.2.2 Long range interactions.....	14
2.3 Newton's equation of motion.....	15
2.4 NVT ensemble.....	18

## Chapter 3 Density Functional Theory

3.1 Elementary quantum chemistry.....	21
3.2 Hartree-Fock scheme.....	24
3.3 Density Functional theory (DFT).....	25
3.3.1 Electron density.....	25
3.3.2 DFT models.....	26
3.3.3 Exchange-correlation functional approximations.....	29
3.3.4 Estimations of atomic charges.....	32

## **Chapter 4 Molecular Weight Dependence of Surface Tensions of Normal Alkanes and Methyl Methacrylate Oligomers**

4.1 Introduction.....	33
4.2 Molecular dynamics simulation.....	39
4.2.1 Simulation details.....	39
4.2.2 Solubility parameter.....	46
4.2.3 Self diffusion coefficient.....	46
4.2.4 Surface area.....	48
4.3 Results and discussion.....	49
4.3.1 Solubility parameter.....	49
4.3.2 Self diffusion coefficient.....	52
4.3.3 Surface area.....	52
4.3.4 Surface tension.....	59
4.4 Concluding remarks.....	74

## **Chapter 5 Adsorption Behavior of Normal Alkanes on a Relaxed**

### **$\alpha - Al_2O_3(0001)$ Surface**

5.1 Introduction.....	75
5.2 Simulation models and methods.....	79
5.2.1 Relaxation of $\alpha - Al_2O_3(0001)$ surface using density functional theory (DFT).....	79
5.2.2 Molecular dynamics simulation.....	83
5.3 Results and discussion.....	89



5.3.1 Relaxation of $\alpha - Al_2O_3$ (0001) surface.....	89
5.3.2 Adsorption behavior of normal alkanes ( $C_{11}$ and $C_{200}$ ) on relaxed $\alpha - Al_2O_3$ (0001) surface.....	92
5.3.3 Adsorption energy of alkanes ( $C_{11}$ and $C_{200}$ ).....	99
5.3.4 Adsorption of normal alkanes ( $C_{11}$ and $C_{200}$ ) on unrelaxed $\alpha - Al_2O_3$ (0001) surface.....	101
5.4 Concluding remarks.....	109

## **Chapter 6 Effect of Solvent Adsorption on the Morphology of Glycothermally Produced $\alpha - Al_2O_3$ Particles**

6.1 Introduction.....	111
6.2 Simulation models and methods.....	114
6.3 Results and discussion.....	124
6.3.1 Validation of the COMPASS force field.....	124
6.3.2 Adsorption of solvent molecules.....	124
6.3.3 Effect of solvent adsorption on crystal growth.....	137
6.3.4 Diffusivity of 1, 4-butanediol.....	140
6.3.5 Addition of methanol molecules.....	144
6.4 Concluding remarks.....	147

## **Chapter 7 Stability of Water/Toluene Interfaces Saturated With Adsorbed Naphthenic Acids**

7.1 Introduction.....	151
7.2 Simulation details.....	156

7.3 Results and discussion.....	162
7.3.1 Validation of the COMPASS force field.....	162
7.3.2 Diffusion coefficients of naphthenic acids.....	162
7.4 Concluding remarks.....	169

## **Chapter 8 Summary and Suggestions for Future Work**

8.1 Surface tensions of chains molecules.....	170
8.2 Adsorption behavior of chain molecules at solid surface.....	171
8.3 Stability of water/oil interfaces.....	172

<b>Bibliography.....</b>	<b>174</b>
--------------------------	------------

## List of Tables

4-1 Equations and parameters used in the modified DRIEDING 2.21 force field...	41
4-2 Characteristics of the normal alkane models with chain lengths from 13 to 200 carbons.....	43
4-3 Characteristics of the MMA oligomer models with chain lengths from 10 to 200 repeat units.....	44
4-4 Self diffusion coefficients and radii of gyration of normal alkanes.....	55
4-5 Self diffusion coefficients and radii of gyration of MMA oligomers.....	56
4-6 Probe sizes for the normal alkanes used in this work.....	60
4-7 Probe sizes for the MMA oligomers used in this work.....	61
5-1 Functional forms used in the COMPASS force field.....	85
5-2 Lennard-Jones parameters used to describe non-bonded interactions between various atomic species.....	86
5-3 Computed surface energies of relaxed $\alpha - Al_2O_3(0001)$ surfaces containing different numbers of repeat units by DFT calculations.....	91
5-4 Computed adsorption energies of $C_{11}$ and $C_{200}$ adsorbed on relaxed and unrelaxed alumina (0001) surface.....	100
6-1 Parameters of slabs made from originally cleaved crystal faces.....	118
6-2 Dimension of the rearranged simulation cell (alumina surface + solvent confined layer) and thicknesses of solvent layers with 200 solvent molecules above each crystal face.....	121

6-3 Dimension of the rearranged simulation cell (alumina surface + solvent confined layers) and numbers of solvent molecules involved with the solvent layer thickness of $58 \text{ \AA}$ for each system.....	122
6-4 Adsorption energy of 1, 4-butanediol at different crystal faces for systems with 200 solvent molecules.....	134
6-5 Adsorption energy of 1, 4-butanediol molecules at different crystal faces for systems with a fixed thickness of $58 \text{ \AA}$ .....	135
6-6 Diffusion coefficients of 1, 4-butanediol at different crystal faces for systems with same number of solvent molecules.....	143
6-7 Dimension of the rearranged simulation cell (alumina surface + solvent confined layer) and thicknesses of solvent layers with 200 1, 4-butanediol molecules and 20 methanediol molecules above each crystal face.....	145
6-8 Adsorption energy of 1, 4-butanediol molecules at different crystal faces for systems with 200 1, 4-butandiol molecules and 20 methanediol molecules...	146
6-9 Diffusion coefficients of 1, 4-butanediol molecules at different crystal faces for systems with methanol molecules added.....	149
7-1 Average diffusion coefficients of naphthenic acids obtained from the calculations with water/ <i>n</i> -heptane and water/toluene flat interfaces at $25^\circ\text{C}$ .....	164

## List of Figures

4-1 Liquid and thin film models of normal alkane (C <sub>30</sub> ) .....	38
4-2 Molecular surface models: (A) Van der Waals surface, (B) Solvent accessible surface.....	44
4-3 Simulation procedure employed to calculate cohesive energy density and solubility parameter of an oligomer.....	47
4-4 Molecular weight dependence of the solubility parameter of normal alkanes .....	50
4-5 Molecular weight dependence of the solubility parameter of MMA oligomers .....	51
4-6 Mean square displacement of normal alkane with 30 backbone carbon atoms.....	53
4-7 Mean square displacement of MMA oligomer with 30 repeat units.....	54
4-8 Probe size dependence of solvent accessible surface area and the corresponding total volume of the thin film models for the normal alkane chains with 30 carbon atoms .....	57
4-9 Probe size dependence of solvent accessible surface area and the corresponding total volume of the thin film models for the MMA oligomer with 30 repeat units .....	58
4-10 Molecular weight dependence of surface tension for normal alkanes obtained from our simulations (solid circles) compared with experimental data (open circles).....	62

4-11 Molecular weight dependence of surface tension for MMA oligomers obtained from our simulations (solid circles) compared with experimental data (open circles).....	63
4-12 Molecular weight dependence of surface tension components for normal alkanes with solvent accessible surface area (opening circles) labeling on the left vertical axis and energy difference $\langle E_{2D} - E_{3D} \rangle$ (solid circles) labeling on the right vertical axis.....	65
4-13 Molecular weight dependence of cohesive energy density components for normal alkanes, with molar volume (opening circles) labelling on the left vertical axis and energy difference $\langle E_{vac} - E_{3D} \rangle$ (solid circles) labeling on the right vertical axis.....	66
4-14 Molecular weight dependence of surface tension components for MMA oligomers with solvent accessible surface area (opening circles) labeling on the left vertical axis and energy difference $\langle E_{2D} - E_{3D} \rangle$ (solid circles) labeling on the right vertical axis.....	67
4-15 Molecular weight dependence of cohesive energy density components for MMA oligomers, with molar volume (opening circles) labeling on the left vertical axis and energy differenc $\langle E_{vac} - E_{3D} \rangle$ (solid circles) labeling on the right vertical axis.....	68
4-16 Solvent accessible surfaces of normal alkane chains .....	71
4-17 Solvent accessible surfaces of MMA oligomer chains (left PMMA10, right PMMA200).....	72

5-1 Hexagonal vacuum slab of $\alpha - Al_2O_3$ (0001) surface (a) before relaxation (b) after relaxation.....	80
5-2 The non-polar surface structure of $\alpha - Al_2O_3$ (0001) surface before and after relaxation. The atomic layers that are perpendicular to the alumina (0001) surface, interlayer distances, the relaxation magnitude in percentage, and the nonpolar repeat unit for building the surface are shown.....	81
5-3 Conformations of $C_{200}$ at different simulation time: (a) before energy minimization; (b) after energy minimization (0 ps); (c) 18,000 ps.....	88
5-4 Density distribution profile of $C_{11}$ along the z direction (z being the direction perpendicular to the alumina (0001) surface) at different simulation times (423 K, relaxed surface): (a) before and after energy minimization; (b) at different simulation times: 0, 100, 500 and 1,000 ps.....	93
5-5 Density distribution profile of $C_{200}$ along the z direction (z being the direction perpendicular to the alumina surface) at different simulation times (423 K, relaxed surface): (a) before and after energy minimization; (b) at different simulation times: 0, 5,000, 10,000 and 18,000 ps.....	94
5-6 Orientation of the molecular axes of the first adsorption layer of $C_{11}$ (image shown as $3 \times 3$ supercell of the original simulation cells).....	96
5-7 Orientation of the molecular axes of the first adsorption layer of $C_{200}$ (image shown as $3 \times 3$ supercell of the original simulation cells): As shown the molecular axes of the adsorbed alkane segments tilt communally to a small angle with respect to the lattice boundaries in the substrate surface.....	97

5-8 Density distribution profile of C <sub>11</sub> along the z direction (z being the direction perpendicular to the alumina (0001) surface) at different simulation times (423 K, unrelaxed surface): (a) before and after energy minimization; (b) at different simulation time: 0, 100, 500 and 1,000 ps.....	102
5-9 Orientation of the molecular axes of the first adsorption layer of C <sub>11</sub> at unrelaxed alumina surface at 423 K (image shown as 3×3 supercell of the original simulation cells).....	103
5-10 Density distribution profile of C <sub>11</sub> along the z direction (z being the direction perpendicular to the alumina (0001) surface) at different simulation time (100 K, unrelaxed surface) at different simulation times: 0, 100, 500 and 1,000 ps.....	105
5-11 Orientation of the molecular axes of the first adsorption layer of C <sub>11</sub> at unrelaxed alumina surface at 100 K (image shown as 3×3 supercell of the original simulation cells).....	106
5-12 Density distribution profile of C <sub>200</sub> along the z direction (z being the direction perpendicular to the alumina (0001) surface) at different simulation time (423 K, unrelaxed surface): (a) before and after energy minimization; (b) at different simulation times: 0, 5,000, 10,000 and 17,000 ps.....	107
5-13 Orientation of the molecular axes of the first adsorption layer of C <sub>200</sub> (image shown as 3×3 supercell of the original simulation cells) on unrelaxed alumina surface: As shown the molecular axes of the adsorbed alkane segments almost perpendicular to the lattice boundaries in the substrate surface.....	108



6-1 Structure of bulk alumina crystal and slabs of cleaved $\alpha$ -alumina crystal faces (a) bulk crystal; (b) (001) face; (c) (010) face; (d) (012) face; (e) (102) face; (f) (110) face; (g) (111) face; (h) (113) face.....	116
6-2 Relative concentration profile of 1, 4-butanediol molecules near various alumina crystal faces: (a) (001) face; (b) (010) face; (c) (012) face; (d) (102) face; (e) (110) face; (f) (111) face; (f) (113) face.....	128
6-3 Pair correlation functions of (a) Al-C; (b) Al-H; (c) Al-O; (d) O-C; (e) O-H; (f) O-O, where for each pair, the former atom represents those of the alumina slab while the latter those of 1, 4-butanediol.....	132
6-4 Effects of solvent layer thickness on adsorption energy of solvent molecules on (001), (012), (102), (110), and (113) crystal faces.....	138
6-5 Time dependence of mean square displacement of 1, 4-butanediol above various $\alpha$ -alumina crystal faces.....	142
6-6 Total self diffusion coefficients of solvent molecules above various crystal faces with methanol molecules added to the systems.....	148
7-1 Chemical structure of 6-methyl-2-naphthatenepropionic acid.....	159
7-2 Snapshots for the simulated system (a) Initial structure; (b) 1000 picoseconds.....	161
7-3 The influence of the linking group chain length on the mobility of the naphthenic acid molecules.....	168

## Nomenclature

$A$	.....variable, Helmholtz free energy
$a$	.....eigenvalue, acceleration
$D$	.....Transport coefficient, diffusion coefficient
$E$	.....Energy
$\hat{f}$	.....effective one-electron operator
$G$	.....Gibbs free energy
$\hat{H}$	.....Hamiltonian operator
$L$	.....dimension of system
$M_n$	.....number average molecular weight
$N$	.....number of molecules
$n$	.....number of molecules
$P$	.....pressure
$r$	.....coordinates of particles
$S$	.....entropy
$T$	.....temperature
$\hat{T}$	.....kinetic energy
$t$	.....time
$U$	.....potential energy
$V$	.....molar volume, growth rate
$\hat{V}$	.....potential energy

$v$  .....velocity of particles  
 $\alpha$  .....operator  
 $\chi$  .....one-electron wave function  
 $\delta$  .....solubility parameter  
 $\varepsilon$  .....orbital energy  
 $\phi$  .....Kohn-Sham orbital wave function  
 $\gamma$  .....surface tension  
 $\rho$  .....density, electron density  
 $\sigma$  .....surface area  
 $\Delta t$  .....time step  
 $\Psi$  .....wave function

## Chapter 1 Introduction

Chain molecules contain long sequences of constitutional units which are composed of molecules of relatively low molecular mass. Rotation of the single bonds in the backbone of such molecules leads to a wide range of conformations. Some of these conformations may be rather unfavorable compared with others, due to hindered rotation by the bulky side groups. The properties of chain molecules can be described statistically, by taking averages over all the numerous allowed conformations. Chain molecules usually exhibit random coil conformation in their liquid state. However, their conformations can change as they approach a surface. The proper theoretical treatment of conformational statistics of chain-like molecules in the presence of a surface is one of the main challenges in the polymer community.

### 1.1 Chain molecules in the melt

Flory first stated that in a pure polymer melt, each chain should be Gaussian and ideal [Flory, 1988]. This is the basis of Flory's analysis of chain structure and is a fundamental premise underpinning the rotational isomeric state (RIS) theory approximations [Mattice and Suter, 1994]. However, it took a long time for this notion to be accepted by the polymer community.

In a pure polymer melt, each polymer chain is surrounded by other polymer chains of the same type. One argument is that the expansion of a given chain to relieve long-range intramolecular steric interactions, the so-called excluded volume effect, only serves to create an equal number of intermolecular steric interactions with neighboring chains. These opposing volume exclusion effects exactly counteract each

other and so in a pure amorphous polymer melt the polymer chains adopt their unperturbed dimensions. Another argument is that in a dense polymer system, the entropy of the system could be translated into an effective interaction, which shows a repulsive core and an attractive well in finite separations followed by oscillations in sign at farther distances and drops to zero beyond certain cut-off distances. The attractive part due to the surrounding chains tends to “screen out” the repulsive core representing the bare interaction which is present even without the surrounding polymer chains. With Flory and Huggins’ model, it can be shown that for long chains there is efficient cancellation between the attractive and repulsive parts of the effective interaction, i.e. a dilute solution of monomers in the melt is ideal [de Gennes, 1979]. Flory’s statement has been proven by neutron scattering experiments by probing a few labeled (deuterated) chains in the melt of identical (hydrogenated) chains. The experiment also shows that in a three dimension polymer melt, the individual molecular coils interpenetrate each other and become highly entangled [de Gennes, 1979].

## **1.2 Chain molecules at surfaces and interfaces**

As typical macromolecular movements which involve large segments and the molecule as a whole control many of the properties of chain molecules in the melt, expansion of chains from the bulk towards the surface or short-ranged reorganization of segments in the local domain surface structure deeply affects the surface properties of chain molecules [Garbassi *et al.*, 1994].

Generally speaking, all kinds of motions are enhanced in the surface region of the chain molecule layer. Mansfield and Theodorou’s molecular dynamics simulation

showed that there is a considerable enhancement of atomic mobility in the outmost region compared to the internal regions [Mansfield and Theodorou, *et al.*, 1991]. The displacements parallel to the surface are much greater than displacements normal to it. Besides, there may also be some structural variation parallel to the surface due to the inhomogeneity of the layers [Garbassi *et al.*, 1994]. It was also found that the surface activity of chain end groups were driven both entropically and enthalpically. There are theoretical methods to examine the entropic contributions to the conformations of chain molecules at melt surfaces. Theodorou *et al.* studied the estimation of chain end excesses driven by entropic effects [Theodorou, 1988; Hariharan *et al.*, 1990]. The entropic penalty for having a polymer coil situated at the polymer melt liquid-vapor interface has been suggested theoretically to be quite small, on the order of a 10% increase in the value of the surface tension at elevated temperatures [Hong and Noolandi, 1981; Rabin, 1984].

The dimensions of the very sharp vapor-melt interface widths are of the order of  $10 \text{ \AA}$  for most polymers and oligomers at experimentally attainable temperatures [Dee and Sauer, 1992]. The concentration profiles normal to the surface or interface could be measured with very high sensitivity by using neutron reflection or X-ray reflection techniques [Russell, 1990]. Chain ends at the surfaces and interfaces lead to oscillations in the chain end concentration in the direction normal to the surface, the period for which is of the order of the coil dimensions of chain molecules [Elman *et al.*, 1994].

Adsorption of chain molecules on the substrate must change their conformations. Jenkel and Rumbach first proposed [Jenkel and Rumbach, 1951] the usual

descriptions for conformations at an adsorbing interface. The segments of the chain molecules were divided into three types: trains, which contain all the segments in contact with the substrate; loops, which are segments between two trains and have no contact with the substrate; and tails which are non-adsorbed chain ends. More structural information of the adsorbed chain molecules resides in the concentration profiles along the direction perpendicular to the substrate surface.

The overall properties of the material also depend on its dynamic properties. However, most of the literatures was devoted to the study of dynamics of bulk chain molecules. This may probably be due to the fact that great challenges exist in the experimental investigation of surface layers of chain molecules, compared with those of bulk chain molecules. On the other hand, the study of chain molecules at surface and interfaces is still in its infancy; no general theory or systemic approaches are available to solve the problem. It was found that chain molecules at surfaces could rearrange their structures to tune their surface properties to the interfacing medium. And the kinetics of motion at the surface of chain molecules could be quick enough to affect the surface properties. Besides, the orientation of surface groups is affected by the nature of the interfacing environment. Several experimental methods were developed to evaluate the polymer surface dynamics. For example, experimental evidence of surface-enhanced polymer segment diffusion could be found in the healing behavior of crazes and fractures [Berger and Sauer, 1991; Kambour, 1964; Yang and Kramer, 1985]. Among them, the work of Berger and Sauer is one of the most direct and conclusive pieces of experimental evidence of the enhanced mobility of polymer surfaces [Berger and Sauer, 1991]. They measured the polymer mobility

within the fibrils by thermally stimulated depolarization currents (TSC) and observed that the TSC spectrum of the crazed sample exhibits a strong increase in depolarization current, comparing with uncrazed samples which were almost featureless. Their results revealed that significant polymer mobility is present at the surface region even at a temperature nearly 100 °C below the glass transition temperature of the polymer.

Minimization of the interfacial free energy between polymer chains and the environment leads to surface restructuring of the polymer adsorption layer. The enhanced kinetics of polymer surfaces makes it possible to observe restructuring with various experimental techniques. Most reports are based on contact angle or interfacial energetics measurements [Pennings and Bosman, 1979; Van Damme, *et al.*, 1986; Everhart and Reilley, 1981]. Van Damme, Hogt and Reiley discussed the contact angle hysteresis of a series of poly (n-alkylmethacrylate) in terms of the reorganization of macromolecules side chains or segments at the polymer surface [Van Damme, 1986]. They documented the effects of side-chain length and of the temperature on the measured contact angle hysteresis. Everhart and Reilley discussed the effect of functional groups mobility on the results of surface analysis [Everhart and Reilley, 1981]. From their results, it is clear that functional groups can migrate back and forth on the surface and subsurface region, depending on the environmental conditions.

### **1.3 Computer modeling of chain molecules**

Many important fluctuations of molecular liquids occur over short range time intervals. Therefore, most properties of molecular liquids may be determined by short



range interactions. However, simulation of chain molecules needs more extensive computational efforts. A full description of chain molecules requires consideration from the size of a single monomer repeat unit to the end-to-end length of the whole chain [Colbourn, 1994]. Besides, the variety of the movement types involved in the chain molecule systems including from vibration of bonds to the fluctuation of the end-to-end distance in a chain molecules melt cover widely from several femto second to the order of micro seconds.

Atomistic simulation method provides a possible way to deal with this problem. As known ab initio methods such as Hartree-Fock [Szabo and Ostlund, 1989] or density functional theory [Hohenberg and Kohn, 1964; Parr and Yang, 1989; Koch and Holthausen, 2001] methods and most semi-empirical methods such as Tight-bonding MNDO or INDO/S [Jensen, 1999; Gray and Gubbins, 1984; Maquarrie, 2000] are only able to handle small systems containing several atoms, it is obviously infeasible to do calculations on systems containing chain molecules. While mesoscale approaches such as Lattice methods, Brownian Dynamics or Dissipative Particle Dynamics and Continuum approaches [Frenkel and Smit, 2002; Zwanzig, 2001; Mazo, 2002] sacrifice too many atomistic details. Fortunately, atomistic simulation method in continuous space offers an opportunity to diminish this problem. This method disregards all the chemical details in the chain and use the “bead” model to describe the bond and non-bond interactions, where the beads represent corresponding statistical units of the chains [Colbourn, 1994]. The atomic simulation method ignores some of the chemical detail but retains the essential features of connectivity and restricted flexibility in a fairly realistic way. Atomistic simulation

methods are able to deal with calculations on systems of sizes from  $10^{-9}$  meter (nanometer) to  $10^{-7}$  meter, and the time interval from  $10^{-12}$  s (pico-second) to  $10^{-6}$  s (micro-second), where some properties of chain molecules could be studied [Hung *et al.*, 2004].

Connectivity, chain flexibility, and van der Waals interactions are essential properties that any chain molecules model should consider. One problem is that the relaxation times in chain molecules are so long that sometimes it may not be really possible to fully sample the equilibrium state of the system using molecular dynamics. Instead methods of selecting chain molecule conformations from the correct distribution have to be developed. Most of the methods so far used include generating chain molecules using some kind of random walk rules and then relax the structures using molecular mechanics at 0 K or using molecular dynamics at high temperatures. One widely accepted criterion is that once the mean square displacement of the center of mass of the system reaches the square of radius of gyration of the chain molecules, the equilibrium is considered to be reached [Abrams, 2003]. Another problem is induced by the use of periodic boundary conditions. It is almost infeasible to construct a simulation cell which is large enough to prevent interactions between molecules in the primary cell and their neighboring images [Allen and Tildesley, 1987]. One widely used but controversial approach is to use a simulation cell which is larger than the correlation lengths important to the phenomena being studied [Colbourn, 1994].

Simulation can predict a wide range of properties for polymer systems such as solubility and miscibility, dynamics properties, surface properties, transition

temperature, optical and opto-mechanical properties, and thermophysical properties, etc [Allen and Tildesley, 1987].

#### **1.4 Scope of the thesis**

The major thrust of this thesis is to study the behavior of chain molecules at surfaces and interfaces by using molecular dynamics simulation techniques.

Surface tension is generally believed to be a critical thermodynamic property that determines behavior of molecules at surfaces and interfaces. Nowadays, researchers can accurately measure surface tensions of a wide range of liquids using various experimental techniques. Over the past two decades, Molecular dynamics (MD) simulation techniques have also been developed to compute surface tensions of materials. However, inadequacies still exist in most current MD simulation approaches that are used to calculate surface tensions of chainlike molecular systems. One objective of this work is to propose a MD simulation strategy for two series of chain molecules: normal alkanes and methyl methacrylate (MMA) oligomers. Normal alkanes are chosen because of their simple structure and availability of literature values for comparison. MMA oligomers are chosen because of their wide applications and interests in industry.

The second objective of this work is to study the adsorption behavior of normal alkanes on the relaxed  $\alpha - Al_2O_3$  (0001) surface. Experimental and theoretical exploration of interaction between chain molecules and alumina surfaces has been an active research topic as alumina play important roles in many areas such as catalysts and catalyst supports. In terms of modeling metal oxide surfaces, infinite flat alumina surfaces are chosen in our MD simulation. Adsorption behavior of chainlike

molecules at the relaxed  $\alpha - Al_2O_3(0001)$  surface is investigated in this work due to the fact that  $\alpha - Al_2O_3(0001)$  surface has the lowest energy among all the alumina surfaces and usually is the crystal growth surface. Simulations of the adsorption behavior of chain molecules on relaxed  $\alpha - Al_2O_3(0001)$  surfaces are expected to provide a theoretical basis and comparison for the exploration of more complex interactions between those molecules and inorganic nanocrystals in organic solvents.

1, 4-butanediol molecules are widely used as solvents in the glycolthermal synthesis of  $\alpha - Al_2O_3$  nanoparticles. Experimental measurements [Bell and Adair, 1999; Sohnle and Garside, 1993] show that adsorption of 1, 4-butanediol molecules have effects on the growth habit of alumina crystals and morphology control of alumina particles. Therefore the third objective of this work is to study the adsorption behavior of 1, 4-butanediol molecules on various  $\alpha - Al_2O_3$  crystal faces, and to explore a possible way to relate the adsorption effects of solvents to the growth habit of  $\alpha$ -alumina particles synthesized in 1, 4-butanediol solution.

This work also includes a MD study on the stability of water/toluene interfaces saturated with adsorbed naphthenic acids. Naphthenic acids are a class of organic monoacids and usually accumulate at the water/oil interfaces in the production of petroleum reserves. They organize to form monolayers, liquid crystalline films, or other colloidal structures, therefore stabilize the water-in-oil emulsions. Based on previous work in our research group, the objective of this part of our work is to explore the nature of the solvent effects on the stability of the water/oil interface and water-in-oil emulsions with the presence of naphthenic acids.

The thesis is organized into three major sections. In section 1 (chapter 2 and 3), MD simulation techniques and density functional theory (DFT) are reviewed. Some important concepts such as force fields and NVT ensemble are introduced. The underlying statistical mechanical and quantum mechanical fundamentals are also presented. In section 2 (chapters 4, 5, 6 and 7), simulation details of study on molecular weight dependence of surface tensions of normal alkanes and MMA oligomers; the adsorption behavior of normal alkanes on relaxed  $\alpha - Al_2O_3(0001)$  crystal face; the effects of solvent adsorption on glycothermally produced  $\alpha - Al_2O_3$  particle morphology and stability of water/toluene interfaces saturated with adsorbed naphthenic acids are presented. Results and discussions are also given accordingly for different part of work. In the last section (chapter 8), we will briefly give the final conclusion of this work and discuss the possible directions for future work.

## Chapter 2 Molecular Dynamics Simulation

### 2.1 Fundamentals of molecular dynamics

Statistical thermodynamics is the theoretical basis of molecular dynamics (MD) simulation [Andersen, 1980]. The thermodynamic state of a many molecule system is usually determined by a small number of variables (number of molecules  $N$ , temperature  $T$ , pressure  $P$ , etc.). It could also be defined as many but finite number of microstates which are specified by the positions and velocities of each atom involved in the system. Classical MD simulation employs effective inter-atomic potentials and generates time evolutions of those microstates by integrating the equations of motion. The ergodic postulate proposes that given that the simulation time is long enough, the time average and the ensemble average of dynamic variables of the system become consistent [Hill, 1986]. Many thermodynamic properties therefore could be determined through equations of state and the fundamental thermodynamic equations. In the following sections of this chapter, some of the key features of MD simulation are presented. One may refer to other references [Rapaport, 2004; Haile, 1992; Allen and Tildesley, 1987] for detailed description of the methodologies of MD simulation.

### 2.2 Force field

#### 2.2.1 Force field

Molecular systems are composed of nuclei and electrons. The Hamiltonian of the molecular systems is extremely complicated as it contains so many terms such as the kinetic energy of nuclei and electrons, electron-electron interactions, electron-nuclei interactions, and nuclei-nuclei interactions even without the consideration of factors

such as spin-orbit coupling and hyperfine structure, etc. The Born-Oppenheimer approximation simplifies the problem greatly by separating the motions of nuclei and electrons. But the full calculation of so called “Potential Energy Surface” for complex molecular systems is still a formidable task [Frenkel and Smit, 2002]. Progress is being made in the use of direct electronic structure calculations to obtain forces. There are two available ways for the calculation of the electronic structure. One is the Car-Parrinello method [Szabo and Ostlund, 1989] with approximate density functional theory [Parr and Yang, 1989], the other one is ab initio MD methods which are designed to obtain, in principle, exact forces [Szabo and Ostlund, 1989]. However, for complex molecular systems, say, the system sizes can reach  $10^6$  atoms and more, and the potential and its derivatives is calculated  $\sim 10^6$  configurations and more, the quantum calculations of electronic structures are far beyond the reach of the current computer technology. A compromise is that a model can be built up which only includes the important interactions in a molecular system.

A force field is actually such an approximate model which contains energy terms as functions of the configurations of the system. A common form of this is:

$$\begin{aligned}
 E_{total} = & \sum_{bonds} K_r (r - r_{eq})^2 + \sum_{angles} K_\theta (\theta - \theta_{eq})^2 + \sum_{dihedrals} \frac{V_n}{2} [1 + \cos(n\phi - \gamma)] \\
 & + \sum_{i < j} \left[ \frac{A_{ij}}{R_{ij}^{12}} - \frac{B_{ij}}{R_{ij}^6} \right] + \sum_{i < j} \frac{q_i q_j}{\epsilon R_{ij}}
 \end{aligned} \tag{2-1}$$

As can be seen from the above equation, the energy terms usually contain bond stretch energy, bond angle deformation energy, dihedral angle (torsion) energy, and

non-bond energies such as van der Waals and electrostatic interactions. Depending on the energy expressions contained, force fields could be roughly divided into three categories [Sun, 1998]. One is generic force fields such as UFF [Rappe *et al.*, 1992], DREIDING [Mayo *et al.*, 1990], AMBER [Cornell *et al.*, 1995; Cornell *et al.*, 1996], and CHARMM [Mackerell *et al.*, 1995], etc., which contain simple functional forms for the diagonal terms of the force-constant matrix. These force fields were designed to cover a wide range of materials but only reasonable predictions of molecular structure. Another type includes new versions of those generic force fields (CHARMM [Mackerell *et al.*, 1995], OPLS/AMBER [Jorgensen *et al.*, 1996], etc.). These force fields still employ simple functional forms, but were extended in such a way that the quality of prediction is improved and area of applications becomes rather focused. The last category refers to the force fields designed to predict various molecular properties and cover a wide range of substances at the same time. Examples include MM3/MM4 [Lii and Allinger, 1989; Allinger *et al.*, 1996], CFF93 [Hwang *et al.*, 1994], and MMFF [Halgren, 1996], etc. These force fields usually contain complicated functional forms, such as cross terms for additional description of the coupling between the various energy expressions, and are usually well parameterized by fitting of high-quality experimental data [Jorgensen *et al.*, 1996; Lii and Allinger, 1989] or quantum mechanics *ab initio* data [Allinger *et al.*, 1996; Hwang *et al.*, 1994]. Unfortunately, most of the above mentioned force fields were developed for biological molecules. The COMPASS force field is an *ab initio* force field optimized for condensed-phase applications, especially for organic and inorganic substances. This force field was developed based on the CFF93 force field.



Some other newly developed force fields contain polarizable models, or mixed quantum mechanical and molecular mechanical models (QM/MM). However, calculations based on these force fields would be very expensive and unnecessary for certain research problems. The energy term expressions and selected parameters for the DREIDING and COMPASS force fields, which are the ones used in the present thesis, will be presented in the later chapters.

### **2.2.2 Long range interactions**

One of the most challenging problems in MD simulation is how to deal with long range interactions. Long range interactions are defined as the interactions which decay on the order of  $r^{-d}$  or slower (where  $d$  is dimensionality of the system) [Allen and Tildesley, 1987]. Within a three dimensional simulation, Coulomb energy ( $\sim r^{-1}$ ) and dipole-dipole interactions ( $\sim r^{-3}$ ) are usually referred to as the long range interactions. Different from short range ones, which could be easily dealt with using the cut-off method, long range interactions are very challenging due to the well known fact that the size of the simulation system is finite (usually less than 10 nm) and the effects of neighboring images of particles on themselves always cause very serious problems. Various techniques have been developed to study long range interactions in different systems. Examples include the Ewald sum method [Ewald, 1921; Heyes, 1981], the reaction field method [Onsager, 1936], the particle-particle and particle-mesh (PPMM) algorithm for ionic crystals [Eastwood *et al.*, 1980], and Ladd methods for dipolar systems [Ladd, 1977; Kadd, 1978], etc. The Ewald sum method was originally developed for the study of ionic crystals, by efficiently summing up the interactions between an ion and all its periodic images. It includes an

extra distribution of charges with equal magnitude and opposite sign surrounding each point charge, which screens the interactions between neighboring charges. The screened interactions become short-ranged and could be calculated by summing over all the molecules in the central cube and all their images in the real space. This addition of extra charge distribution is then cancelled out by applying the same shape of charge distribution of the same sign as the original charge in reciprocal space and therefore recovers the correct results. Besides, the Ewald sum method can be easily extended to dipoles and quadrupoles interactions, by representing those dipoles and quadrupoles as partial charges within the core of a molecule. It tends to overemphasize the periodic nature of the model fluid, but is still one of the most widely used methods.

### 2.3 Newton's equation of motion

The time sequences of position and velocity of each atom in a simulation system are obtained by integrating its equation of motion. Various equations exist such as Lagrangian equation of motion, Hamiltonian equation of motion, and Newton's equation of motion; all of these equations are essentially equivalent. Among them, the Lagrangian equation of motion is the most fundamental form:

$$\frac{d}{dt}(\partial L / \partial \dot{q}_k) - (\partial L / \partial q_k) = 0 \quad (2-2)$$

where  $L(q, \dot{q})$  is the Lagrangian function defined in terms of kinetic and potential energies

$$L = \hat{T} - \hat{V} \quad (2-3)$$

$q_k$  and  $\dot{q}_k$  are the generalized coordinates and their time derivative for the  $k$  th particle in an  $N$  particle system. Besides,  $\hat{T}$  is the kinetic energy and  $\hat{V}$  is the potential energy of the system.

While for atomic systems with Cartesian coordinates  $r_i$ , the Lagrangian equation of motion becomes Newton's form:

$$m_i \ddot{r}_i = f_i \quad (2-4)$$

where  $m_i$  is the mass, and  $f_i$  is the force on atom  $i$ , which is also defined as

$$f_i = \nabla_{r_i} L = -\nabla_{r_i} \hat{V} \quad (2-5)$$

On the other hand, the Hamiltonian equation of motion is defined by the equation

$$H(p, q) = \sum_k \dot{q}_k p_k - L(q, \dot{q}) \quad (2-6)$$

where

$$H = \hat{T} + \hat{V} \quad (2-7)$$

and

$$p_k = \partial L / \partial \dot{q}_k \quad (2-8)$$

These equations are solved numerically in computer simulation [Allen and Tildesley, 1987]. The simplest numerical solution is Taylor expansion series. It is not accurate in practice and is not used in real simulations; however, it illustrates what is required to integrate equations of motion. Energy conservation, the ability to handle long time step, and time reversibility are three most important factors to evaluate a good algorithm. Specific examples of algorithms in common use include the Verlet algorithm [Verlet, 1967; Gear, 1971], Leap-frog algorithm [Hockney, 1970], the Gear predictor-corrector algorithm [Berendsen and Van Gunsteren, 1986], etc. The Verlet algorithm was one of the most widely used methods for integrating equations of motion. The method is based on positions  $\vec{r}(t)$ , accelerations  $\vec{a}(t)$ , and the positions  $\vec{r}(t - \Delta t)$  from the previous step

$$\vec{r}(t + \Delta t) = 2\vec{r}(t) - \vec{r}(t - \Delta t) + \Delta t^2 \bullet \vec{a}(t) \quad (2-9)$$

The only drawback is that it can not handle the velocity explicitly. Half-step leap-frog scheme was developed to modify the Verlet algorithm, but it still can not handle the

velocities in a satisfactory way. Its stored quantities are the current positions  $\vec{r}(t)$ , accelerations  $\vec{a}(t)$  and the mid-step velocities  $\vec{v}(t - \frac{1}{2}\Delta t)$ :

$$\vec{r}(t + \Delta t) = \vec{r}(t) + \Delta t \bullet \vec{v}(t + \frac{1}{2}\Delta t) \quad (2-10a)$$

$$\vec{v}(t + \frac{1}{2}\Delta t) = \vec{v}(t - \frac{1}{2}\Delta t) + \Delta t \bullet \vec{a}(t) \quad (2-10b)$$

The velocity Verlet algorithm solves this problem successfully and has become the most popular method until nowadays due to its numerical stability, convenience, and simplicity:

$$\vec{r}(t + \Delta t) = \vec{r}(t) + \Delta t \bullet \vec{v}(t) + \frac{1}{2}\Delta t^2 \bullet \vec{a}(t) \quad (2-11a)$$

$$\vec{v}(t + \Delta t) = \vec{v}(t) + \frac{1}{2}\Delta t \bullet [\vec{a}(t) + \vec{a}(t + \Delta t)] \quad (2-11b)$$

Besides, the Gear predictor-corrector algorithm can also be easily adapted to handle modified first- and second-order equations of motion.

## 2.4 NVT ensemble

Molecular dynamics simulations are usually carried out in certain ensembles. Commonly used ensemble includes: the microcanonical (constant NVE), the canonical (constant NVT), the grand canonical (constant  $\mu$  VT), and the isothermal-

isobaric (constant NPT) ensemble [Allen and Tildesley, 1987]. Different sets of variables were fixed within these ensembles, respectively, through which other thermodynamic properties could be averaged or derived from these ensembles. But theoretically, in the thermodynamic limit, all these ensembles would be equivalent and standard transformation methods exist between different ensembles. Newton's equations of motion conserve the total energy of a system; therefore, only NVE ensemble can be studied and the conjugate intensive thermodynamic properties such as  $P$  and  $T$  can only be calculated indirectly. Thanks to the development of "thermostats" and "barostat", ensemble such as NVT and NPT etc. can also be studied. Atoms and molecules in the system interact with imaginary thermo or baro bath, which constrains the temperature and pressure of the system.

Several temperature controlling methods have been developed. In stochastic method [Andersen, 1980], selected particles in the system collide with imaginary heat-bath particles with a certain frequency, and velocities of these particles are changed accordingly. Between the collision intervals, microcanonical evolution still takes place. In this way, all of the important regions in the phase space can be explored given sufficiently long simulation time. The limiting distribution probability density is expected to be the canonical one. Nose presented the extended system method which includes an extra degree of freedom representing the heat-bath in contact with the system [Nose, 1984b]. The probability density for the whole extended system is microcanonical, while the canonical distribution is obtained after integrating over the system. Hoover's constraint technique introduced a "friction coefficient" which is chosen to constrain kinetic temperature to a constant value and

to perturb the classical Newton's equation of motion as little as possible [Hoover, 1985]. The resulting equations of motions generate a canonical distribution for configurational properties of the system. Later Hoover combined the two methods by using the extra degree of freedom of Nose as time-scaling parameter [Hoover, 1985]. The newly derived equations steer the temperature towards the target value in a gentle way, and generate the canonical ensemble.

## Chapter 3 Density Functional Theory

### 3.1 Elementary quantum chemistry

According to classical mechanics, exact values can be assigned to the position and momentum of a particle at the same time. However, quantum mechanics denies this possibility. Instead, in quantum mechanics, the more precisely the position of a particle is given, the less precisely one can say what its momentum is. Quantum mechanics assumes that the state of a system can be completely specified by a wave function  $\Psi(r,t)$  which depends on the coordinates ( $r$ ) of the particles in the system and the time ( $t$ ). The wave function has the important property that  $\Psi^*(r,t)\Psi(r,t)d\tau$  is the probability of finding the particle at a certain position, where  $\Psi^*(r,t)$  is the complex conjugate of  $\Psi(r,t)$ . For every observable, there is a corresponding operator, and the value of the observable can be obtained by the Eigen equation:

$$\alpha\Psi = a\Psi \quad (3-1)$$

where  $\alpha$  is the operator, and  $a$  is the eigenvalue. In particular, the total energy of the system can be calculated by the Schrödinger equation [Park, 1974; Kohn and Sham, 1965]

$$\hat{H}\Psi = E\Psi \quad (3-2)$$



where  $\hat{H}$  is the Hamiltonian operator for the molecular system;  $E$  is the total energy of the system. The ultimate goal of most quantum chemical approaches is to approximately solve the time-independent, non-relativistic Schrödinger equation [Lewars, 2003], where the Hamiltonian operator can be written as:

$$\begin{aligned}\hat{H}(\vec{r}, \vec{R}) &= \hat{T} + \hat{V} \\ &= \hat{T}_e(\vec{r}) + \hat{T}_N(\vec{R}) + \hat{U}_{ee}(\vec{r}) + \hat{U}_{NN}(\vec{R}) + \hat{U}_{eN}(\vec{r}, \vec{R})\end{aligned}\quad (3-3)$$

where  $\vec{r}$  is the positions of the electrons and  $\vec{R}$  is the positions of the nuclei. The first two terms represent the kinetic energy of electrons and nuclei, respectively. The remaining three terms account for the repulsive potential due to the electron-electron, nucleus-nucleus interactions and the attractive interactions between electrons and nuclei, respectively.

The Schrödinger equation can be further simplified according to the famous Born-Oppenheimer approximation [Born and Oppenheimer, 1927], which states that due to the significant differences between the masses of nuclei and electrons, the electrons can be considered as moving in the field of fixed nuclei. Therefore, the kinetic energy of the nuclei is zero and the repulsive potential energy between nuclei can be simply considered as a constant. Thus the Schrödinger equation given in equation (3-2) reduces to the electronic Schrödinger equation [Schrödinger 1926A, 1926B]:

$$\hat{H}_{elec} \Psi_{elec} = E_{elec} \Psi_{elec} \quad (3-4)$$

Where  $\hat{H}_{elec}$  is the electronic Hamiltonian operator:

$$\hat{H}_{elec} = \hat{T}_e(\vec{r}) + U_{ee}(\vec{r}) + U_{eN}(\vec{r}, \vec{R}) \quad (3-5)$$

$E_{elec}$  is the electronic energy. And the total energy is then the sum of  $E_{elec}$  and the constant nuclear repulsion term. Here  $U_{eN}(\vec{r}, \vec{R})$  is also termed as the external potential  $V_{ext}$  in the density functional theory (DFT) [Bethe, 1964; Joubert, 1997].

In order to solve the electronic Schrödinger equation for an arbitrary molecular system, the specific Hamiltonian operator of that system has to be set up first. In the second step, the eigenfunction  $\Psi$  and the corresponding eigenvalue  $E$  can be determined, and then all properties of interest can be obtained by applying the appropriate operators to the wave function. The variational principle states that the trial wave function which yields the lowest energy expectation value is the one which is closest to the exact wave function, and the energy computed as the expectation value of the Hamiltonian operator from a guessed  $\Psi_{trial}$  will be an upper bound to the true energy of the ground state. By searching through all acceptable N-electron wave functions, energy  $E$  as a function of  $\Psi$  is minimized. Usually some subsets are chosen such that the minimization of the energy can be done in some algebraic scheme. According to the variational principle, the ground state energy of a molecular system is a functional of the number of electrons  $N$  and the nuclear potential  $V_{ext}$ .

### 3.2 Hartree-Fock scheme

Hartree-Fock (HF) approximation is the corner stone of almost all conventional wave function based quantum chemical methods and is also of great conceptual importance. In this scheme, the N-electron wave function is approximated by an antisymmetrized product of N one-electron wave functions [Bethe, 1964; Levine, 2000]. The product is usually referred as a Slater determinant, while these one-electron functions  $\chi_i(\vec{x}_i)$  are called spin orbitals. The physical interpretation of spin orbitals is that  $\left| \chi_i(\vec{x}_i) \right|^2 d\vec{x}$  represents the probability of finding the electron within the volume element  $d\vec{x}$ . By applying the variational principle, it was found that the HF energy could be presented by the so-called Coulomb and exchange integrals [Eichkorn *et al.*, 1995], and the variational freedom in the expression of HF energy is in the choice of the orbitals. Therefore, by solving Hartree-Fock equations, which determines the “best” spin orbitals, the best Slater determinant which yields the lowest HF energy could also be obtained.

$$\hat{f} \chi_i = \varepsilon_i \chi_i, i = 1, 2, \dots, N. \quad (3-6)$$

where  $\varepsilon_i$  is the orbital energy, and  $\hat{f}$  is an effective one-electron operator defined as following:

$$\hat{f}_i = -\frac{1}{2} \nabla_i^2 - \sum_A \frac{Z_A}{r_{iA}} + V_{HF}(i) \quad (3-7)$$

The first two terms represent the kinetic energy and the potential energy due to the electron-nucleus attraction; while  $V_{HF}(i)$  is the Hartree-Fock potential which contains two components related to the Coulomb operator and the Exchange operator, counts for the average repulsive potential experienced by the  $i$ 'th electron due to the remaining  $N - 1$  electrons.

### 3.3 Density functional theory (DFT)

The conventional quantum chemistry approach uses the wave function  $\Psi$  as the central quantity. However, the wave function is very complicated and cannot be measured in experiments. Besides, it depends on  $4N$  variables, three spatial and one spin variable for each of the  $N$  electrons, which makes the calculation of many-atom systems computationally inaccessible. By using the density functional theory (DFT) [Dreizler and Gross, 1990; Parr and Yang, 1989] in which the electron density is the central quantity, the equation that needs to be solved only depends on 8, rather than  $4N$  variables, independent of the system size.

#### 3.3.1 Electron density

The electron density  $\rho(\vec{r})$  determines the probability of finding any of the  $N$  electrons within the volume element  $d\vec{r}_1$  with arbitrary spin while the other  $N-1$  electrons have arbitrary positions and spins in the state represented by  $\Psi$ . It is defined as the following multiple integral over the spin coordinates of all electrons and over all but one of the spatial variables:

$$\rho(\vec{r}_1) = N \int \dots \int \left| \Psi(\vec{r}_1, \vec{r}_2, \dots, \vec{r}_N) \right|^2 ds_1 d\vec{r}_2 \dots d\vec{r}_N \quad (3-8)$$

The electron density is a non-negative function of the three spatial variables. It integrates to the total number of electrons, and vanishes at infinity. Besides, it is an experimental observable [Parr and Yang, 1989; Shusterman and Shusterman, 1997; Bader, 1990]. The concept of electron density can be extended to the pair density, which defines the probability of finding a pair of two electrons with spins  $\sigma_1$  and  $\sigma_2$  at the same time within two volume elements  $d\vec{r}_1$  and  $d\vec{r}_2$ , while the remaining N-2 electrons have arbitrary positions and spins. The pair density contains all information about electron correlation and therefore is of great importance.

### 3.3.2 DFT models

In the earliest attempt to use the electron density to describe atomic and molecular systems, Thomas-Fermi model treats the nuclear-electron and electron-electron contributions in a classical way and takes into account only the kinetic energy, which is expressed based on the uniform electron gas [Thomas, 1927; March, 1975]. In this way, the energy for an atom can be described completely in terms of the electron density. Thomas-Fermi model employs the variational principle to find the correct density needed for the energy equation with the constraint that the electron density integrates to the total number of electrons.

Hohenberg and Kohn published their classical paper in the Physical Review in 1964 pronouncing the birth of density functional theory [Hohenberg and Kohn, 1964]. The theorem of Hohenberg-Kohn (HK) proves that the total ground state

energy of an electron system is a unique functional of the ground state electron density. Moreover, the ground state electron density determines all properties of all states of the electron systems. The theorem also states that the ground state energy of the system attains its minimum value with respect to all allowed densities if and only if the input density is the true ground state density. However, the HK theorem did not provide how to construct the functional, and what kind of approximation should be used for the unknown functions.

In 1965, Kohn and Sham proposed a method of combining wave function and density method to construct the unknown functional. They introduced the concept of a non-interacting reference system, which is built from a set of orbitals such that the major part of the kinetic energy can be computed to good accuracy. The remainder, which is a rather small part of the total energy, is determined by an approximate functional. By using this method, as much information as possible is computed exactly. They repartitioned the total energy functional into the following parts:

$$E[\rho] = T_0[\rho] + \int [\hat{V}_{ext}(r) + \hat{U}_{cl}(r)]\rho(r)dr + E_{xc}[\rho] \quad (3-9)$$

where  $T_0[\rho]$  is the kinetic energy of non-interacting reference system with the same density as the real, interacting one;  $\hat{V}_{ext}(r)$  is the external potential, i.e., the potential coming from nuclei;  $\hat{U}_{cl}(r)$  is the classical Coulomb interactions between electrons;  $E_{xc}[\rho]$  is the exchange-correlation energy term which contains the non-classical effects of self-interaction correction, exchange and correlation, and the residual part

of the true kinetic energy of the interacting system comparing with the non-interacting reference system [Levy, 1996]. By applying the variational principle, this energy expression is minimized under certain constraints and the resulting equations can be solved iteratively:

$$\left[-\frac{1}{2}\nabla_i^2 + \hat{V}_{eff}(r)\right]\phi_i^{ks}(r) = \varepsilon_i\phi_i^{ks}(r) \quad (3-10)$$

where  $\phi_i^{ks}(r)$  is the Kohn-Sham orbital and  $\hat{V}_{eff}(r)$  is an effective potential. The equation is very similar to the eigen equation of the Hartree-Fock method. Most importantly, the Kohn-Sham orbitals, which can be quite easily derived from the above equation, are used to obtain the total density of the system:

$$\rho(r) = \sum_{i=1}^N |\phi_i^{ks}(r)|^2 \quad (3-11)$$

where the density is used to calculate an improved potential  $\hat{V}_{eff}(r)$  and leads to a new cycle of self-consistent field. Therefore, the Kohn-Sham orbitals have no actual physical significance and their only connection to the real world is that the summation of their squares adds up to the exact electron density.

It is worth noting that if the exact form of  $E_{xc}[\rho]$  and the functional derivative of it with respect to  $\rho$  were known, the Kohn-Sham approach is in principle exact. Unlike the Hartree-Fock model, where the wave function is assumed to be a single

Slater determinant, where the approximation is introduced from the very beginning and can never obtain the true solution, the approximation of the Kohn-Sham approach only enters when an explicit form of the  $E_{xc}[\rho]$  and its corresponding potential with respect to  $\rho$  have to be determined. Therefore, the main challenge of modern density functional theory is to explore better and better approximations to these two quantities.

### 3.3.3 Exchange-correlation functional approximations

As discussed above, the quality of the density functional approach is solely determined by the accuracy of the chosen approximation to  $E_{xc}[\rho]$ . Unfortunately, unlike the conventional wave function based methods, there is no systematic way towards improving approximate functionals in the density functional theory.

All approximate exchange-correlation functionals are based on a simple model system of the local density approximation (LDA) [Hohenberg and Kohn, 1964; Kohn and Sham, 1965; Hedin and Lundqvist, 1969; Perdew and Zunger, 1981]. The central idea of this model system is a concept of uniform electron gas [Ceperley and Alder, 1980], which is a hypothetical system where electrons move on a positive background charge distribution such that the total system is electrically neutral. The uniform electron gas has been shown a fairly good physical model for simple metals, but is quite far away from any realistic situation in atoms or molecules which are usually characterized by rapidly varying densities. However, the uniform electron gas is still considered to be a very important part of the density functional theory because it is the only system for which the exact (or at least to very high accuracy) forms of the exchange-correlation functionals are known:



$$E_{xc}^{LDA}[\rho] = \int \rho(\vec{r}) \varepsilon_{xc}(\rho(\vec{r})) d\vec{r} \quad (3-12)$$

where  $\varepsilon_{xc}(\rho(\vec{r}))$  is the exchange-correction energy per particle of a uniform electron gas of density  $\rho(\vec{r})$ . Surprisingly, although the LDA model and the true exchange-correlation hole differ in many details, the LDA model has been proved not a bad approximation and sometimes is even comparable to the Hartree-Fock approximation for the determination of molecular properties such as equilibrium structures, harmonic frequencies or charge moments. But it performs rather poorly when it comes to the energetic details such as bond energies due to overbinding.

In early 1980s, the first successful extensions to the purely local approximation were developed. Besides the information about the density  $\rho(\vec{r})$  at a particular point  $r$ , the information about the gradient of the charge density was also considered to take into account the non-homogeneity of the true electron density. The energy functional of the following form is termed the gradient expansion approximation (GEA) [Chrétien and Salahub, 2001]:

$$E_{xc}^{GEA}[\rho_\alpha, \rho_\beta] = \int \rho \varepsilon_{xc}(\rho_\alpha, \rho_\beta) d\vec{r} + \sum \int C_{xc}^{\sigma, \sigma'}(\rho_\alpha, \rho_\beta) \frac{\nabla \rho_\sigma}{\rho_\sigma^{2/3}} \frac{\nabla \rho_{\sigma'}}{\rho_{\sigma'}^{2/3}} d\vec{r} + \dots \quad (3-13)$$

where  $\sigma$  and  $\sigma'$  indicate  $\alpha$  or  $\beta$  spin;  $\nabla \rho$  is the gradient of the charge density. Unfortunately, GEA does not lead to the desired improved accuracy as expected, but

frequently performs even worse than the simple LDA method. The reason was considered to be that the exchange-correlation hole [Ziegler, 1991; Baerends and Gritsenko, 1997] associated with this functional has lost many of the properties which made the LDA hole physically meaningful.

By truncating the exchange and correlation holes in the GEA models such that the models do not violate the requirement of the exchange holes being negative everywhere, generalized gradient approximation (GGA) [Perdew, 1985; Perdew and Yue, 1986; Becke, 1988; Perdew, 1986a; Perdew, 1986b; Perdew, 1992; Perdew, 1993; Perdew, *et. al.*, 1996; Becke, 1992] provide notable improvements. Its expansion tries to find the right asymptotic behavior and right scaling for the usually nonlinear expansion. The functionals depend not only upon the density, but also upon the magnitude of the gradient of density at a given point. GGA works quite well and becomes one of the most popular methods in the current density functional theory.

Going beyond the GGA method, meta-generalized gradient approximation (meta-GGA) [Becke and Roussel, 1989] takes second order gradients and the (non-interacting) kinetic energy density into account and leads to a new family of functionals. Another new exchange-correlation functional termed VSXC [Van Voorhis and Scuseria, 1998] depends not only on  $\rho$  and  $\nabla\rho$ , but also on the non-interacting kinetic energy. Besides, empirical density functionals make heavy use of parameterization. Interestingly, all these latter new functionals achieve their promising performance without exact exchange. And none of them has gained a significant popularity.

### 3.3.4 Estimation of atomic charges

The type of bonding in a material is reflected by the distribution of the electron density around the atoms in the material. Therefore, atomic charges in a material can be calculated by DFT methods. For a covalent bond, charges are strongly aggregated and direction-dependent between the neighboring atoms. However, in the case of an ionic bond, the charge density distribution resembles a superposition of spherically symmetric atomic charge densities.

The calculated DFT charge density can be integrated to yield a measure of the ionicity of the atoms. And the ionicity of the material can be determined by summing up the charges around each atom. One method is to divide the unit cell into so called Voronoi cells and sum up the charges in each cell. A drawback of this method is that it is not suitable for molecular systems where various atoms with different ionic radii are involved. Another better method is to define that an arbitrary point  $r$  belongs to the Voronoi-like cell around atom  $j$ , if

$$\frac{|r - R_j|}{b_j} \leq \frac{|r - R_i|}{b_i} \quad (3-14)$$

are for all atoms  $i \neq j$  [Yourdshahyan *et. al.*, 1999; Ruberto *et. al.*, 2003]. In this equation,  $R_i$  and  $b_i$  are the position and ionic radius of atom  $i$ , respectively.

# Chapter 4 Molecular Weight Dependence of Surface Tensions of Normal Alkanes and Methyl Methacrylate Oligomers

## 4.1 Introduction

Inasmuch as the relevancy of the concept of surface tension to a variety of physical phenomena and engineering applications, there exists a wealth of information about it in the literature [Dee and Sauer, 1992; Dee and Sauer, 1993; Aubouy *et al.*, 2000; Stanton and Jurs, 1992; Carre and Vial, 1993; Brostow *et al.*, 2003; Hapke *et al.*, 1998; Vial and Carre, 1991; Patterson and Siow, 1970; Escobedo and Mansoori, 1996; Patterson and Rastogi, 1970; Flour and Paplrer, 1982]. Especially, numerous theoretical and experimental methods for surface tension of polymer liquids have been reviewed in a paper by Dee and Sauer [Dee and Sauer, 1992]. As mentioned in their paper, it was early observed that surface tension  $\gamma$  varies with  $M_n^{-2/3}$  (where  $M_n$  is the number-averaged molecular weight) for oligomers and low molecular weight polymers [LeGrand and Gaines, 1969], and recent experimental studies show that the surface tension of polymer melts with moderate to high molecular weights actually exhibits a  $M_n^{-1}$  dependence [Sauer and Dee, 1991; Sauer and Dee, 1994; Dee and Sauer, 1993; Jalbert *et al.*, 1993].

Over the past two decades, MD techniques have also been developed to compute

---

Another version of this chapter has been published as **Chunli Li** and Phillip Choi, Molecular Dynamics Study of the Molecular Weight Dependence of Surface Tensions of Normal Alkanes and Methyl Methacrylate Oligomers, *Journal of Physical Chemistry B*, **2006**, *110*, 6864

surface tension [Kirkwood and Buff, 1949; Gloor and Jackson, 2005; Bennett, 1976; Binder, 1982; Buff *et al.*, 1965; Bowlinson and Widom, 1982; Theodorou, 1988]. Three general types of simulation techniques to determine the surface tension of fluids were discussed in details in a paper written by Gloor and coworkers [Gloor and Jackson, 2005]. Within the context of such techniques, these general approaches are referred as mechanical approaches [Kirkwood and Buff, 1949], thermodynamic approaches [Bennett, 1976], and finite-size scaling concept based approaches [Binder, 1982; Buff *et al.*, 1965]. One is to use the distribution function approach in which the tangential component of the pressure tensors ( $P_t(z)$ ) of the molecules in the interfacial region bound by the coordinates  $z_\alpha$  and  $z_\beta$  in the normal direction of the interface of a model system is used to calculate surface tension [Theodorou, 1988]. This is based upon the classical equation developed by Kirkwood and Buff in 1949 [Kirkwood and Buff, 1949]:

$$\gamma = \int_{z_\alpha}^{z_\beta} [P - P_t(z)] dz \quad (4-1)$$

where  $\gamma$  is the surface tension and  $P$  is the uniform normal pressure of the model system. This equation essentially provides the link between the intermolecular forces experienced by the molecules in the interfacial region and surface tension measured macroscopically. However, since most of the generic force fields used in molecular simulation cannot reproduce pressure tensors very well, use of such an approach, especially for chain like molecules, would lead to inaccurate prediction of surface tension.

Another approach is to calculate the internal energy change upon creation of surfaces to a bulk model system (i.e.,  $\left(\frac{\partial U}{\partial \sigma}\right)_{n,V,T}$ ) and combine it with the experimental information about the corresponding entropy change (i.e.,  $T\left(\frac{\partial S}{\partial \sigma}\right)_{n,V,T}$ ) to obtain surface tension [Mansfield and Theodorou, 1990]. This is because the entropy term cannot be evaluated directly from molecular simulation. The approach is based on the most common definition of surface tension as shown in the following equation:

$$\gamma = \left(\frac{\partial A}{\partial \sigma}\right)_{n,V,T} = \left(\frac{\partial U}{\partial \sigma}\right)_{n,V,T} - T\left(\frac{\partial S}{\partial \sigma}\right)_{n,V,T} \quad (4-2)$$

where  $\gamma$  is the surface tension of the model system;  $A$  is the Helmholtz free energy of the system; and  $\sigma$  is area of the surface that separates the bulk liquid phase and its equilibrium vapour phase.  $U$  and  $S$  are the internal energy and entropy of the system. The subscripts  $n$ ,  $V$  and  $T$  denote the number of molecules, total volume and temperature of the system. In particular, Mansfield and Theodorou demonstrated that reasonably accurate  $\left(\frac{\partial U}{\partial \sigma}\right)_{n,V,T}$  values could be obtained by calculating the internal energy difference between a thin film model and a bulk liquid model with the same number of molecules at the same temperature [Mansfield and Theodorou, 1990]. In their approach, the thin film model was generated by imposing two well-defined

surfaces which were located at the upper and lower extremes of the bulk cell and normal to the z axis.  $\left(\frac{\partial U}{\partial \sigma}\right)_{n,V,T}$  is simply calculated using the following expression:

$$\left(\frac{\partial U}{\partial \sigma}\right)_{n,V,T} = \frac{\langle U_{2D} \rangle - \langle U_{3D} \rangle}{\sigma} \quad (4-3)$$

where  $\sigma$  denotes the total surface area of the two surfaces created on both sides of the bulk cell. (i.e,  $2 L_x L_y$ ). Here,  $L_x$  and  $L_y$  are the dimensions of the thin film in the  $x$  and  $y$  directions ( $z$  being the direction normal to film surface).  $\langle U_{2D} \rangle$  and  $\langle U_{3D} \rangle$  represent the average internal energy of the model system in the bulk and thin film states and such quantities are calculated from the corresponding molecular dynamics (MD) simulations at the same  $T$ . However,  $V$  has changed considerably in the process. This is because such equilibrated thin film structure would contain two interfacial regions that have a higher volume per unit mass than the bulk region of the system. Therefore, the total volume occupied by the same number of molecules in the thin film model would be larger than the volume of the 3D periodic bulk model. Obviously, this is not an issue for a macroscopic system because the volume of the interfacial region is much smaller than the total volume of the system. In addition, the total volume of such a small thin film model is difficult to define as its surfaces are fairly rough. In our view, it is more appropriate to define the area using the concept of solvent accessible surface area (see discussion below) and use it to define the total volume of the thin film model [Connolly, 1985].

Nonetheless, Mansfield and Theodorou were able to reproduce the experimental data even with the use of a surface area of  $2L_xL_y$  and showed that the entropy term in equation (3-2) is not negligible. The latter finding is somewhat expected as surface tensions of polymer melts are generally measured at relatively high temperatures (e.g., 400 K). Unless the entropy term is extremely small, say on the order of  $10^{-4} \text{ mJ/K} \cdot \text{m}^2$ , it would lead to erroneous predictions when the entropy term is neglected. However, it is worth noting that Mattice and coworkers used a different method and found that reasonable predictions of surface tensions of polymer melts such as poly(1,4-cis-butadiene) [He *et al.*, 1997], polyethylene [Misra *et al.*, 1995], polybenzoxazine [Kim and Mattice, 1998], etc., could be obtained by ignoring the entropy term in equation (4-2). The method by which the authors used to create surfaces is to elongate the three-dimensional periodic liquid model cell in one direction up to a point that the parent chains in the periodic simulation cell do not sense the existence of their periodic images in the elongating direction (see Figure 4-1).

In view of the difficulty associated with the second approach, we propose here a new approach to compute  $\gamma$  using a less popular definition of surface tension as shown in the following equation [Becher, 1983]:

$$\gamma = \left( \frac{\partial U}{\partial \sigma} \right)_{n,V,S} \quad (4-4)$$

Obviously, use of the definition shown in equation (4-4) suffers from the volume and surface area issues mentioned above as well. But it provides the basis for the direct



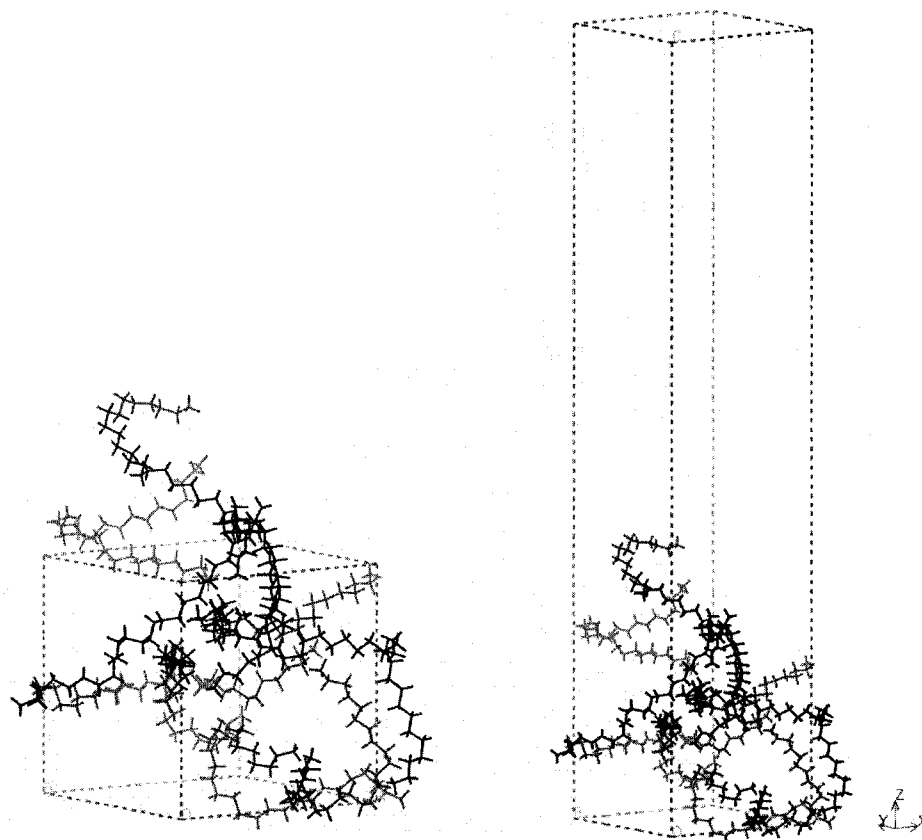


**Figure 4-1** Liquid and thin film model of normal alkane (C<sub>30</sub>)

calculation of surface tension without the need to evaluate the entropy term as  $S$  is supposed to be fixed. The key issue here is how to keep  $S$  constant. In this regard, we adopted an approach similar to a procedure that is commonly used in the calculation of cohesive energy density (CED) for such a purpose [Zhao and Choi, 2004; Maranas *et al.*, 1998]. In order to test the validity of the new strategy, we applied it to two fairly different series of low molecular weight compounds – normal alkanes and methyl methacrylate (MMA) oligomers to check if we could reproduce their surface tension values and the corresponding experimentally observed molecular weight dependence. The choices of the oligomers were made simply because of the availability of surface tension data and molecules of respective oligomers interact with each other through different types of intermolecular forces. In general, it has been observed experimentally that oligomers exhibit a  $M_n^{-2/3}$  rather than  $M_n^{-1}$  dependence of surface tension [Dee and Sauer, 1998].

## **4.2 Molecular dynamics simulation**

### **4.2.1 Simulation details**

All simulations were carried out on a Silicon Graphics (SGI) workstation cluster along with the use of commercial software – Cerius2 version 4.0 purchased from Accelrys. A generic force field DREIDING 2.21 developed by Mayo *et al.* was used for both series of oligomers which were represented by explicit atomistic models [Mayo *et al.*, 1990]. However, for the alkane models, instead of using the default Lennard-Jones (LJ) parameters for carbon-carbon interactions, LJ parameters of Ryckaert and Bellemans were used as such parameters yield satisfactory estimation of cohesive energy density for low molecular weight alkanes as demonstrated previously

[Rychaert and Bellemans, 1975]. Typical equations and parameters used in the modified DREIDING 2.21 force field (not the complete set) are presented in Table 4-1. The choice of the force field and LJ parameters was based on the balance of the availability of computational resources and accuracy of the results. For the normal alkane models, zero charges were assigned while the charge equilibration method was used to determine the partial atomic charges for all atoms made up of the MMA oligomers. For each series of oligomers, five models with chain lengths ranging from about 10 to 200 backbone carbons, which cover the so-called low molecular weight ranges as defined experimentally, were used. Multiple chain models were used for simulating the condensed phase of the normal alkanes except the model with 200 backbone carbons. However, single chain models were used for MMA oligomers as their chain architecture is much more complex than that of normal alkanes. Characteristics of the above described models are presented in Table 4-2 and Table 4-3. The experimental bulk densities at the simulation temperatures (150 °C for normal alkanes and 180 °C for MMA oligomers) and the corresponding cubic simulation cell sizes are also given in the same tables [Doolittle, 1964]. For the MMA oligomers, owing to the lack of experimental density data on the oligomers at various chain lengths, density of PMMA at 180 °C was used for all models.

The initial liquid state models of the oligomers were built using the method of Theodorou and Suter along with their experimental density values [Theodorou and Suter, 1985]. Each initial three-dimensional periodic simulation cell, after energy minimization, was subjected to a 1,000 K MD annealing for a period of 100 picoseconds (ps) before the low temperature MD simulations at the corresponding

**Table 4-1** Equations and parameters used in the modified DRIEDING 2.21 force field

Interaction		Equation
Valence terms	Bond energy	$E_b = 1/2K_b(R - R_0)^2$
	Angle energy	$E_\theta = 1/2K_\theta(R - R_\theta)^2$
	Torsion energy	$E_\phi = \sum_{n=1}^2 1/2K_\phi n[1 \pm \cos(n\phi)]$
	Out-of-plane angle	$E_{inv} = K_{inv}(\cos \chi - \cos \chi_0)^2$
Nonbond terms	Coulombic interaction	$E_{coul} = 332.0637q_i q_j / \epsilon r_{ij} \operatorname{erfc}(r_{ij} / \beta)$
	Hydrogen Bonding	$E_{hb} = \epsilon_0 [5(R_0 / R)^{12} - 6(R_0 / R)^{10}] \cos^4 \phi$
	Van der Waals energy	$E_{vdw} = \epsilon_0 [(\sigma_0 / R)^{12} - 2(\sigma_0 / R)^6]$

$$K_b = 2.93 \times 10^5 \text{ kJ/mol/nm}^2; R_0 = 0.15 \text{ nm}; K_\theta = 418 \text{ kJ/mol/rad}^2; R_\theta = 1.91 \text{ rad}$$

$$K_\phi = 20.9 \text{ kJ/mol}; K_{inv} = 20.9 \text{ kJ/mol}; \chi_0 = 2.09 \text{ rad}; \beta = 0.234 \text{ nm}; \epsilon = 1$$

**Hydrogen bonding:**  $\epsilon_0 = 16.72 \text{ kJ/mol}; R_0 = 0.275 \text{ nm}$

**van der Waals energy:**

**H atom:**  $\epsilon_0 = 0.00042 \text{ kJ/mol}; \sigma_0 = 0.3195 \text{ nm}$

**O atom:**  $\epsilon_0 = 0.4 \text{ kJ/mol}; \sigma_0 = 0.3405 \text{ nm}$

**C atom:**  $\epsilon_0 = 0.6985 \text{ kJ/mol}; \sigma_0 = 0.3923 \text{ nm}$

**Off-diagonal interactions:**  $\epsilon_0 = 1.2607 \text{ kJ/mol}; \sigma_0 = 0.4237 \text{ nm}$

simulation temperatures (150 °C for normal alkanes and 180 °C for MMA oligomers) were carried out. The simulation time was set at 1 nanosecond (ns) and the time step used was 1 femtosecond (fs). Ten snapshots of the last 100 ps, recorded every ps, of the 1 ns simulation were used for the calculation of the potential energy of the liquid state model, denoted as  $E_{3D}$  respectively. And for each of such snapshots, the z-direction of the 3D periodic simulation cell was elongated manually until it was long enough that no interactions between neighboring periodic cells in the z direction could be found (see Figure 4-1). And the corresponding  $E_{2D}$  was calculated. The total volume of the thin film model was determined based on the volume bounded by the two solvent accessible surfaces (see Figure 4-2 and the discussion about solvent accessible surface area below). Here, a series of hard spherical probes with different radii were used to identify the area that would yield the total volume which was equal to that of the original 3D model. The average total volume of the thin film model was also calculated by averaging the total volumes of the last 100 snapshots.

In this way, all subscript variables appearing in equation (4-4) (i.e.,  $n$ ,  $V$  and  $S$ ) are kept constant. It should be emphasized that  $\langle U_{2D} \rangle$  appears in equation (4-3) does not require the entropy (i.e., conformations of the molecules) to be fixed. Therefore, equilibrated structures of the thin film model should be used. However, when equation (4-4) is used,  $E_{2D}$  should be calculated using the same conformations of the molecules from the 3D periodic simulation cell but with interactions in the z direction removed. This procedure is essentially identical to a well accepted procedure used for the calculation of the cohesive energy density of chain molecules in which the potential energy of the molecules in an ideal gas state is calculated using the same

**Table 4-2** Characteristics of the normal alkane models with chain lengths from 13 to 200 carbons

<b>Model</b>	<b>Molecular weight (<i>g/mol</i>)</b>	<b>Density (<i>g/cm<sup>3</sup></i>)</b>	<b>Number of chains for calculation</b>	<b>Cell side length (<i>Å</i>)</b>
PEC13	184.4	0.6604	10	16.67
PEC20	282.6	0.7009	10	18.85
PEC30	422.9	0.7276	10	21.30
PEC60	843.6	0.7533	4	19.52
PEC200	2807	0.7706	1	18.22

**Table 4-3** Characteristics of the MMA oligomer models with chain lengths from 10 to 200 repeat units

<b>Model</b>	<b>Molecular weight (<i>g/mol</i>)</b>	<b>Density (<i>g/cm</i><sup>3</sup>)</b>	<b>Cell side length (<i>Å</i>)</b>
PMMA10	1003	1.11	11.45
PMMA30	3006	1.11	16.51
PMMA50	5008	1.11	19.57
PMMA100	10014	1.11	24.66
PMMA200	20026	1.11	31.06

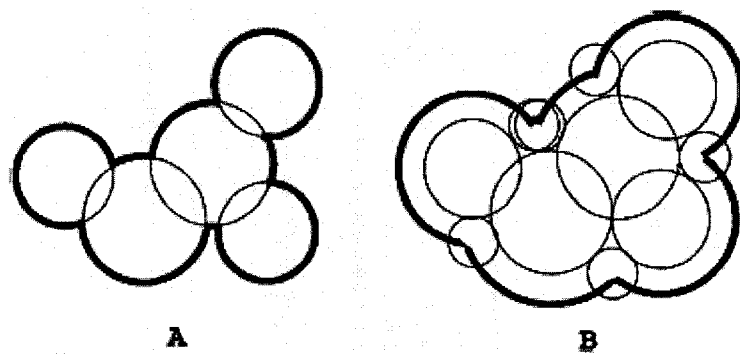


**Figure 4-2** Molecular surface models: (A) van der Waals surface, (B) Solvent accessible surface



conformation of the molecules obtained from the bulk cell but with all three dimensional periodic boundary conditions removed [Rodgers, 1993].

#### 4.2.2 Solubility parameter

The solubility parameters of normal alkanes and MMA oligomers were calculated according to the following equation [Zhao and Choi, 2004; Maranas *et al.*, 1998]:

$$\delta^2 = \frac{\rho(E_v - E_b)}{M} \quad (4-5)$$

where  $\delta$  is solubility parameter;  $\delta^2$  is cohesive energy density;  $\rho$  is density of oligomers;  $E_v$  is potential energy of the isolated chains in vacuum;  $E_b$  is potential energy of the chains in bulk state and  $M$  is molecular weight of the polymer chains modeled. Figure 4-3 depicts the procedure to calculate the solubility parameters of the oligomers. Ten frames of the last 100 ps were chosen to do these calculations separately and the results were then averaged. Standard deviation was obtained from the 10 results statistically.

#### 4.2.3 Self diffusion coefficient

Self diffusion coefficients of normal alkanes and MMA oligomers were calculated according to Einstein's diffusion equation [Allen and Tildesley, 1987]:

$$D = \frac{1}{6} \lim_{t \rightarrow \infty} \frac{d \langle |r(t) - r(0)|^2 \rangle}{dt} \quad (4-6)$$

$$\delta^2 = \frac{\langle E_{\text{vacuum}} - E_{3D} \rangle}{V}$$

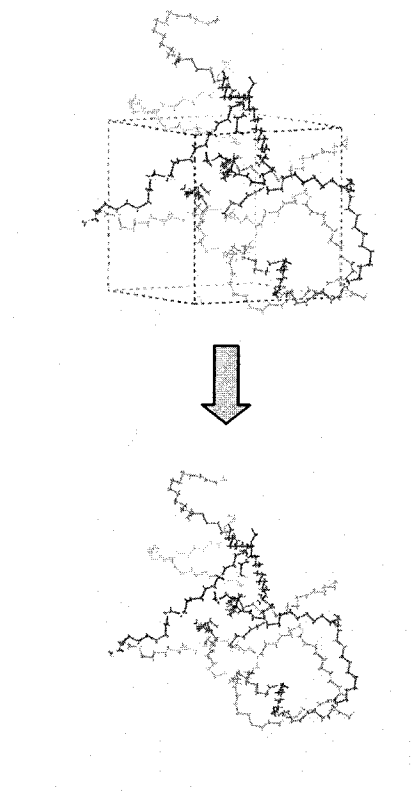


**Figure 4-3** Simulation procedure employed to calculate cohesive energy density and solubility parameter of an oligomer

As it shows, the three-dimensional self diffusion coefficient ( $D$ ) of a molecule is related to the time derivative of its mean square displacement. And the mean square displacement could be obtained readily through molecular dynamics simulation.

#### 4.2.4 Surface area

As mentioned, use of the flat surface areas (i.e.,  $2L_xL_y$ ) as  $\sigma$  shown in equation (4-3) for the thin film models with thicknesses in the length scale of few nanometer (either the equilibrated or non-equilibrated one) is not appropriate as surfaces of such models are “rough”. In our view, such “rough” surfaces are better described by the concept of solvent accessible surface area [Mansfield and Theodorou, 1990]. Solvent accessible surface area is generated by the center of a solvent molecule probe (modeled as a rigid sphere) when it is being “rolled” over the van der Waals surface of the model molecules as depicted in Figure 4-2. Obviously, different surface areas would be obtained using probes with different radii. Therefore, specifying the radius of the spherical probe for such a “rolling” process is critical. In this regard, we tested a series of probes with radii ranging from 0.5 to 3.5 Å. And the solvent accessible surface area that would yield a total volume that is equal to volume of the liquid state model would be used in the calculation of  $\gamma$ . Owing to the time consuming nature of such calculations, only 10 snapshots of the last 100 ps of each MD simulation were obtained and used for calculating the average.

## 4.3 Results and discussion

### 4.3.1 Solubility parameter

Figure 4-4 and 4-5 depict our simulation results on the molecular weight dependence of solubility parameters for normal alkanes and MMA oligomers, respectively. Solubility parameters are widely used to estimate the mutual solubilities of ordinary liquids, but are not measurable for polymers [Hildebrand and Scott, 1964]. However, values of solubility parameters could be inferred from data on internal pressure. Internal pressure is obtained from PVT measurements and their values are equal to cohesive energy densities for van der Waals liquids. Available experimental measurements on internal pressure for normal alkane series include 235 MPa for n-heptane at 20 °C [Allen *et al.*, 1960] and 312 MPa for polyethylene samples at 167 °C [Krishnamoorti *et al.*, 1996]. In another words, the solubility parameters inferred from internal pressure are  $15.3 (J/cm^3)^{1/2}$  and  $17.7 (J/cm^3)^{1/2}$ , respectively. Maranas *et al.* [Maranas *et al.*, 1998] reported their MD simulation results on the chain length dependence of cohesive energy density and internal pressure for polyethylene. Comparing with available experimental measurements and Maranas' simulation results, our simulation values show slightly underestimated values. Besides, Goudeau *et al.* [Goudeau *et al.*, 2000] calculated solubility parameters of MMA oligomers from data of internal pressure. Their reported values are  $20.1 (J/cm^3)^{1/2}$  and  $20.2 (J/cm^3)^{1/2}$  for MMA oligomers with molecular weight of 1 K and 15 K, respectively. Compared with these values, our simulation results show underestimation to some extent.

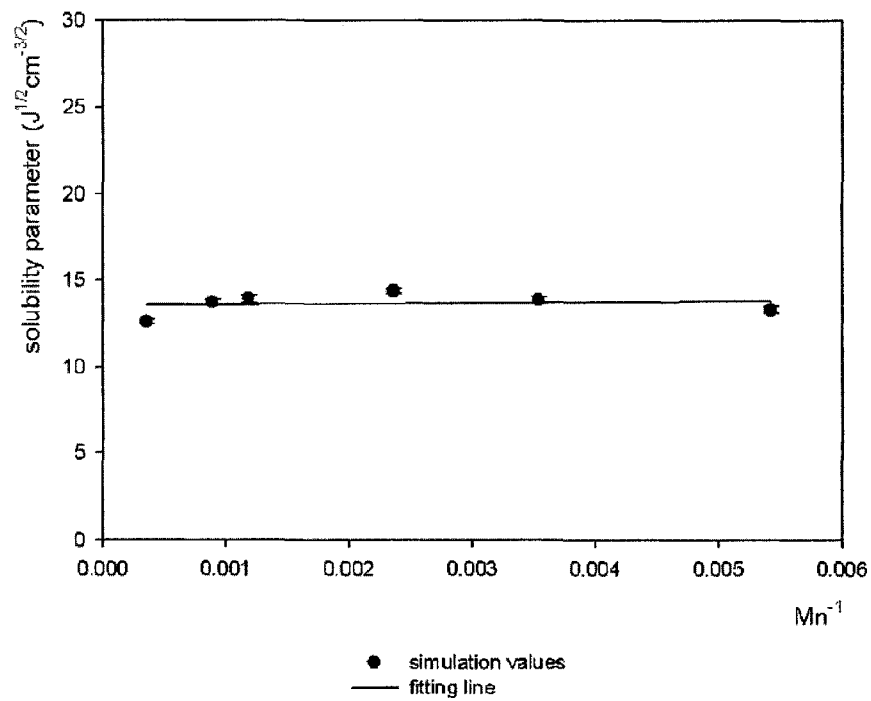


**Figure 4-4** Molecular weight dependence of the solubility parameter of normal alkanes

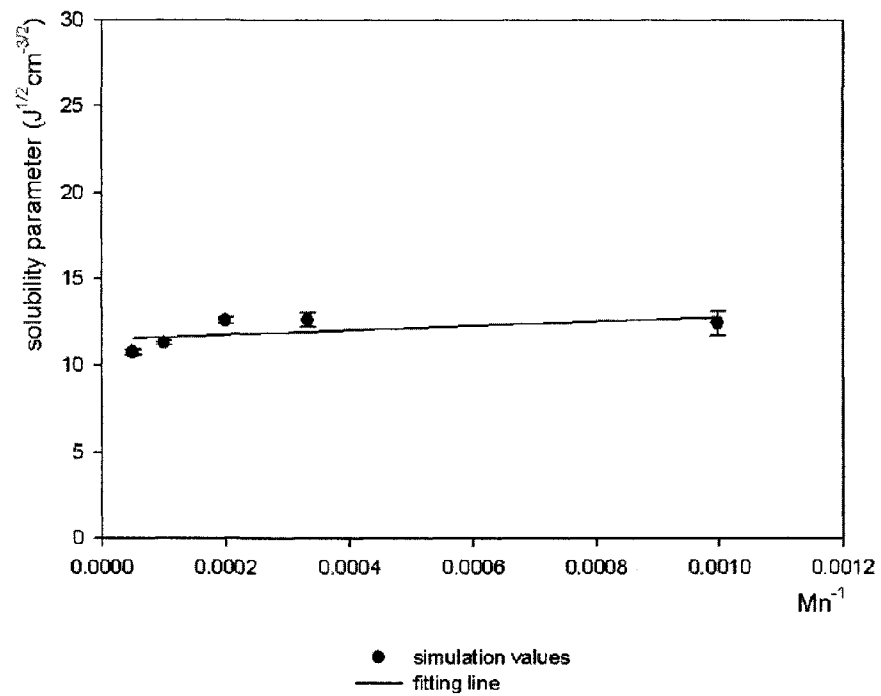


**Figure 4-5** Molecular weight dependence of the solubility parameter of MMA oligomers

### **4.3.2 Self diffusion coefficient**

Figure 4-6 and 4-7 depict the mean square displacements of the normal alkane with 30 backbone carbon atoms and MMA oligomer with 30 repeating units, respectively. Similar results for the two oligomers at various chain lengths are omitted for clarity. Self diffusion coefficients of the normal alkanes and MMA oligomers are also listed in Table 4-4 and 4-5. Note again that the criterion for the system to reach equilibrium state is that the mean square displacement reaches the square of radius of gyration. This criterion has been achieved for each of the normal alkane models. However, as shown in Figure 4-7, equilibrium of the MMA oligomers system has by far not been reached for the simulation. Much longer simulations were also carried out but the results were not substantially improved. Another possible reason is that DREIDING force field may not be able deal with the electrostatic interactions in those MMA oligomers correctly. Different combinations of force field parameters were validated to calculate the electrostatic interactions, but surprisingly, even the combination of Ewald summation method and COMPASS force field can not obviously do a better job. Besides, we used the same density value for all MMA oligomers, which could also possibly affect the evaluation of self diffusion coefficient values of MMA oligomers.

### **4.3.3 Surface area**

The probe size dependence of the solvent accessible surface area and the corresponding total volume of the thin film models of the normal alkane with 30 backbone carbon atoms and MMA oligomer with 30 repeating units are shown in Figures 4-8 and 4-9, respectively. Similar results for the two oligomers at various

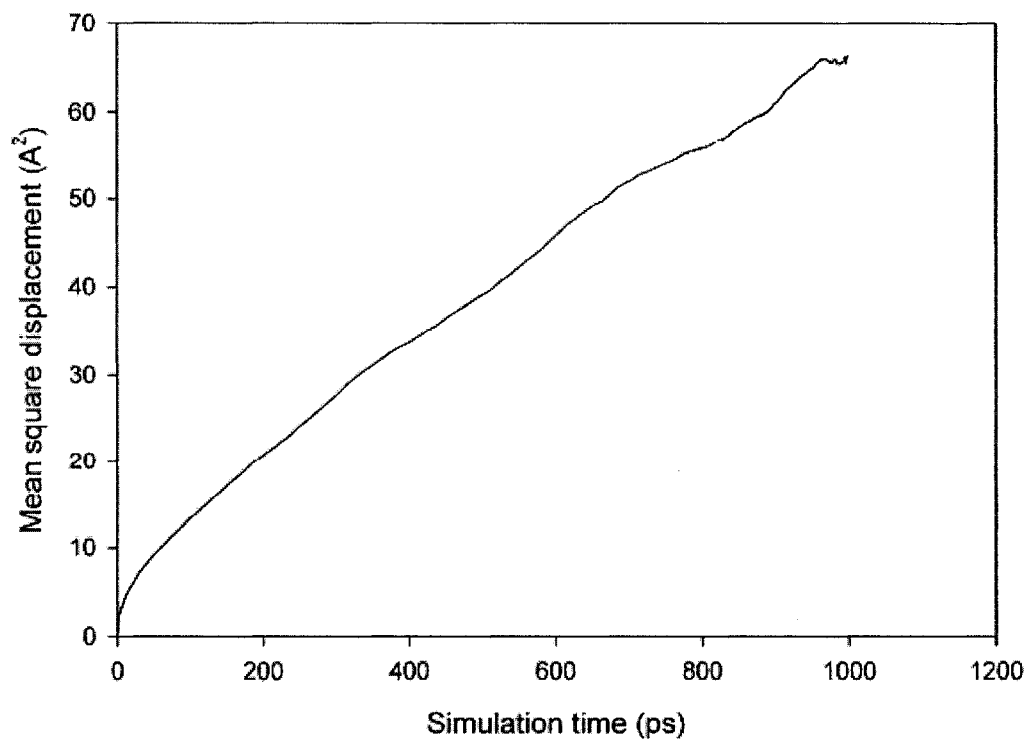


**Figure 4-6** Mean square displacement of normal alkane with 30 backbone carbon atoms



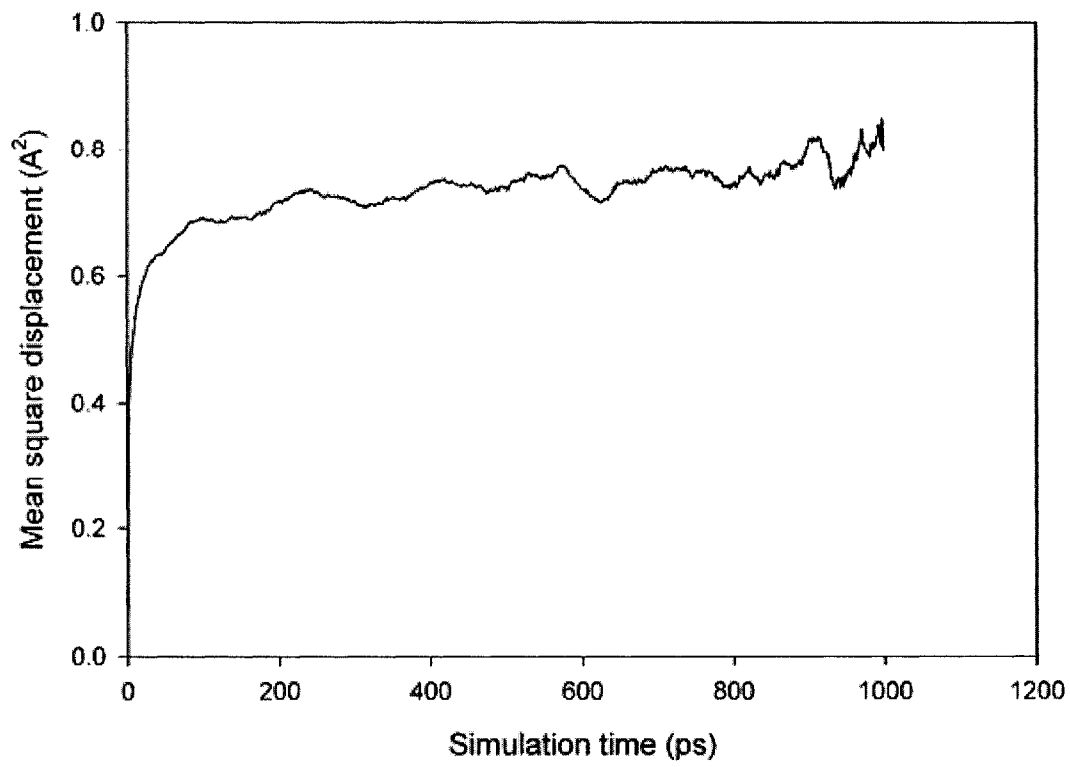


**Figure 4-7** Mean square displacement of MMA oligomer with 30 repeat units

**Table 4-4** Self diffusion coefficients and radii of gyration of normal alkanes

<b>Model</b>	<b>Diffusion coefficient</b> $\text{\AA}^2 / ps$	<b>Radius of gyration</b> $\text{\AA}$
PEC13	0.0804	4.1
PEC20	0.0268	6.6
PEC30	0.0614	8.3
PEC60	0.0361	9.0
PEC200	0.0156	12.8

**Table 4-5** Self diffusion coefficients and radii of gyration of MMA oligomers

<b>Model</b>	<b>Diffusion coefficient</b> $\text{\AA}^2 / ps$	<b>Radius of gyration</b> $\text{\AA}$
PMMA10	0.0002	5.9
PMMA30	0.00007	8.8
PMMA50	0.0012	13.1
PMMA100	0.0014	21.1
PMMA200	0.0011	21.4

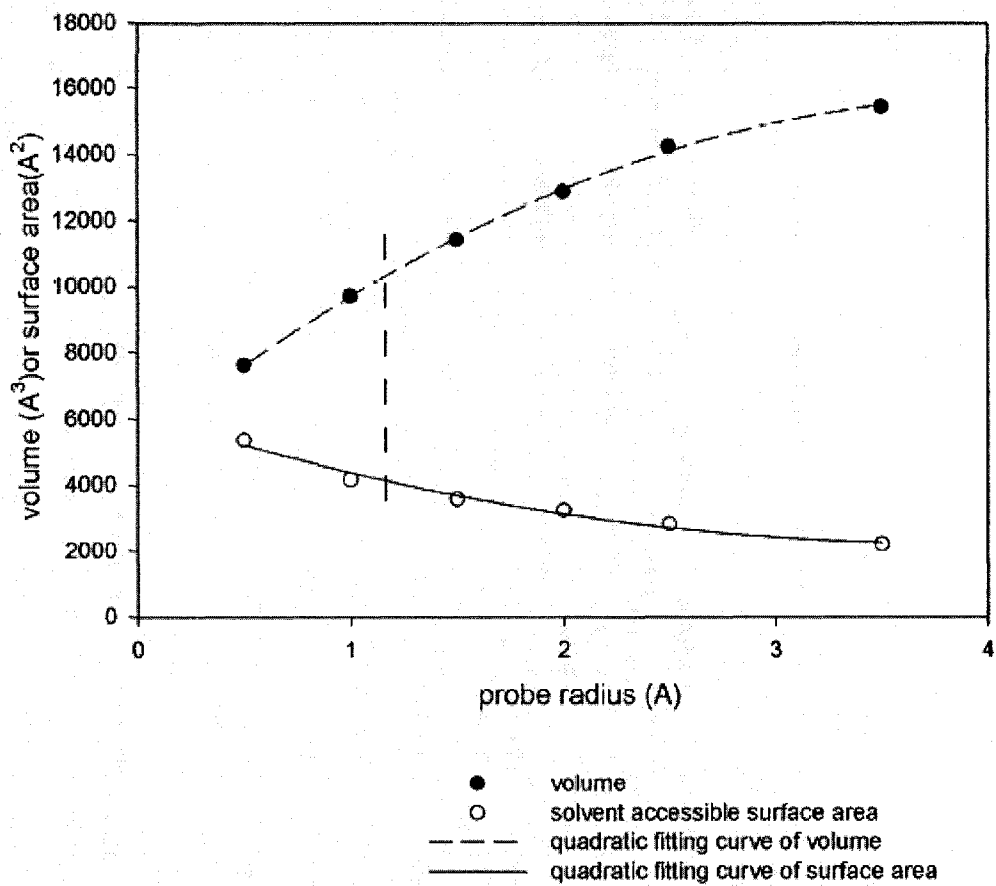


**Figure 4-8** Probe size dependence of solvent accessible surface area and the corresponding total volume of the thin film models for the normal alkane chains with 30 carbon atoms (the probe size marked by the dash line corresponds to the one used in this paper)

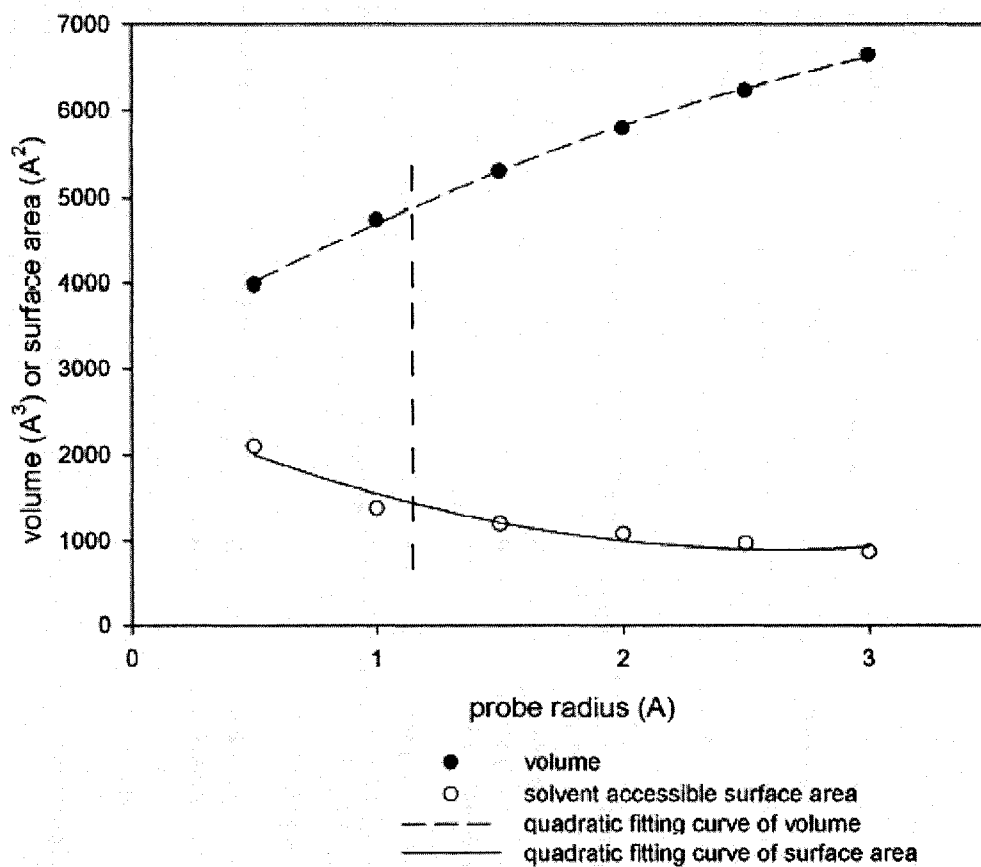


**Figure 4-9** Probe size dependence of solvent accessible surface area and the corresponding total volume of the thin film models for the MMA oligomer with 30 repeat units (the probe size marked by the dash line corresponds to the one used in this paper)

chain lengths are omitted for clarity. As can be seen, the solvent accessible surface area decreases with increasing probe size while the total volume of the thin film bounded by the solvent accessible surfaces exhibits an opposite trend. The first observation is simply attributed to the fact that larger probes would not be able to detect the detailed contour of the surfaces. As a result, the solvent accessible surface area and its roughness would decrease. Hence, the total volume enclosed by the solvent accessible surfaces would include considerable amount of free volumes leading to a larger total volume. As mentioned, in order to determine the area that should be used in the calculation of surface tension, we chose the solvent accessible surface area that would yield a total volume which was equal to the volume of the 3D periodic simulation cell from which the thin film model was generated. The probe size and the solvent accessible surface area of normal alkane and MMA oligomers models are shown in Table 4-6 and 4-7, respectively.

#### **4.3.4 Surface tension**

It should be noted again that the molecules in the thin film model possess the same conformation as those in the 3D periodic simulation cell. Consequently, the energy difference between the thin film and liquid state models is purely attributed to the internal energy change due to the difference in the intermolecular interactions (not from the change in the bonded energy). The respective simulation results, plotted against  $M_n^{-2/3}$  for the normal alkanes and MMA oligomers are shown in Figure 4-10 and 4-11 along with the corresponding experimental results. It is obvious in both cases that the computed data points are highly linear, indicating that the surface tension of these two chemically different oligomers exhibit the expected  $M_n^{-2/3}$

**Table 4-6** Probe sizes for the normal alkanes used in this work

<b>Model</b>	<b>Probe size</b> $\overset{\circ}{(A)}$	<b>Surface area</b> $\overset{\circ^2}{(A)}$
PEC13	1.00	2740 $\pm$ 235
PEC20	0.99	4097 $\pm$ 79
PEC30	0.98	4110 $\pm$ 107
PEC60	0.93	2244 $\pm$ 96
PEC200	0.86	3102 $\pm$ 82

**Table 4-7** Probe sizes for the MMA oligomers used in this work

<b>Model</b>	<b>Probe size</b> $\overset{\circ}{\text{Å}}$	<b>Surface area</b> $\overset{\circ^2}{\text{Å}}$
PMMA10	1.50	$676 \pm 17$
PMMA30	0.79	$1569 \pm 38$
PMMA50	0.77	$3830 \pm 26$
PMMA100	0.81	$6764 \pm 32$
PMMA200	0.87	$9978 \pm 155$



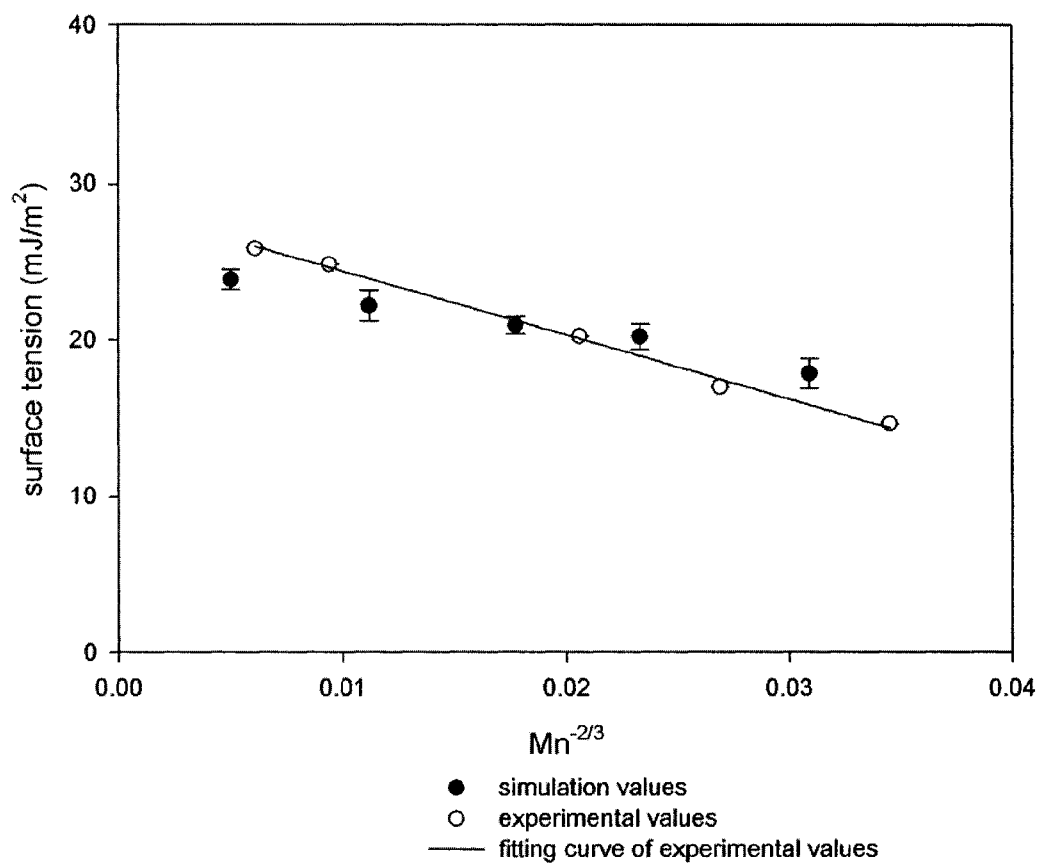


**Figure 4-10** Molecular weight dependence of surface tension for normal alkanes obtained from our simulations (solid circles) compared with experimental data (open circles)

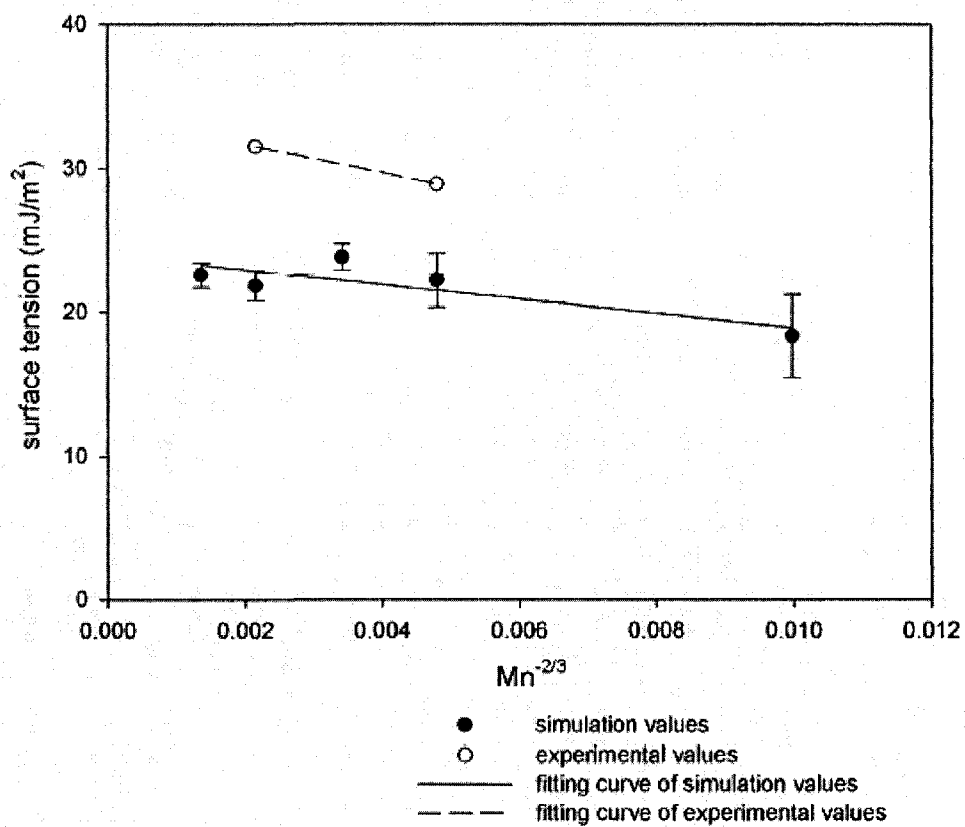


**Figure 4-11** Molecular weight dependence of surface tension for MMA oligomers obtained from our simulations (solid circles) compared with experimental data (open circles)

dependence. Using slopes of the regression lines obtained for the experimental surface tension data (no error bars) as referenced [Becher, 1983; Goudeau *et al.*, 2000; Wu, 1982; Wu, 1970], we consider the slopes we obtained to be in good agreement with experiment; especially in the case of MMA oligomers (there are only two experimental data points available for the MMA oligomers). Nonetheless, the experimental and our simulation results indicate that the  $M_n^{-2/3}$  dependence of surface tension is universal but the proportional constant (i.e., the slope) depends on the chemical characteristics of the oligomer. Compared with normal alkanes, it is clear that the numerical values of the computed surface tension of MMA oligomers deviate significantly from experiment. The deviation may be due to two reasons. One is that DRIEDING 2.21 is not optimized for MMA oligomers; the other is that our assumption of constant density for all MMA oligomers with different chain lengths may not be valid. However, it is interesting to note that the newly proposed molecular simulation procedure, even with the use of a generic force field, yielded the molecular weight dependence of surface tension ( $M_n^{-2/3}$ ) quite well for the two drastically different oligomers. In other words, our models implicitly captured the physics involved. To this end, we further analyze both the surface tension and CED data to identify the root cause for the observed behavior.

Figures 4-12 and 4-14 show the molecular weight dependence of  $\langle E_{2D} - E_{3D} \rangle$  and of the corresponding solvent accessible surface area for the normal alkanes and MMA oligomers while Figures 4-13 and 4-15 are for  $\langle E_{vac} - E_{3D} \rangle$  and molar volume for the two set of models, respectively. It should be noted that the molar volumes shown in Figures 4-12 and 4-14 are from experiment while all other data points in

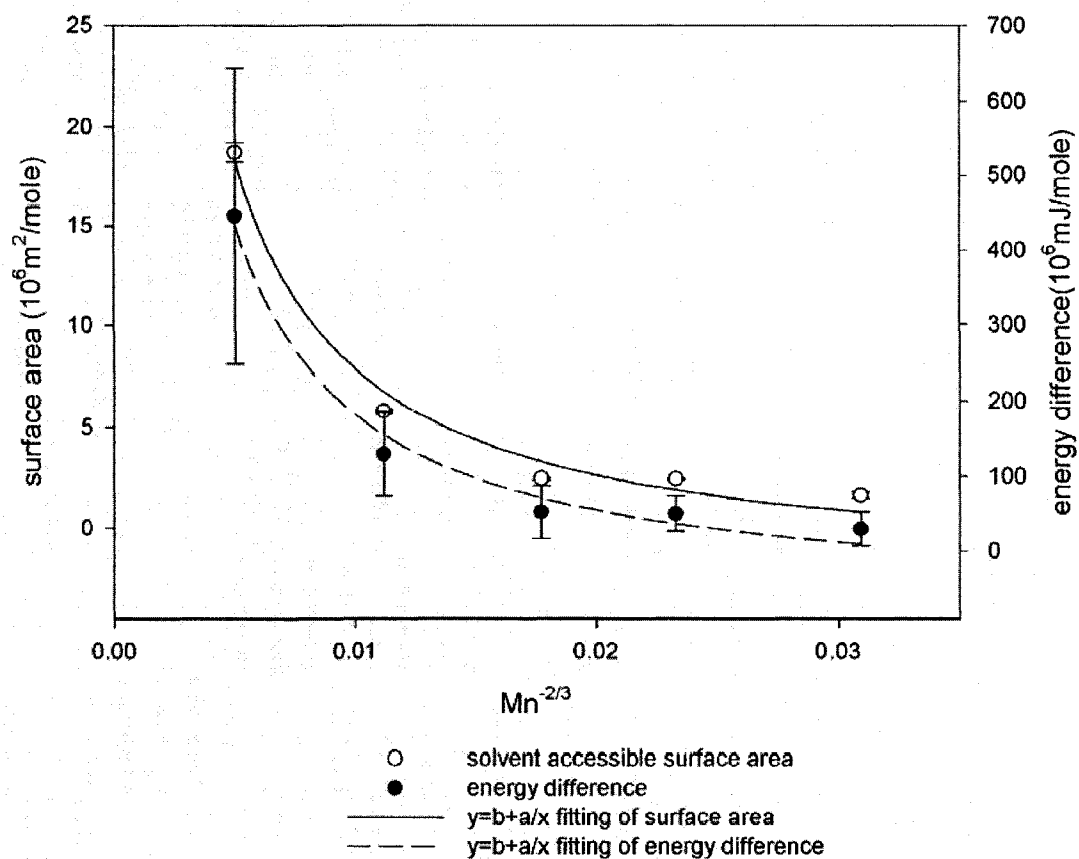


**Figure 4-12** Molecular weight dependence of surface tension components for normal alkanes with solvent accessible surface area (opening circles) labeling on the left vertical axis and energy difference  $\langle E_{2D} - E_{3D} \rangle$  (solid circles) labeling on the right vertical axis

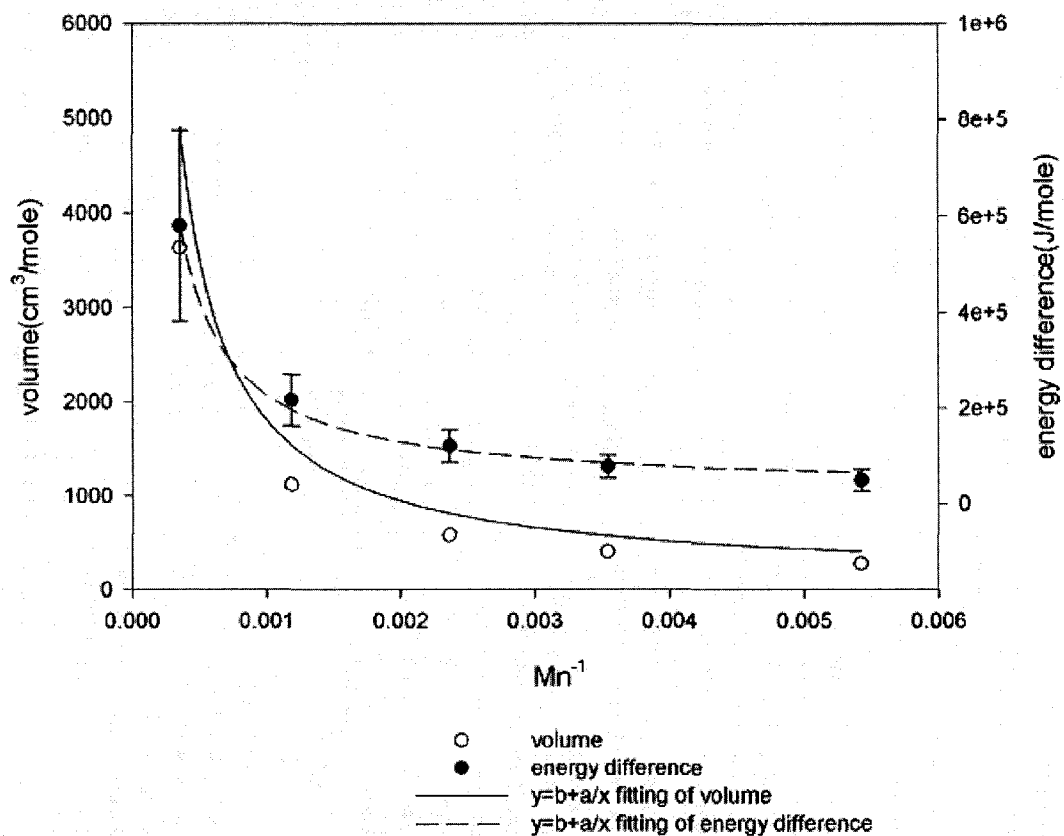


**Figure 4-13** Molecular weight dependence of cohesive energy density components for normal alkanes, with molar volume (opening circles) labeling on the left vertical axis and energy difference  $\langle E_{vac} - E_{3D} \rangle$  (solid circles) labeling on the right vertical axis

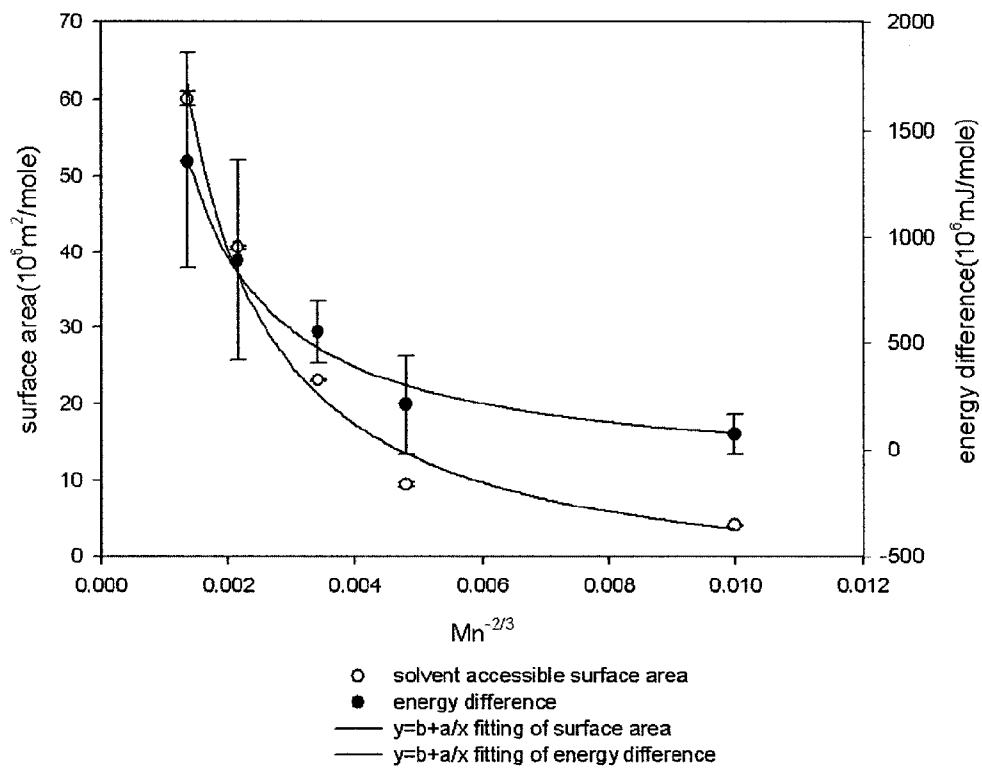


**Figure 4-14** Molecular weight dependence of surface tension components for MMA oligomers with solvent accessible surface area (opening circles) labeling on the left vertical axis and energy difference  $\langle E_{2D} - E_{3D} \rangle$  (solid circles) labeling on the right vertical axis

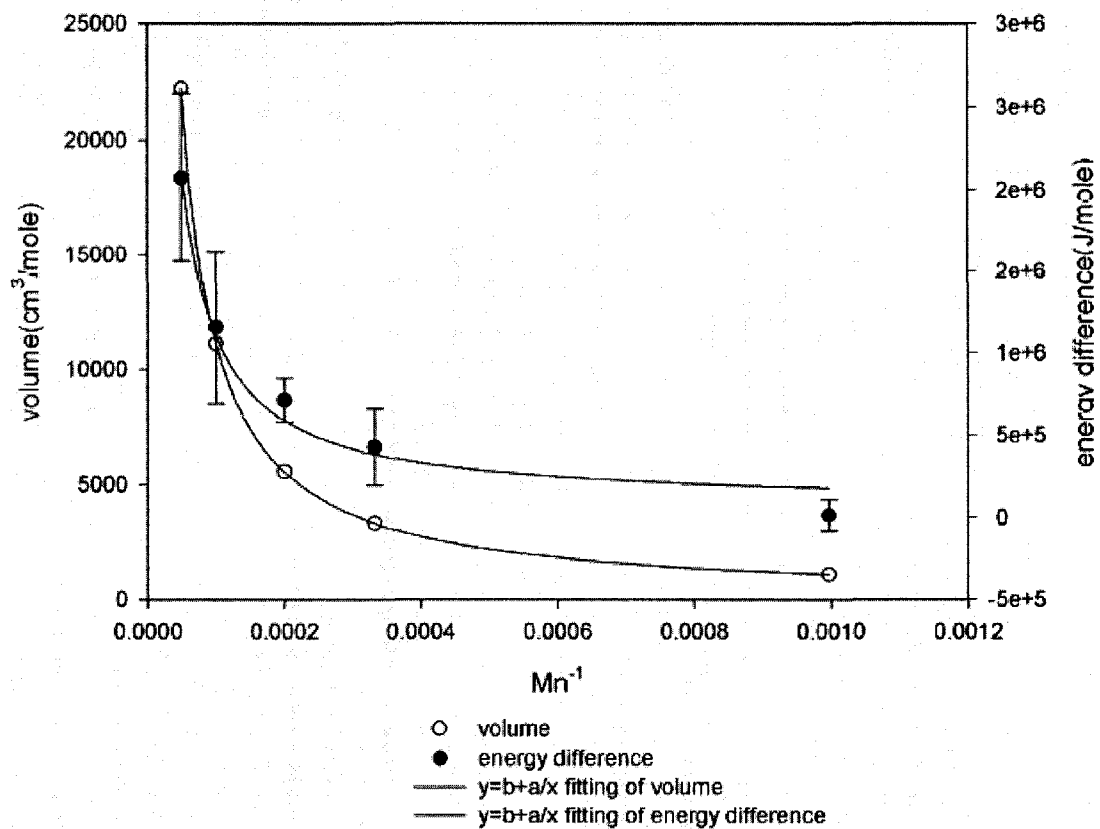


**Figure 4-15** Molecular weight dependence of cohesive energy density components for MMA oligomers, with molar volume (opening circles) labeling on the left vertical axis and energy difference  $\langle E_{vac} - E_{3D} \rangle$  (solid circles) labeling on the right vertical axis

Figures 4-12, 4-13, 4-14, 4-15 were obtained from our MD simulations. It is interesting to observe that molecular weight dependence of the solvent accessible surface area and the associated  $\langle E_{2D} - E_{3D} \rangle$  as well as of the molar volume and  $\langle E_{vac} - E_{3D} \rangle$  resemble each other when they were plotted against  $M_n^{-2/3}$  and  $M_n^{-1}$ , respectively. In particular, the molar volume shows an inverse dependence of  $M_n^{-1}$  while the solvent accessible surface area also shows an inverse dependence but on  $M_n^{-2/3}$ . The inverse dependence of  $M_n^{-1}$  for the molar volume and the associated  $\langle E_{vac} - E_{3D} \rangle$  simply means that both quantities are linearly proportional to the average size of the molecules. The former dependence is expected based upon the definition of molar volume. The latter also seems reasonable as the vaporization process involves the elimination of the intermolecular forces experienced by the molecules in the three-dimensional space which should vary linearly with the average size of the molecules. And such dependence should not change as the size of the molecules becomes larger and is applicable to the whole molecular weight range as observed experimentally.

Regarding the solvent accessible surface area, our simulation results show that it depends, to a less extent, on the size of the oligomers, only to the power of 2/3 (i.e.,  $1/M_n^{-2/3}$ ) rather than 1. The corresponding  $\langle E_{2D} - E_{3D} \rangle$  also exhibits a similar functional dependence. Consequently, when both quantities were combined, that led to a  $M_n^{-2/3}$  dependence of surface tension. Since high molecular weight normal alkanes ( $M_n > 500$  g/mol) exhibit a  $M_n^{-1}$  dependence of surface tension (experimental observation) [Hapke, 1998], it is conjectured that the exponent of the molecular weight dependence of the solvent accessible surface area for high molecular weight



normal alkanes may have a value of 1. If that is the case, what is required to explain is why do low molecular weight normal alkanes exhibit a  $M_n^{-2/3}$  dependence on the solvent accessible surface area (therefore surface tension) while high molecular weight ones a  $M_n^{-1}$  dependence. Considering the manner by which solvent accessible surface areas were evaluated in the present work, it seems that the higher the molecular weight of the oligomer is, the rougher the surface is. Figures 4-16 and 4-17, which show the solvent accessible surfaces for the lowest and highest molecular weight normal alkane and MMA oligomers used, are used to illustrate such observation. In other words, the molecular weight dependence of the solvent accessible surface area seems to be related to the roughness of the non-equilibrium surfaces created by the elongation process. In particular, it was observed that surfaces of the oligomers with 200 backbone carbons tend to exhibit more chain bending that leads to rougher surfaces. For low molecular weight oligomers, roughness seems to be related to the orientations of the molecules (no chain bending) rather than their size. One can imagine that in the extreme case, when all such small molecules line up in the direction normal to the surface, roughness of the surface would be a weak function of the size of the molecules. On the other hand, when all molecules lie in the plane of the surface, the surface accessible surface area covered by the molecules would depend, to a larger extent, on the size of the molecules. However, since all of these molecules orient randomly, the exponent of the molecular weight dependence of the solvent accessible surface area should be expected to be less than 1. We believe the observed exponent of  $2/3$  could probably be derived mathematically based upon the orientations of the molecules and the radius of the

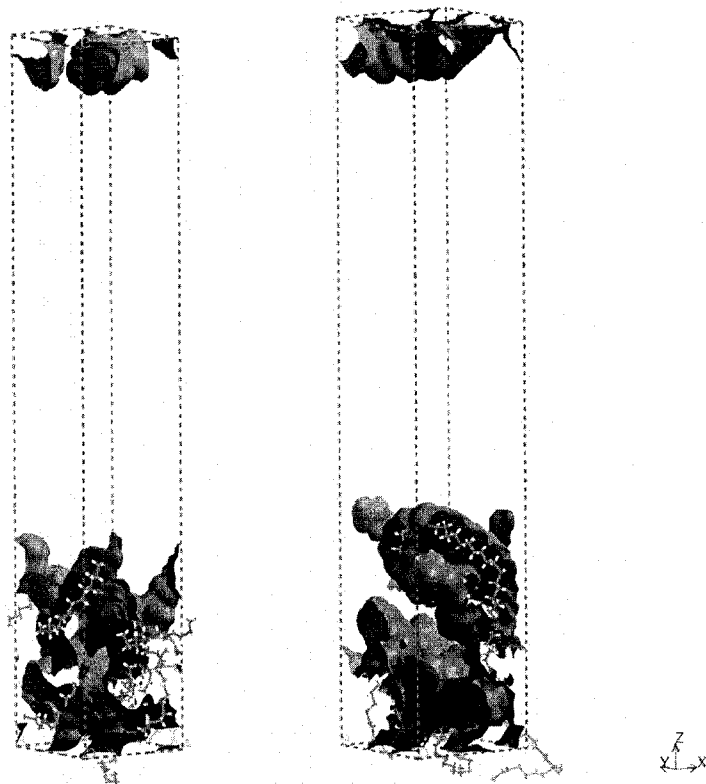


**Figure 4-16** Solvent accessible surfaces of normal alkane chains (left PEC13, right PEC200)

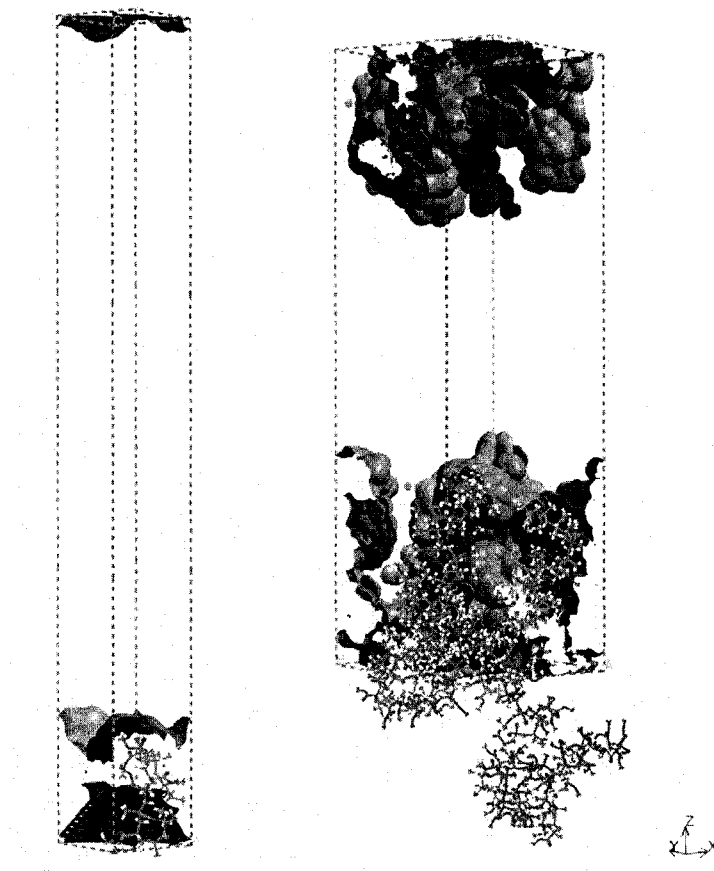


**Figure 4-17** Solvent accessible surfaces of MMA oligomer chains (left PMMA10, right PMMA200)

probe used. Since the critical molecular weight above which normal alkanes start to chain fold in vacuum is about 500 g/mol, it is speculated that above such a molecular weight, the roughness of the surfaces of normal alkanes would depend on the orientations of the segments exposed to the surface, which would depend on the chain length of the molecules. It should be pointed out that the chain segments of the high molecular weight molecules would orient themselves more or less in a random fashion.

Finally, it should be pointed out that the above discussion is based on the non-equilibrium surfaces created by the elongation process; the orientations and/or conformations of the molecules are identical to those in their corresponding bulk state. The conformations of the molecules correspond to a hypothetical state of the systems that we created to evaluate surface tension in accordance with the surface tension definition shown in equation (4-4). In reality, those surfaces would not be as rough as shown in Figures 4-16 and 4-17 as the surface molecules would move closer to each other to form the interfacial region at a density value lower than that of the bulk to minimize the interaction with the vacuum. In doing so, there is an entropy penalty associated with it. And the entropy penalty would be different for molecules in different size ranges. In particular, the entropy penalty for small oligomers would be much smaller than that of the high molecular weight molecules as reeling of the chain segments into the interfacial region is not required. Therefore, the entropy penalty of molecules in the low molecular weight range should depend, to a less extent, on the size of the molecules and such dependence manifests itself in the surface tension measurements.

#### 4.4 Concluding remarks

A novel MD simulation procedure, based upon a less common definition of surface tension, has been proposed to compute the surface tension of oligomers. In particular, the new procedure was tested on normal alkanes and MMA oligomers. It was found that the deviation of the surface tension for MMA oligomers is very likely attributed to the generic nature of the force field used. Nonetheless, the new method is able to yield the molecular weight dependence of these two vastly different series of oligomers. Simulation results are in good agreement with the experimental observation of  $M_n^{-2/3}$  dependence of surface tension. Analysis of the data revealed that it may originate from the fact that the roughness of the surface determine such molecular weight dependence. In particular, for molecules in the low molecular weight range, roughness of their surfaces depends on the orientations of the molecules and to a less extent on the size of the molecules. However, in the high molecular weight range, surface roughness would likely depend on the orientations of the segments (i.e., conformation) made up of the molecules in the interfacial region, therefore on the size of the molecules.

## Chapter 5 Adsorption Behavior of Normal Alkanes on a Relaxed $\alpha\text{-Al}_2\text{O}_3$ (0001) Surface

### 5.1 Introduction

Adsorption of chain molecules on solid surfaces has intrigued many researchers as the process is relevant to a wide range of practical applications such as colloidal suspensions, lubricants, coatings, paints [Baschnagel *et al.*, 2003], polymer molding, and surface modification of medical implants [Norde, 1995], etc. More recently, the subject has attracted additional interest in the field of nanoparticle synthesis because behavior of chain molecules, used as a dispersant, influences significantly the shape and size, therefore, the properties of inorganic colloidal nanocrystals synthesized in an organic environment. This increasing attention is simply attributed to the potential applications of such nanoparticles in biomedical applications (e.g., drug delivery). It is obvious that behavior of chain molecules adsorbed on solid surfaces with drastically different chemical characteristics from themselves would not be the same as that on organic surfaces. To obtain desired properties of systems containing such interfaces, it is imperative to obtain molecular level insights into the spatial arrangement and intermolecular interactions of the chain molecules at such “organic-inorganic” interfaces. In this regard, atomistic level simulation techniques have a great potential for providing us with the insights needed.

---

Another version of this chapter has been published as **Chunli Li** and Phillip Choi, A Molecular Dynamics Study of the Adsorption Behavior of Normal Alkanes on a Relaxed Alpha-Alumina (0001) Surface, *the Journal of Physical Chemistry C*, **2007**, *111*, 1747

Molecular dynamics (MD) simulation has been routinely applied to study structure and dynamic behavior of chain molecules in their bulk and thin film states over the past few decades with considerable success. However, great challenges still exist for studying interactions between organic molecules and inorganic solid surfaces by MD. One major stumbling block is that most existing force fields cannot predict the structure of solid substrates accurately as such force fields are not optimized for inorganic materials. Another problem is that since the relaxation time scales of most inorganic substrates of interest (e.g. metals or metal oxides) and those of chain molecules differ by several orders of magnitude, this makes classical MD simulation infeasible for equilibrating both the organic and inorganic parts of the system simultaneously. It is worth noting that Monte Carlo (MC) simulation works no better as an alternative approach than MD simulation in this regard [Abrams, 2004]. To simplify the calculations, uniform metal surface models are usually employed in most of these MD simulations because structures of these metal surfaces are simple and well characterized by experiments. On the other hand, adsorption of chain molecules onto heterogeneous surfaces (such as those of metal oxides) is poorly understood, even though most of the applications involve such systems. At present, the only computational chemistry technique that would be able to precisely predict the structure and relaxation dynamics of metal oxides is the density functional theory (DFT) first principle calculations [Hass *et al.*, 1998; Lodziana and Norskov, 2003; Lodziana *et al.*, 2004]. Nevertheless, it is infeasible to perform MD simulation using such an *ab initio* approach for systems containing chainlike molecules interacting with metal oxide surfaces as the computational cost is prohibitively high. For

instance, Dkhissi *et al.* carried out quantum chemical calculations on the grafting of chain organosilane compounds on SiO<sub>2</sub>-hydroxylated solid surfaces, unfortunately only one single molecule with a few alkyl chains could be involved [Dkhissi *et al.*, 2005]. In general, coarse grained models are employed to represent chain molecules by using united atoms to represent repeat units, which could have different chemical composition, in a given chain molecule [Baschnagel *et al.*, 2003; Delle Site *et al.*, 2002; Delle Site and Kremer, 2005] and DFT calculations are performed to determine the interactions between such united atoms and the uniform metal surface of interest. The resultant interaction energy will then be used for performing MD simulation [Delle Site *et al.*, 2002; Delle Site, 2005]. Obviously, this approach only works for highly coarse-grained chains and simple inorganic surfaces. Therefore, detailed local packing of the adsorbed segments could not be obtained.

Alumina surface plays an important role in many technological areas simply because alumina (e.g.  $\alpha - Al_2O_3$ ) is frequently used as catalysts and catalyst supports. In addition, owing to oxidation reaction, aluminum surfaces are always covered by a layer of alumina, thereby determining the surface and interfacial properties of aluminum. Despite the importance and relevancy of alumina surface to many applications, few achievements have been obtained in the experimental investigations on the structure and chemistry of alumina surface even in recent years. This is because it is very challenging to prepare a clean and well-defined alumina surface experimentally. Since molecular simulation can be performed on a well defined alumina surface, this, in turn, provides an effective alternative for exploring surface phenomena of alumina surfaces in a well-controlled manner. The key issue here is



whether one can generate proper alumina surfaces computationally or not. This, in fact, can be accomplished by extending DFT calculations that yield correct  $\alpha - Al_2O_3$  crystal structure to alumina surfaces [Hass *et al.*, 1998; Kodziana and Norskov, 2003].

Claire *et al.* investigated the short chain hydrocarbon adsorption and the subsequent water penetration through a hydrocarbon film on a  $\alpha - Al_2O_3$  (0001) surface [Claire *et al.*, 1997]. The surface model they employed to run MD simulation was cleaved directly from the default crystal structure of  $\alpha - Al_2O_3$  listed in a commercial software Cerius<sup>2</sup> structures library and no further treatment was made. However, since atoms in the surface layers of  $\alpha - Al_2O_3$  would experience a rather different environment than in the bulk, it is necessary, in our view, to “correct” the atomic structure of the surface before MD is carried out. In this work, we therefore propose to relax the alumina surface using DFT calculations before the MD study. In this way, equilibration of the alumina surface by the MD simulation is not required. After the relaxation, positions of all alumina surface atoms will then be fixed and classical MD simulation will be carried out with the deposition of the chain molecules of interest onto the surface. Normal alkanes at two fairly different chain lengths (C<sub>11</sub> and C<sub>200</sub>) will be used. The rationale that MD simulation can be performed using such a strategy is that the frequency of the vibration of the aluminum-oxygen bond (on the order of femtoseconds) is by far much faster than that of the relaxations of the alkane chains of interest (on the order of nanoseconds) [Kodziana and Norskov, 2003; Goo, 2002]. To characterize the adsorption behavior of the normal alkanes, orientations and adsorption energy at 150 °C were determined.

## 5.2 Simulation models and methods

### 5.2.1 Relaxation of $\alpha$ - $\text{Al}_2\text{O}_3$ (0001) surface using density functional theory (DFT)

It is well known that molecules near a surface adopt a rather different intermolecular packing from those in the bulk state as such molecules are at a higher free energy state. For solids, surface atoms would undergo a so-called geometry optimization process (i.e., relaxation) by which the atoms move to the lowest free energy state. Since most solid substrates of interest are inorganic in nature, classical force fields are not adequate for such a relaxation process. Rather, use of the *ab initio* approach is more appropriate. Computationally, the relaxation process is performed on structures that are created by cleaving the corresponding crystal [Ruberto *et al.*, 2003]. In this work, the relaxation approach of Ruberto *et al.* will be applied to the  $\alpha$ - $\text{Al}_2\text{O}_3$  (0001) surface [Ruberto *et al.*, 2003]. Here, the bulk structure of the alumina crystal was obtained from an inorganic crystal library of a commercial software so-called Materials Studio (see Figure 5-1(a)). The crystal is composed of “sandwich” like layers of aluminum and oxygen atoms (see Figure 5-2(a)). Each layer (considered to be a repeat unit) contains three sub-layers of atoms in which two are made up of *Al* atoms while the sub-layer in between the two *Al* sub-layers is made up of oxygen atoms. The repeat unit is believed to be non-polar (i.e., no net charges) [Ruberto *et al.*, 2003].  $\alpha$ - $\text{Al}_2\text{O}_3$  (0001) surface was initially obtained by cleaving the alumina bulk structure at an *Al* terminated plane at a chosen depth. The rationale of cleaving the crystal at an *Al* terminated plane is that electrostatic considerations as well as

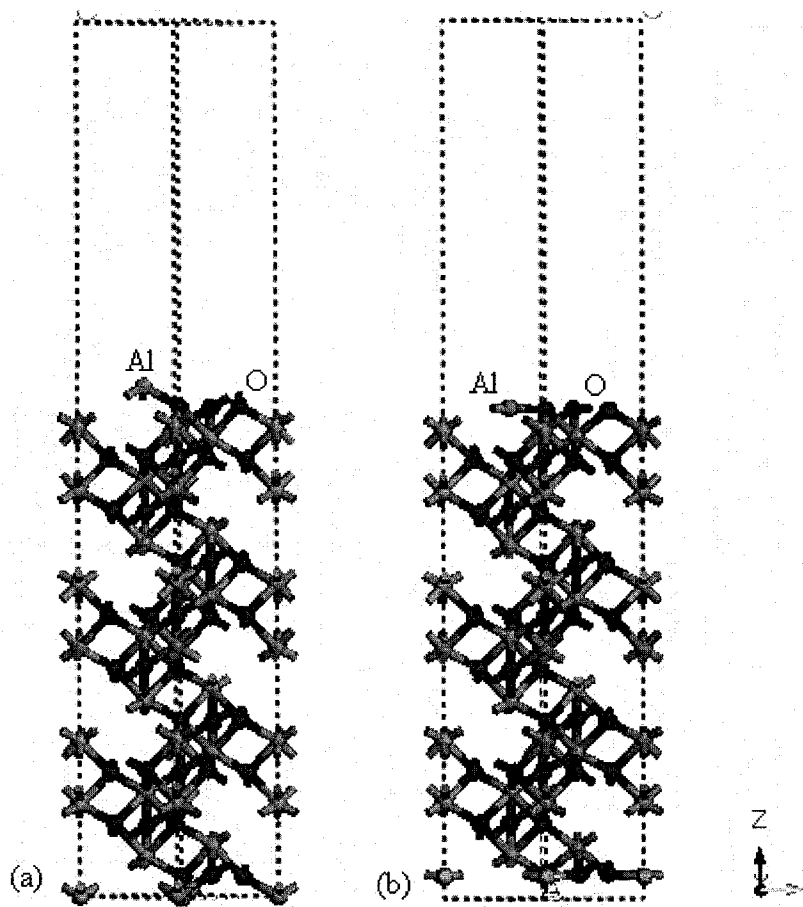


**Figure 5-1** Hexagonal vacuum slab of  $\alpha\text{-Al}_2\text{O}_3(0001)$  surface (a) before relaxation  
(b) after relaxation

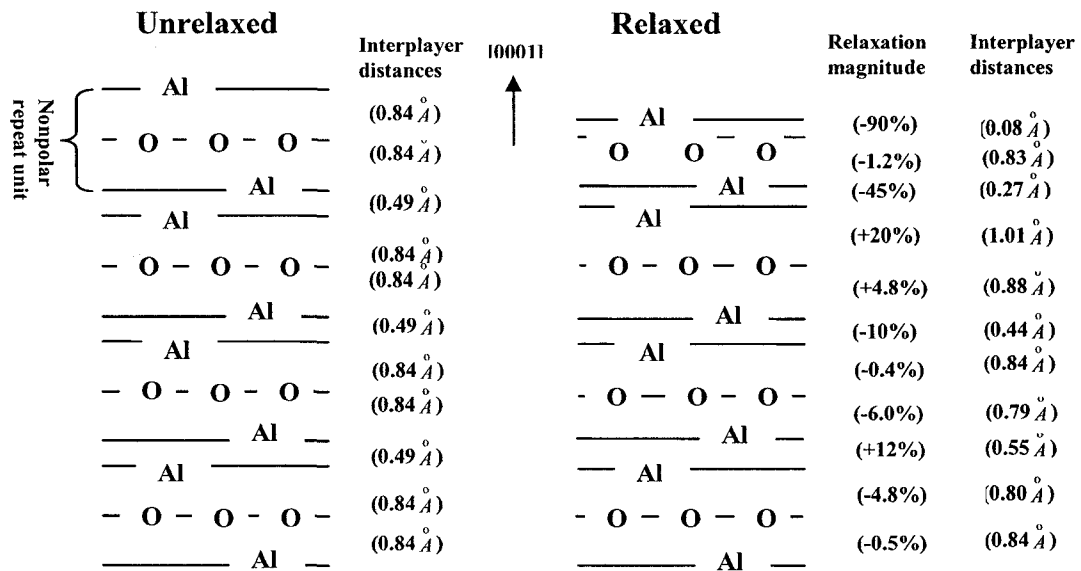


**Figure 5-2** The non-polar surface structure of  $\alpha\text{-Al}_2\text{O}_3(0001)$  surface before and after relaxation. The atomic layers that are perpendicular to the alumina (0001) surface, interlayer distances, the relaxation magnitude in percentage, and the nonpolar repeat unit for building the surface are shown

classical and quantum mechanical calculations indicate that the most favorable (0001) surface of  $\alpha - Al_2O_3$  is terminated by a single plane of  $Al$  atoms [Hass *et al.*, 1998; Claire *et al.*, 1997].

Slabs consisting of different numbers of repeat units were constructed to investigate the effect of the thickness of slab on the relaxation geometry of the surface atoms. This is accomplished by calculating the surface energy of the slabs based on the concept of “cleavage energy” or separation energy  $E_{sep}$  [Ruberto *et al.*, 2003], the energy needed to cleave one infinite crystal into two separate infinite crystals, each of which has one surface. It is worth noting that the separation energy is essentially equal to the surface energy of the slab created in our simulation as two surfaces are created in the cleaving process. The vacuum section in between the two surfaces of the model was set to 15 Å, which ensured that interactions between two neighboring slabs could be ignored [Ruberto *et al.*, 2003]. Since such surfaces are symmetric, the surface energy  $E_s$  could be obtained as

$$E_s = E_{sep} / 2 \quad (5-1)$$

The separation energy could be obtained as

$$E_{sep} = E_{cell}(n) - nE_b \quad (5-2)$$

Where

$$E_b = E_{cell}(n) - E_{cell}(n-1) \quad (5-3)$$

$E_b$  is the bulk binding energy of one repeat unit.  $E_{cell}(n)$  is the calculated total energy of a slab with  $n$  repeat units. The method to calculate surface energy here was believed to be more consistent than a separate bulk crystal calculation, due to the fact that the value of  $E_{sep}$  at sufficiently large  $n$  would converge, thus ensuring the independence of  $E_{sep}$  on the slab thickness [Ruberto *et al.*, 2003]. In fact, when the slab is thick enough, both surfaces of the slab would be fully relaxed with identical spacing while the repeat units in the middle of the slab resemble to that in the bulk. Relaxation of the slabs with different numbers of repeat units was carried out using the CASTEP code available in Materials Studio, a first principle calculation code developed based on the DFT. Exchange and correlation were treated with generalized gradient approximation (GGA) – PW91. Ionic cores were represented by ultrasoft pseudo potentials. A kinetic energy cut-off of 340 eV was used, and the  $k$ -point sampling mesh separation was set to  $0.05 \text{ \AA}^{-1}$ .

### 5.2.2 Molecular dynamics simulation

MD simulations were carried out with the use of commercial software Materials Studio. The COMPASS force field was employed to describe the atomic interactions between the normal alkanes and  $\alpha - Al_2O_3$  (0001) surface. COMPASS is an *ab initio* force field optimized for condensed-phase applications. Simulation results have shown that it can make accurate predictions of structural, conformational, cohesive and other physical properties for a wide range of substances [Accerlys, 2004]. The

expressions used in this force field are presented in Table 5-1 [Sun, 1998]. The functions include two categories of energy terms – valence terms which include diagonal and off-diagonal cross-coupling terms, and non-bonded interaction terms. As can be seen from the table, owing to the complexity of the expressions, a large number of parameters are used. For clarity, not all parameters are listed here (however, they can be found easily from Sun, 1998). Rather, we chose to show only the Lennard-Jones parameters that were used in the present work (see Table 5-2). It is worth noting that we used the 6<sup>th</sup> order combination law to calculate the cross Lennard-Jones parameters. The van der Waals interaction has a cutoff distance of  $9.50 \text{ \AA}$ , spline width of  $1.00 \text{ \AA}$ , buffer width of  $0.50 \text{ \AA}$ . Long-range corrections have also been applied for the effects of cutoff and splining. Here, it should be pointed out that interactions between aluminum and oxygen atoms in alumina were described as non-bonded. Similarly, van der Waals (vdW) energy and Coulombic energy terms describe the interactions between atoms in the alkanes and those in the alumina surface. However, charges of the atoms in the alkane chains are ignored in simulation. Therefore, vdW energy is the only one accounted for the interactions between the normal alkanes and relaxed alumina surface.

Two explicit normal alkane models (i.e., hydrogen atoms were modeled explicitly), one consisted of 40 chains each with 11 backbone carbons ( $C_{11}$ ) while the other is a single chain of 200 backbone carbons ( $C_{200}$ ), were used in the present work. Using the experimental density of the normal alkanes at  $150 \text{ }^\circ\text{C}$  ( $423 \text{ K}$ ) ( $0.6396 \text{ (}C_{11}\text{) g/cm}^3$  and  $0.7706 \text{ (}C_{200}\text{) g/cm}^3$ ) [Doolittle, 1964], thin film initial structures were constructed in such a way that the simulation cells were periodic only in two

**Table 5-1** Functional forms used in the COMPASS force field [Sun, 1998]

Interaction		Equation
Valence terms	Bond energy	$E_b = \sum_b [k_2(b - b_0)^2 + k_3(b - b_0)^3 + k_4(b - b_0)^4]$
	Angle energy	$E_\theta = \sum_\theta [k_2(\theta - \theta_0)^2 + k_3(\theta - \theta_0)^3 + k_4(\theta - \theta_0)^4]$
	Torsion energy	$E_\phi = \sum_\phi [k_1(1 - \cos \phi) + k_2(1 - \cos 2\phi) + k_3(1 - \cos 3\phi)]$
	Out-of-plane angle	$E_\chi = \sum_\chi k_2 \chi^2$
	Cross-coupling terms	$E_{cross} = \sum_{b,b'} k(b - b_0)(b' - b_0') + \sum_{b,\theta} k(b - b_0)(\theta - \theta_0)$ $+ \sum_{b,\phi} (b - b_0)[k_1 \cos \phi + k_2 \cos 2\phi + k_3 \cos 3\phi]$ $+ \sum_{\theta,\phi} (\theta - \theta_0)[k_1 \cos \phi + k_2 \cos 2\phi + k_3 \cos 3\phi]$ $+ \sum_{\theta,\theta'} k(\theta' - \theta_0')(\theta - \theta_0)$ $+ \sum_{\theta,\theta',\phi} k(\theta - \theta_0)(\theta' - \theta_0') \cos \phi$
Nonbond terms	Coulombic interaction	$E_{coul} = \sum_{i,j} \frac{q_i q_j}{r_{ij}}$
	Van der Waals energy	$E_{vdW} = \sum_{i,j} \epsilon_{ij} \left[ 2 \left( \frac{r_{ij}^0}{r_{ij}} \right)^9 - 3 \left( \frac{r_{ij}^0}{r_{ij}} \right)^6 \right]$



**Table 5-2** Lennard-Jones parameters used to describe non-bonded interactions between various atomic species [Sun, 1998]

<i>i</i>	<i>j</i>	$\epsilon_{ij}$ (kJ/mol)	$r_{ij}^0$ (Å)
Al	Al	2.361	3.500
Al	O	1.480	3.566
Al	C	0.752	3.698
Al	H	0.405	3.261
O	O	0.936	3.627
O	C	0.485	3.749
O	H	0.238	3.354
C	C	0.259	3.854
C	H	0.113	3.526
H	H	0.096	2.878

dimensions (i.e.  $x$  and  $y$  directions here). It is worth noting that the density of the inner region of these thin films was equal to that of the corresponding bulk material and interfacial regions on both sides of the thin films with a width of less than 10 Å was present. Each thin film alkane model was assembled with a supercell of alumina surface slab with surface area of 313.82 Å<sup>2</sup> (lattice parameters a: 19.036 Å, b: 19.036 Å;  $\alpha$ : 90°,  $\beta$ : 90°,  $\gamma$ : 60°). It should be noted that similar results were obtained when systems with larger simulation cells were used and that the alkane thin film structures were energy minimized using a convergence criterion of 0.1 kcal/mol Å and equilibrated before they were assembled with the alumina surface slab. Figure 5-3(a) shows the resulting structure for C<sub>200</sub> above the supercell of alumina surface slab. Following the energy minimization, MD simulation was carried out at 150°C. As mentioned, the relaxation behavior of the alumina surface is much faster than that of the alkanes; therefore, atoms in the relaxed  $\alpha$ -Al<sub>2</sub>O<sub>3</sub> (0001) surface were fixed during the MD simulations. The Nose canonical method along with the velocity-Verlet algorithm and a time step of 1 fs was used for generating the MD trajectories [Allen and Tildesley, 1987]. Simulations were carried up to a time period as long as 18,000 ps to ensure the adequate equilibration of the alkane chains near the alumina surface. Different initial alkane conformations were used to test the reproducibility of the simulation.

The adsorption energy  $E_{ads}$  is defined as the energy difference between the system with a thin film of normal alkane chains in close contact with the relaxed alumina surface ( $E_{PE+surf}$ ) and the systems consisting of the alkane chains only  $E_{PE}$ ,

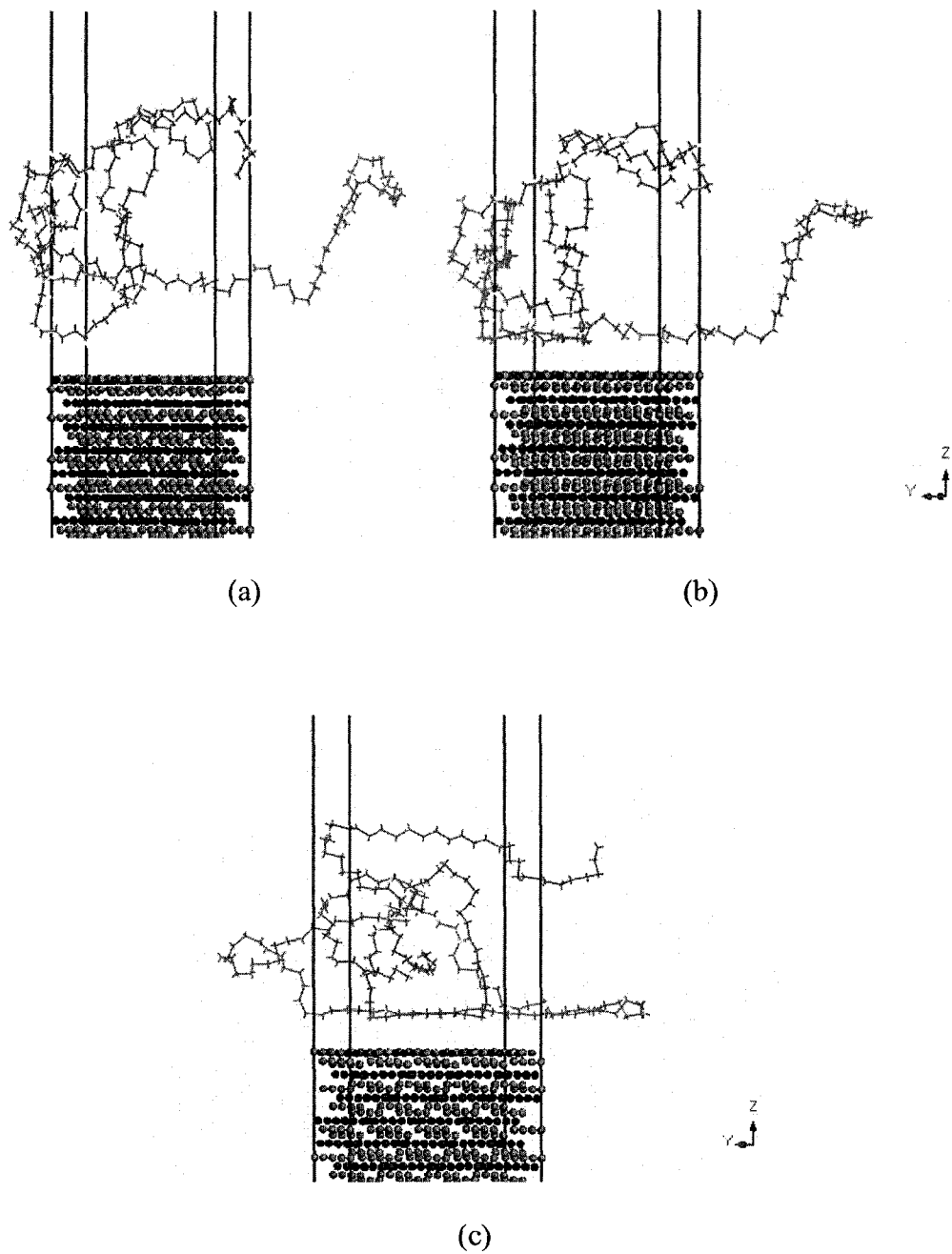


**Figure 5-3** Conformations of C<sub>200</sub> at different simulation time: (a) before energy minimization; (b) after energy minimization (0 ps); (c) 18,000 ps

and of a clean, relaxed alumina surface  $E_{surf}$  in their pure form [Lodziana *et al.*, 2004]:

$$E_{ads} = -E_{PE+surf} + E_{PE} + E_{surf} \quad (5-4)$$

## 5.3 Results and discussion

### 5.3.1 Relaxation of $\alpha$ -Al<sub>2</sub>O<sub>3</sub> (0001) surface

Structures of  $\alpha$ -Al<sub>2</sub>O<sub>3</sub> (0001) surface before and after relaxation are depicted in Figures 5-1(a) and 5-1(b), respectively. Similar to what earlier DFT studies showed [Hass *et al.*, 1998; Kodziana *et al.*, 2004; Delle Site *et al.*, 2002], it was observed that the outmost layer of Al atoms and the O atoms right underneath such a layer lie in nearly the same plane. Our calculated spacings in between the first six layers of atoms (4 Al layers and 2 O layers) were -90%, -1.2%, -45%, +20%, and +4.8% (see Figure 5-2(b)). Other research groups obtained similar simulation results. In particular, results of Lodziana *et al.* are -85%, +3.2%, -45%, +20%, and +4.8%, respectively [Lodziana *et al.*, 2004], and those of Hass *et al.* for the spacings in between the first five layers are -82%, +7%, -52% and +25%, respectively [Hass *et al.*, 1998]. Besides, review of calculated surface relaxations of  $\alpha$ -Al<sub>2</sub>O<sub>3</sub> (0001) surface could be found in Sun's paper [Sun *et al.*, 2006]. Comparison of UV photoelectron spectroscopy (UPS) and meta-stable impact electron spectroscopy (MIES) measurements showed that spacing between the first and second layers of the surface atoms ranges from -63% to -68% [Puchin *et al.*, 1997; Ahn and Rabalais, 1997]. It is worth noting that MIES techniques are only sensitive to the topmost

surface atoms. The discrepancy between the simulation and experimental results was attributed to the difficulty associated with preparing well defined alumina surfaces experimentally [Hass *et al.*, 1998]. Nevertheless, the important point here is that both computational and experimental results illustrate that surface atoms of  $\alpha - Al_2O_3$  (0001) surface do relax. This reinforces our belief that adsorption study should be done on a relaxed rather than unrelaxed surface.

The surface energy values calculated by DFT for slabs containing different numbers of repeat units are listed in Table 5-3. It can be seen from the table that the relaxed surfaces with six or more repeat units satisfy the convergence criterion of  $\Delta E_b < 0.05 eV$  [Ruberto *et al.*, 2003]. This means that a slab containing six or more repeat units (i.e., nine sub-layers of surface atoms on each side of the slab) would have structure of the repeat units in the interior of the slab that resembles to that of the bulk. However, to ensure a good description of the relaxation effect of the surface atoms on the adsorption behavior of normal alkanes, relaxed alumina slabs composed of ten repeat units were used in the subsequent MD calculations. The average surface energy averaging over the slabs with six to ten repeat units was determined to be  $1.40 J/m^2$ , which is slightly lower than the DFT results of Ruberto *et al.* ( $1.60 J/m^2$ ), which was also determined by averaging over up to 10 repeat units [Ruberto *et al.*, 2003]. We speculate that the difference in the computed average surface energy is attributed to the difference in the sizes of the systems used in respective groups.

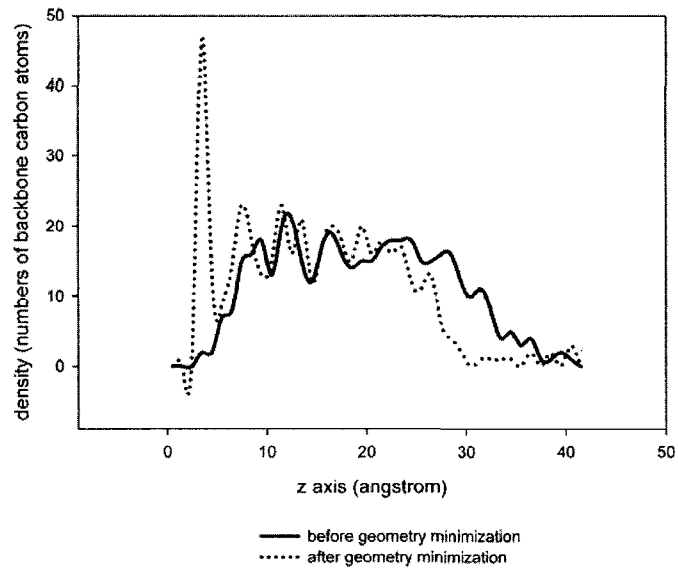
**Table 5-3** Computed surface energies of relaxed  $\alpha-Al_2O_3$  (0001) surfaces containing different numbers of repeat units by DFT calculations

$n$	$E_{cell}$ (eV)	$E_b$ (eV)	$\Delta E_b$ (eV)	$E_s$ (J/m <sup>2</sup> )
3	-4318.0600			
4	-5758.1752	-1440.1152		0.9323
5	-7198.5731	-1440.3979	-0.2827	1.3935
6	-8638.9837	-1440.4106	-0.0127	1.4194
7	-10079.3670	-1440.3833	0.0273	1.3526
8	-11519.7712	-1440.4042	-0.0209	1.4309
9	-12960.1811	-1440.4099	-0.0057	1.4309
10	-14400.5760	-1440.3949	0.0150	1.3758

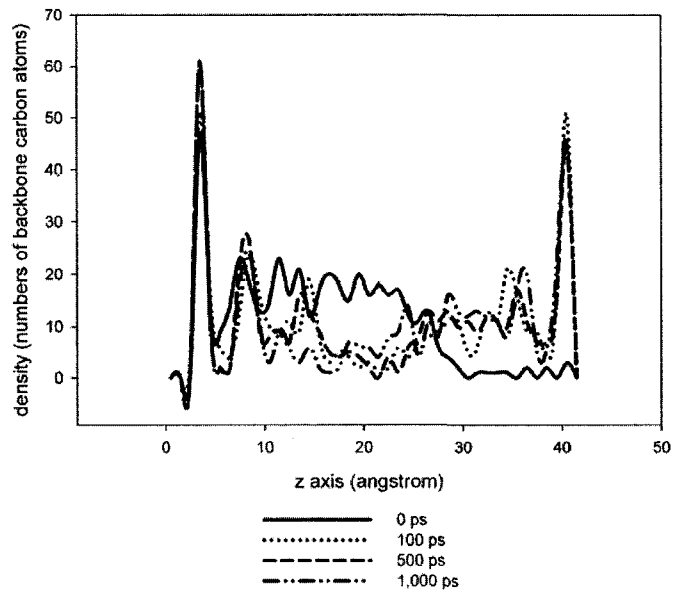
### 5.3.2 Adsorption behavior of normal alkanes ( $C_{11}$ and $C_{200}$ ) on relaxed $\alpha\text{-Al}_2\text{O}_3$ (0001) surface

It should be pointed out that prior to the MD simulations, chains in both  $C_{11}$  and  $C_{200}$  thin film models were pulled significantly towards the alumina surface during the energy minimization step. In particular, there were about 47 and 30 carbon atoms (the first adsorption layer) that were in direct contact with the relaxed surface for  $C_{11}$  and  $C_{200}$ , respectively. This is attributed to the fact that relatively strong van der Waals interaction exists between atoms of normal alkanes and surface atoms of alumina.

Figures 5-4 and 5-5 show the density profiles of both  $C_{11}$  and  $C_{200}$  over the durations of the respective simulations on the same relaxed alumina (0001) surface. It is clear that during the MD simulation, alkane chains (both  $C_{11}$  and  $C_{200}$ ) moved further towards the alumina surface. Specifically, numbers of backbone carbon atoms that formed the first nearest layer to the relaxed alumina surface increased from a value of 47 to 61 and from 30 to 41 for  $C_{11}$  and  $C_{200}$ , respectively. And layers of segments away from the surface also moved towards the surface with change of numbers of atoms involved. Examination of the time dependence of the density profiles of the alkane models shows that the layers of carbon atoms that are near the surface require less time to reach equilibrium number density values while the far ones moved slowly into a multi-layer structure. This is consistent with the fact that interactions between alkane atoms and alumina surface atoms are much stronger than those between atoms among the alkane chains [Claire *et al.*, 1997].



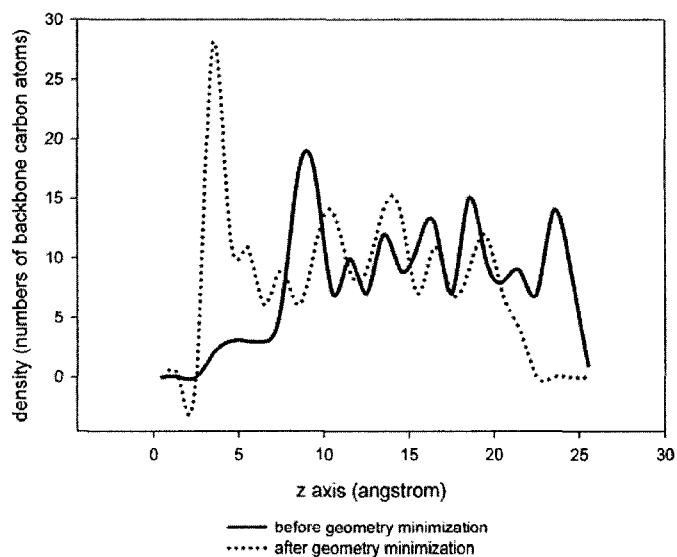
(a)



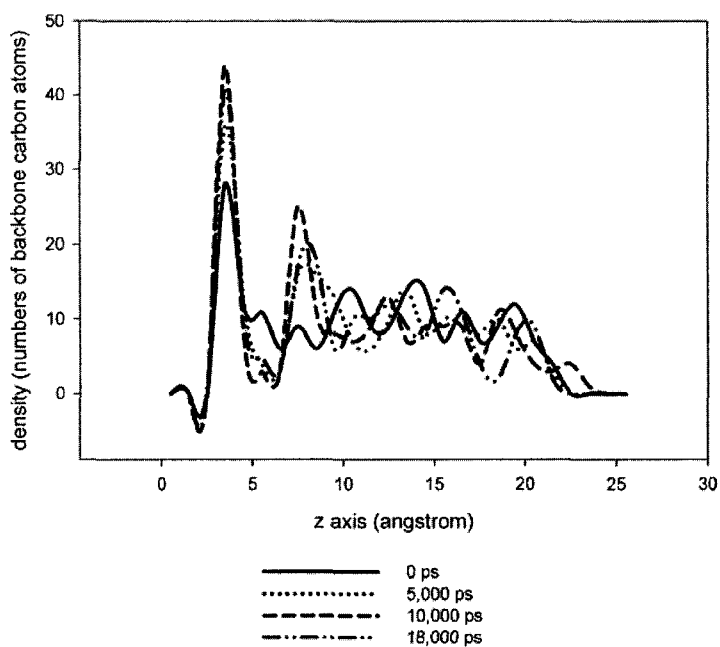
(b)

**Figure 5-4** Density distribution profile of  $C_{11}$  along the  $z$  direction ( $z$  being the direction perpendicular to the alumina (0001) surface) at different simulation times (423 K, relaxed surface): (a) before and after energy minimization; (b) at different simulation times: 0, 100, 500 and 1,000 ps





(a)

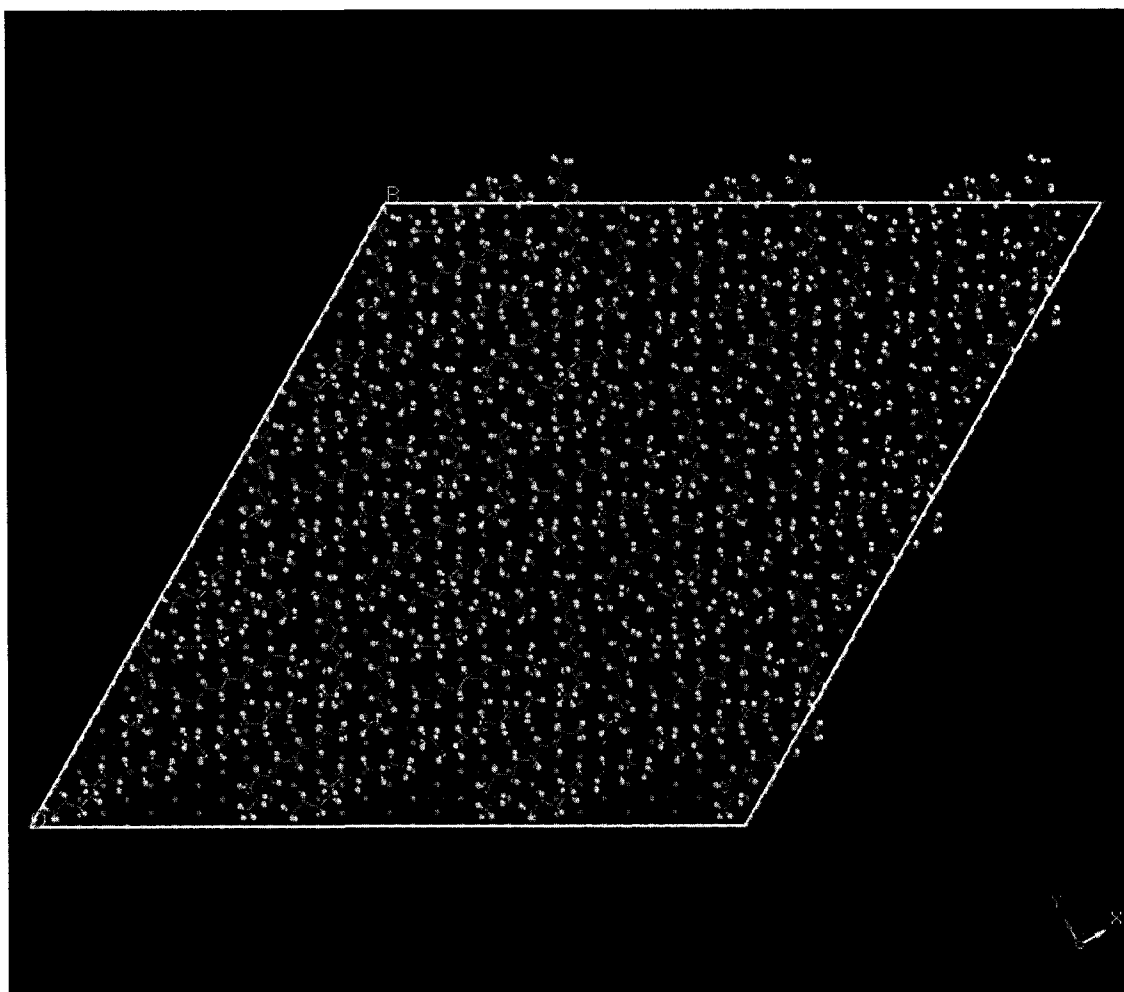


(b)

**Figure 5-5** Density distribution profile of  $C_{200}$  along the  $z$  direction ( $z$  being the direction perpendicular to the alumina surface) at different simulation times (423 K, relaxed surface): (a) before and after energy minimization; (b) at different simulation times: 0, 5,000, 10,000 and 18,000 ps

The separation between the first nearest layer of alkane chains and the outmost surface aluminum atoms is about 3.5 Å for both C<sub>11</sub> and C<sub>200</sub> cases. This result is exactly the same as what Claire *et al.* obtained for the interactions between an alumina surface and butane, octane and dodecane chains [Clair *et al.*, 1997]. This equilibrium separation is simply a result of the balance between repulsive and attractive vdW forces experienced by all the atoms involved in such an interfacial region. It should be noted that all the backbone carbon atoms in the first nearest layer adopt mostly *trans* conformation. However, what is interesting to note is that our simulation results show that the molecular planes of the adsorbed alkane segments prefer to orient parallel rather than perpendicular to the substrate surface, as shown in Figure 5-3, 5-6 and 5-7. Results of Claire *et al.*, for which they used united atom models and an unrelaxed alumina surface at a much lower temperature (100 K), showed perpendicular orientation [Clair *et al.*, 1997]. However, in the case of C<sub>11</sub>, a small fraction of molecular planes exhibited the perpendicular orientation. In general, if adsorbed segments adopt a configuration by which the molecular planes formed by the corresponding skeletal carbons are perpendicular to the surface, there will exist a peak splitting pattern with two peaks separated in the density profile [Gupta *et al.*, 1994]. Such a splitting peak feature was not observed in our data (see Figures 5-4 and 5-5).

As mentioned above, about 61 and 41 backbone carbon atoms for C<sub>11</sub> and C<sub>200</sub> were found to be involved in the first nearest layer to the substrate surface in their equilibrium state and no more atoms could enter this layer during the last portions of the MD simulations suggesting that a saturate adsorption density of alkane chains on



(a)

**Figure 5-6** Orientation of the molecular axes of the first adsorption layer of C<sub>11</sub>  
(image shown as 3×3 supercell of the original simulation cells)

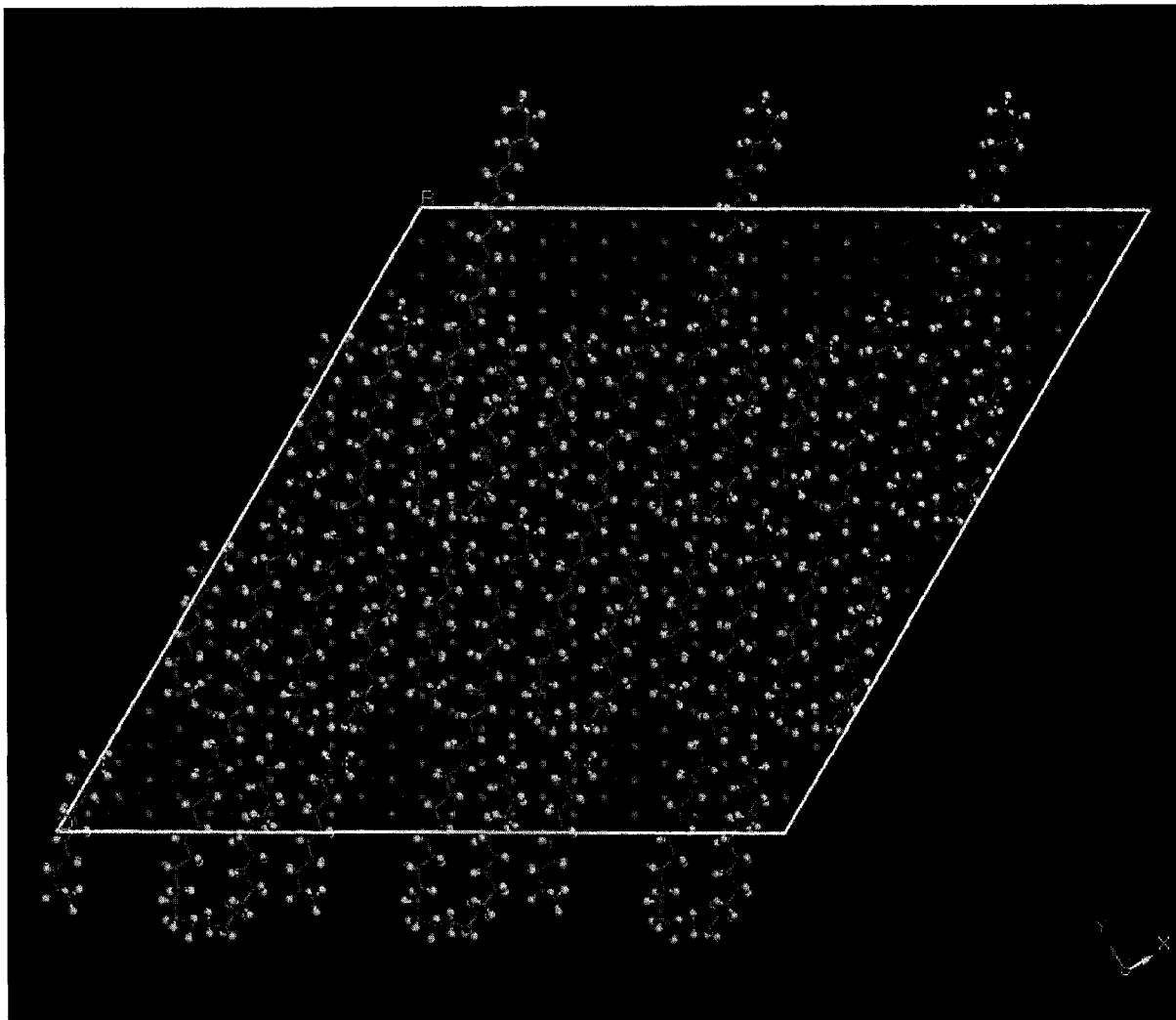


**Figure 5-7** Orientation of the molecular axes of the first adsorption layer of  $C_{200}$  (image shown as  $3 \times 3$  supercell of the original simulation cells): As shown the molecular axes of the adsorbed alkane segments tilt communally to a small angle with respect to the lattice boundaries in the substrate surface

the alumina surface may exist and that such a density value depends on the chain length. However, it is interesting to note that, for both  $C_{11}$  and  $C_{200}$ , the average distance between the skeletal carbons of two neighboring adsorbed segments and that between the first and second layers of the adsorbed segments is about 4.6 Å and 4.0 Å, respectively. These values are slightly lower than the corresponding intermolecular spacings, which are 4.8 Å and 4.2 Å, respectively, in alkane (octadecane) crystals as determined by x-ray diffraction at a much lower temperature (note that our simulation temperature was 423 K) [Rabe *et al.*, 1991]. This observation implies that the region that consists of the first two layers of adsorbed segments possesses a much higher density than that of the bulk to maximize the surface atoms interactions. Another interesting observation is about the position of the adsorbed backbone carbon atoms. The separation between an outmost surface aluminum atom and its secondary neighboring aluminum atoms in the same (0001) surface is found to be about 4.8 Å, which is comparable to the distance between two neighboring adsorbed segments in the first nearest layer (4.6 Å). A previous experimental study on the adsorption of alkane on a graphite surface by Rabe *et al.* showed that the distance between the second from the next carbon rows in graphite amounts to 4.26 Å and that the distance between two alkane segments with perpendicular orientation is about 4.2 Å [Rabe *et al.*, 1991]. These authors latter performed simulations and confirmed this orientation and proposed that it is the commensuration of the adsorbed alkane chains with the graphite substrate that results in the perpendicular orientation of the molecular planes of skeleton carbons relative to the graphite surface [Askin and Inel, 2001]. It seems that, in our case, the

commensuration of the adsorbed alkane segments (with explicit hydrogens) with the alumina (0001) surface induces the parallel orientation. Another observation was that the molecular axes of the adsorbed alkane segments seem to tilt communally to a small angle with respect to the lattice boundaries in the substrate surface (see Figure 5-7) which was not observed in the case when the alumina (0001) surface was not relaxed (will be presented in 5.3.4).

### 5.3.3 Adsorption energy of alkanes ( $C_{11}$ and $C_{200}$ )

Heats of adsorption of n-alkanes on alumina surface evaluated by inverse gas chromatography are 39.28, 46.02, 54.38, and 57.99  $kJ/mol$  for n-pentane, n-hexane, n-heptane, and n-octane, respectively [Askin and Inel, 2001]. Expressed in unit of per mole of  $CH_2$  group, the corresponding values are 7.86, 7.68, 7.77 and 7.25  $kJ/mol$ , respectively. Table 5-4 summaries our computed adsorption energies of  $C_{11}$  and  $C_{200}$  on the relaxed and unrelaxed  $\alpha-Al_2O_3(0001)$  surface. Comparing our computed value of 5.15  $kJ/mol \pm 0.07$  with the corresponding extrapolated value of 6.64  $kJ/mol$  for  $C_{11}$  based upon the aforementioned experimental values, the agreement is reasonably good considering the fact that the COMPASS force field is not optimized for these systems and that inverse gas chromatography measurements normally carry uncertainties of 3 to 5%. Nonetheless, the trend that the adsorption energy decreases with the increasing chain length of alkane was reproduced. We also carried out similar calculations using unrelaxed alumina surface (data also reported in Table 5-4) and found that differences in the adsorption energies between the relaxed and unrelaxed cases could differ up to 20%.

**Table 5-4** Computed adsorption energies of C<sub>11</sub> and C<sub>200</sub> adsorbed on relaxed and unrelaxed alumina (0001) surface

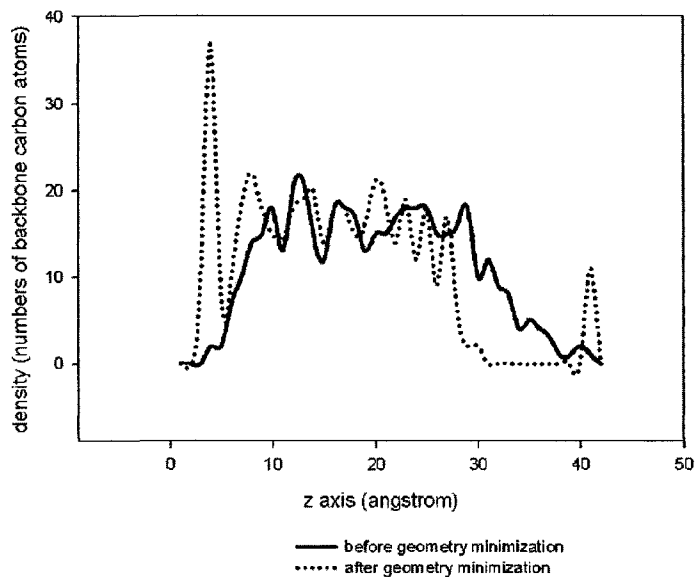
<b>Normal Alkane</b>	<b>Alumina surface</b>	<b>Adsorption Energy (kJ/mol)</b>	<b>Adsorption Energy per Mole of CH<sub>2</sub>, (kJ/mol)</b>
C <sub>11</sub>	Relaxed	2,264 ± 31	5.15 ± 0.07
	Unrelaxed	1,929 ± 32	4.38 ± 0.07
C <sub>200</sub>	Relaxed	919 ± 12	4.60 ± 0.06
	Unrelaxed	745 ± 26	3.73 ± 0.13

(presented in section 5.3.4) This is somewhat expected as locations of *Al* and *O* layers would determine the configuration of alkane molecules near the alumina surface, leading to differences in the interaction energies.

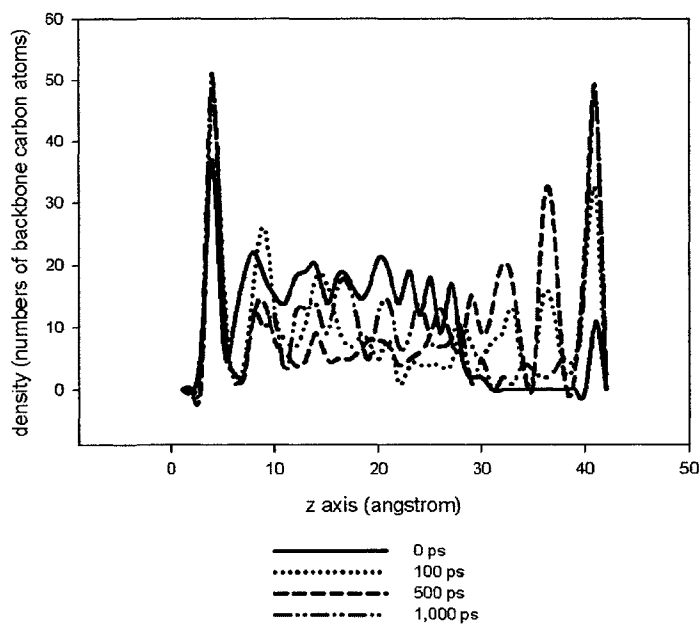
#### **5.3.4 Adsorption of normal alkanes ( $C_{11}$ and $C_{200}$ ) on unrelaxed $\alpha\text{-Al}_2\text{O}_3$ (0001) surface**

For comparison, simulation was also carried out to investigate adsorption behaviors of normal alkanes on unrelaxed  $\alpha\text{-Al}_2\text{O}_3$  (0001) surfaces with the same surface area. Figure 5-8(a) shows the density profiles of  $C_{11}$  system along the *z* direction before and after geometry minimization. After geometry minimization, large numbers of backbone segments moved towards to the substrate surface to constitute several adsorption layers. However, only about 37 backbone carbon atoms were found in the first adsorption layer, which was considerably less than 47 in the relaxed system. This might imply that the interactions between alkanes and unrelaxed alumina surfaces were not as strong as those between alkanes and relaxed alumina surfaces. The separation between the first nearest adsorption layer of alkane chains and the outmost surface aluminum atoms is about 3.5 Å, which is the same as the relaxed case. When MD simulations were carried out, as depicted in Figure 5-8 (b), about 51 backbone carbon atoms were obtained in the first adsorption layer after 1,000 ps, which was also less than the number of 61 in the relaxed case. However, comparing with the time evolution of numbers of backbone segments involved within various adsorption layers in the relaxed case (For instance, the time evolution of the first and second peaks as shown in Figure 5-4 (b)), it seems that alkane chains near the unrelaxed





(a)



(b)

**Figure 5-8** Density distribution profile of  $C_{11}$  along the  $z$  direction ( $z$  being the direction perpendicular to the alumina (0001) surface) at different simulation time (423 K, unrelaxed surface): (a) before and after energy minimization; (b) at different simulation times: 0, 100, 500 and 1,000 ps

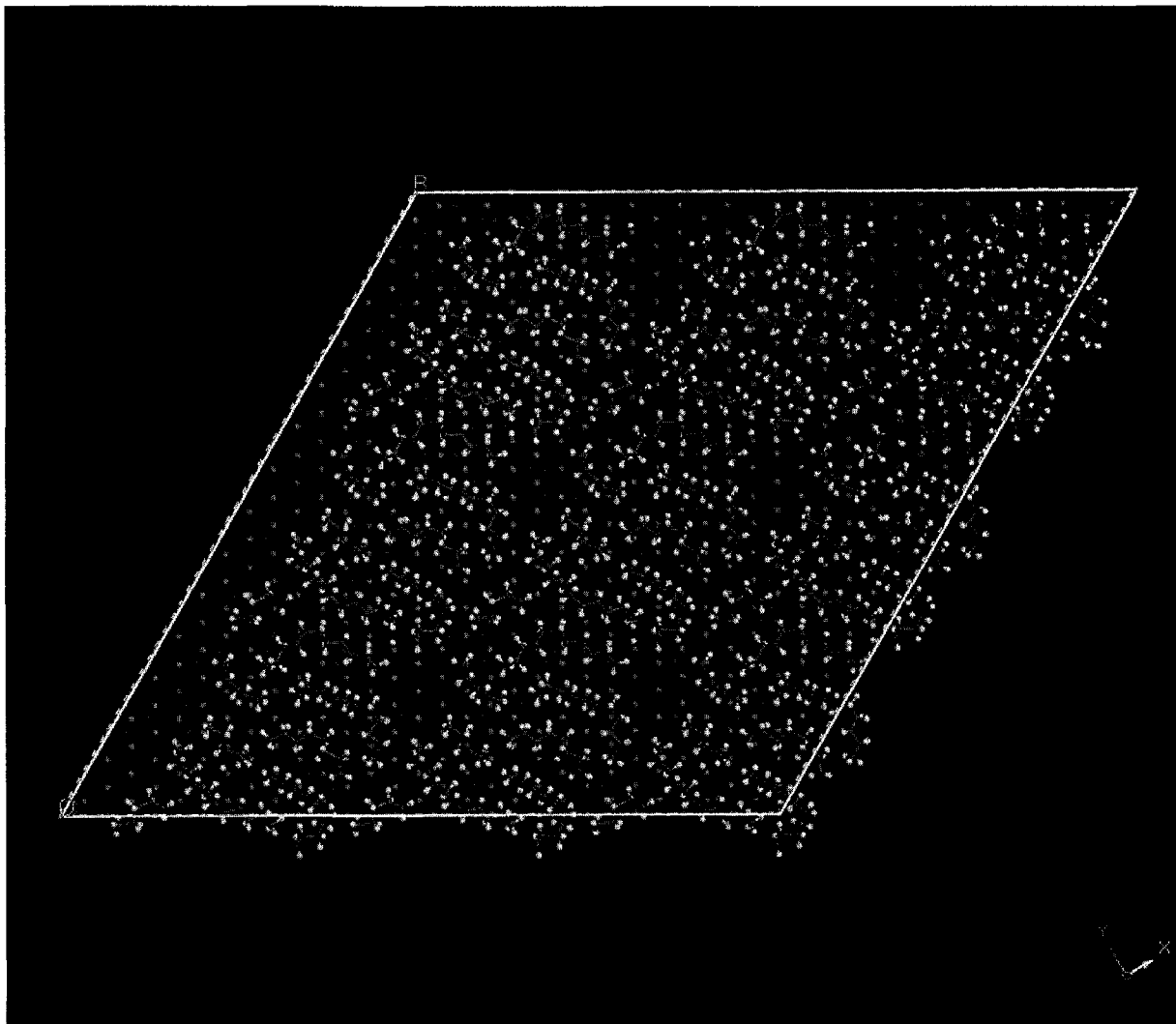


**Figure 5-9** Orientation of the molecular axes of the first adsorption layer of  $C_{11}$  at unrelaxed alumina surface at 423 K (image shown as  $3 \times 3$  supercell of the original simulation cells)

alumina surface need a longer time to move towards the surface to reach an equilibrium state. The orientation of the molecular axes of the first adsorption layer of  $C_{11}$  is shown in Figure 5-9. It can be seen that the molecular planes of some alkane segments are parallel to the substrate surface. The rest of the alkane segments were perpendicular to the alumina surface. The adsorption conformations of  $C_{11}$  above the unrelaxed alumina surface at low temperature (100 K) were also investigated in this research. Figures 5-10 and 5-11 present the density profile of the alkane chains after different simulation time intervals and the orientation of the molecular axes of the first nearest adsorption layer of  $C_{11}$  at 100 K, respectively. It is interesting that at temperature as low as 100 K, the alkane segments involved within the first adsorption layer are shorter than those at high temperature ones (423 K). This observation implies that at least some part of the molecular planes of the alkane chains adsorbed were perpendicular to the substrate surface. However, in this case, large fraction of molecular planes exhibiting the perpendicular orientation was still not observed as reported by Claire *et al.* [Claire *et al.*, 1997]. Besides, the adsorbed alkane segments were not well organized as those at high temperature.

When it comes to the  $C_{200}$  case, however, slightly different observations were obtained. First of all, about same numbers of backbone carbon atoms moved to the first adsorption layers of alkanes after geometry minimization (29 comparing with 30 in the relaxed case). Besides, 41 backbone carbon atoms were obtained after as long as 17,000 ps of molecular dynamics simulation, which is exactly the same comparing with the relaxed case. During the MD simulation, no obvious differences were found comparing with the time required for the alkane chains to

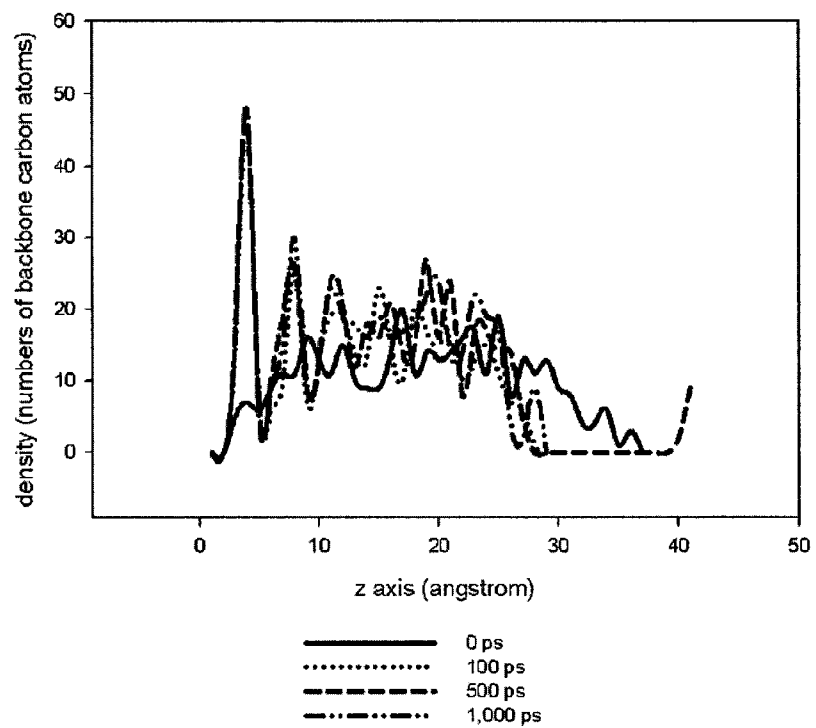


**Figure 5-10** Density distribution profile of C<sub>11</sub> along the z direction (z being the direction perpendicular to the alumina (0001) surface) at different simulation time (100 K, unrelaxed surface) at different simulation times: 0, 100, 500 and 1,000 ps

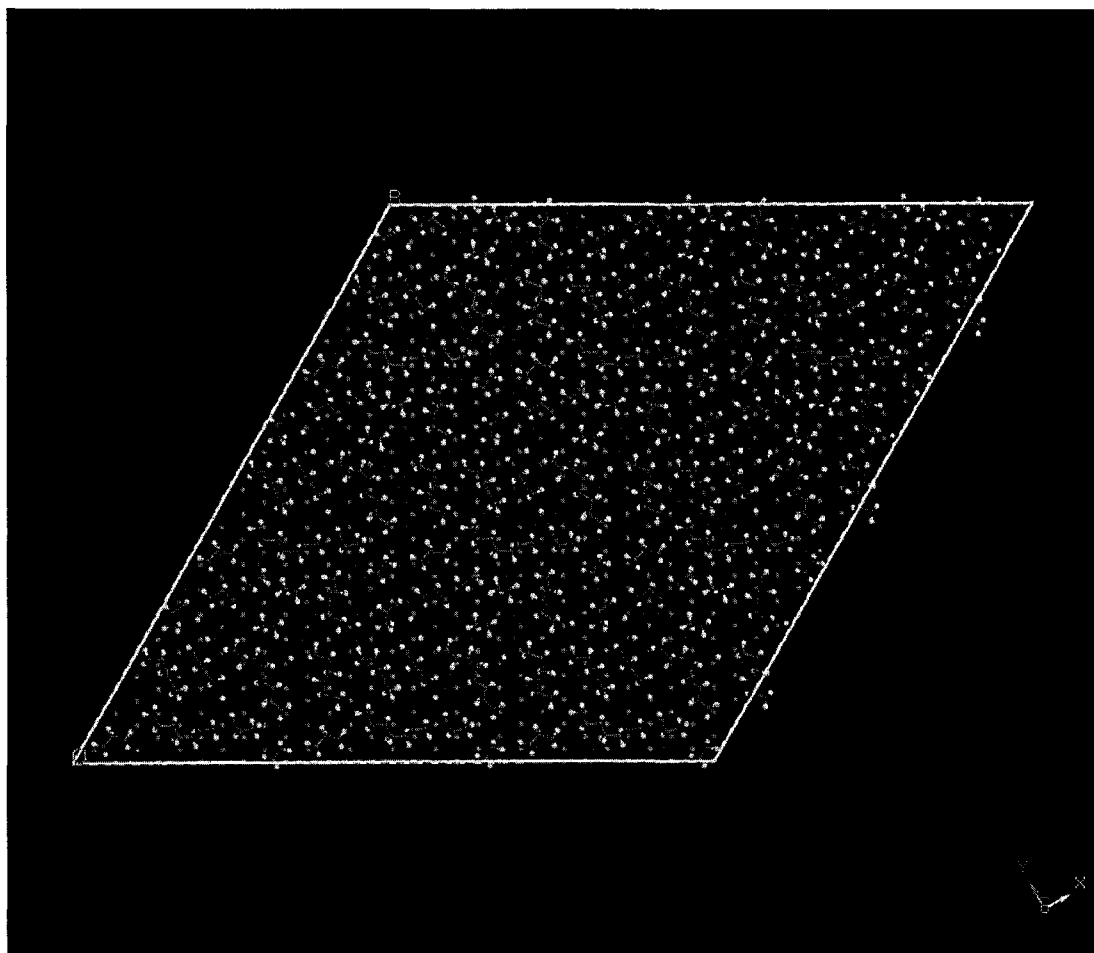
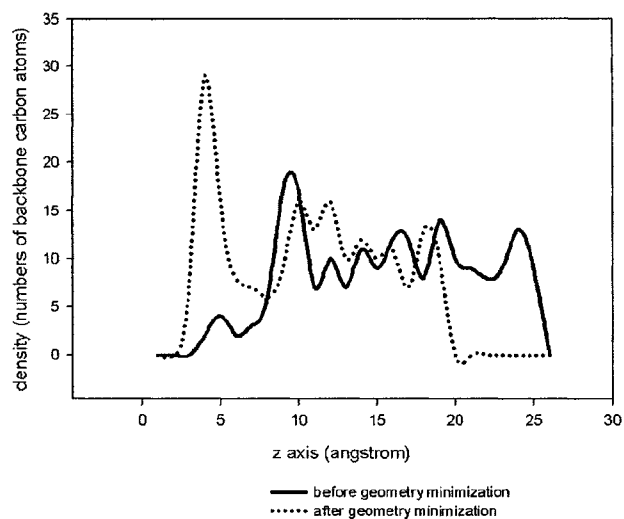
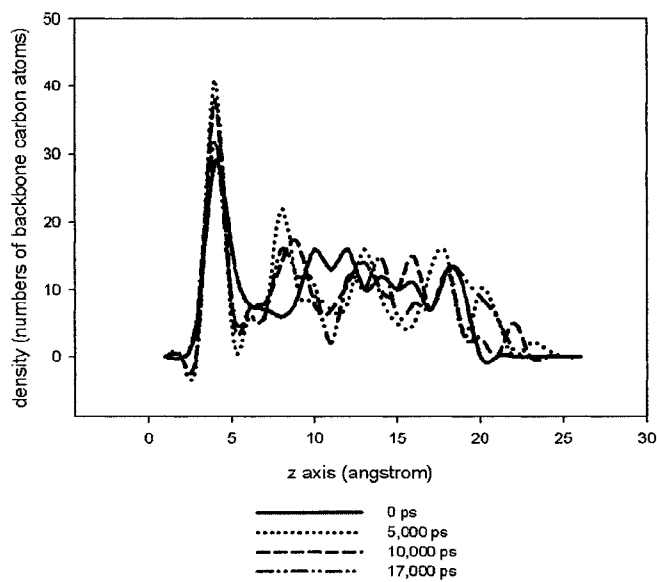


**Figure 5-11** Orientation of the molecular axes of the first adsorption layer of  $C_{11}$  at unrelaxed alumina surface at 100 K (image shown as  $3 \times 3$  supercell of the original simulation cells)



(a)



(b)

**Figure 5-12** Density distribution profile of  $C_{200}$  along the  $z$  direction ( $z$  being the direction perpendicular to the alumina (0001) surface) at different simulation time (423 K, unrelaxed surface): (a) before and after energy minimization; (b) at different simulation times: 0, 5,000, 10,000 and 17,000 ps

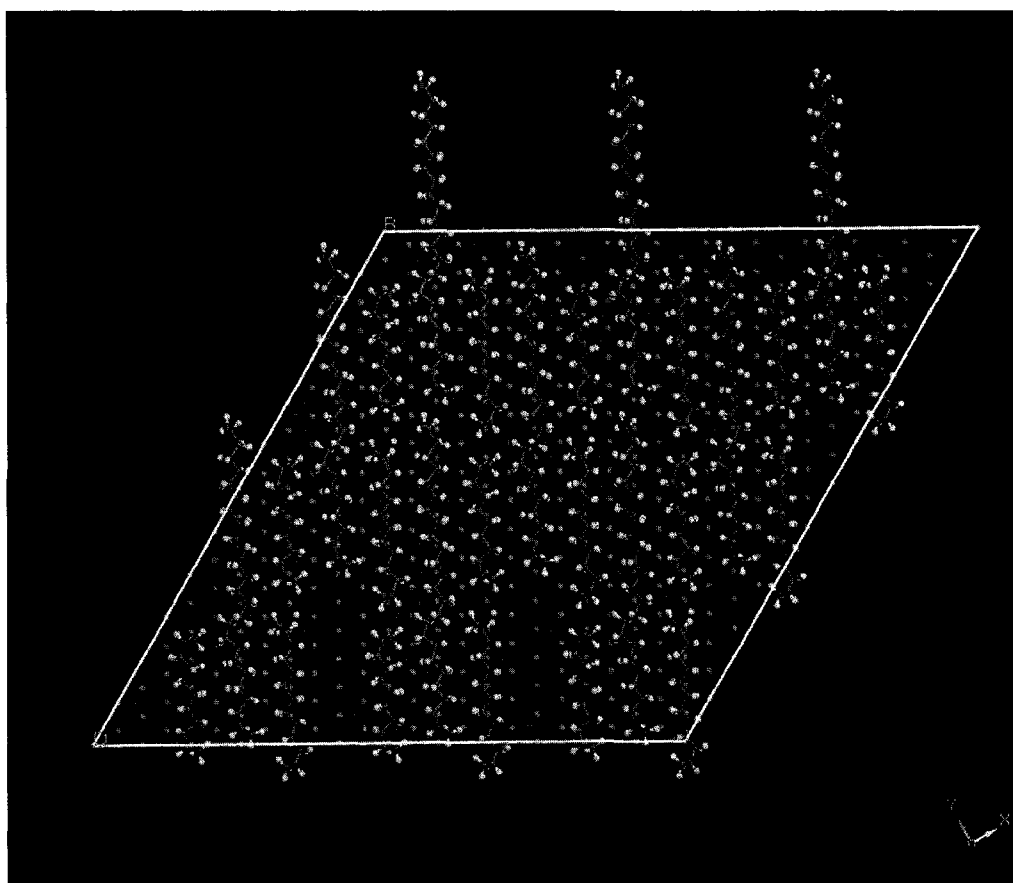


**Figure 5-13** Orientation of the molecular axes of the first adsorption layer of  $C_{200}$  (image shown as  $3 \times 3$  supercell of the original simulation cells) on unrelaxed alumina surface: As shown the molecular axes of the adsorbed alkane segments almost perpendicular to the lattice boundaries in the substrate surface

reach equilibrium above the relaxed and unrelaxed alumina surfaces (Figure 5-12). However, according to Figure 5-13, the molecular axes of the first adsorption layer of  $C_{200}$  on unrelaxed alumina surface are almost perpendicular to the lattice boundaries in the substrate surface.

Adsorption energies of normal alkanes on unrelaxed  $\alpha\text{-Al}_2\text{O}_3$  (0001) surface were calculated as  $4.38 \text{ kJ/mol} \pm 0.07$ ,  $5.23 \text{ kJ/mol} \pm 0.02$  and  $3.67 \text{ kJ/mol} \pm 0.13$  for  $C_{11}$  at 423 K and 100 K, and  $C_{200}$  at 423 K, respectively. Besides, the adsorption energy of  $C_{11}$  is  $5.90 \text{ kJ/mol} \pm 0.03$  for relaxed substrate surface at low temperature. It is found that higher values of adsorption energy are obtained when relaxations of the alumina surfaces are taken into account.

#### 5.4 Concluding remarks

Density functional theory (DFT) and classical molecular dynamics (MD) simulations were employed to investigate the behavior of two normal alkanes ( $C_{11}$  and  $C_{200}$ ) adsorbed on a relaxed alumina (0001) surface. DFT *ab initio* calculations were carried out first to fully relax the alumina surface and the positions of all the aluminum and oxygen atoms in the relaxed alumina (0001) surface were fixed during the subsequent classical MD simulation. For comparison, simulation was also carried out to investigate adsorption behaviors of normal alkanes on unrelaxed  $\alpha\text{-Al}_2\text{O}_3$  (0001) surfaces with the same surface area. It was found that relaxation of the alumina surface plays an important role in determining the configuration of the adsorbed alkane segments. Our simulation results show that molecular planes of the alkane segments in the first adsorption layer prefer to orient parallel rather than perpendicular to the substrate surface, which may be due to the commensuration of



the adsorbed alkane segments with the aluminum atom rows in the substrate surface. Also, the molecular axes of the adsorbed alkane segments seem to tilt communally to a small angle with respect to the aluminum atom rows. The adsorption energies were calculated to be  $5.15 \text{ kJ/mol}$  and  $4.60 \text{ kJ/mol}$  per  $\text{CH}_2$  group for  $\text{C}_{11}$  and  $\text{C}_{200}$ , respectively.

## Chapter 6 Effect of Solvent Adsorption on the Morphology of Glycothermally Produced $\alpha$ - $Al_2O_3$ Particles

### 6.1 Introduction

Morphological control of monodisperse, anisotropic single crystals of metal oxides has been an important issue in the materials industry during the past couple decades.  $\alpha$ -alumina is one of the metal oxides most widely used in applications such as catalysis, microelectronics, lasers, optics, and refractories, etc [Adair *et al.*, 2001]. Conventional synthesis methods of  $\alpha$ -alumina particles involve thermally activated solid-state processes. The precursor materials composed of aluminum hydroxide transform to  $\alpha$ -alumina phase by calcination at a temperature of at least 950 °C [Kumagai and Messing, 1985; McArdle and Messing, 1986; McArdle and Messing, 1987]. Synthesis methods based on hydrothermal and glycothermal approaches improve the processing environment by lowering the reaction temperature and pressure down to about 300 °C and 4 MPa and therefore have made some fundamental studies on the morphological control of  $\alpha$ -alumina particles possible [Li *et al.*, 1999; Li *et al.*, 2000; Inoue, 2004].

The growth habit of metal oxide crystals, especially the relative growth rates of various crystal faces bounding the crystal, plays an important role in determining the

---

Another version of this chapter has been submitted as **Chunli Li** and Phillip Choi, Molecular Dynamics Study on the Effect of Solvent Adsorption on the Morphology of Glycothermally Produced  $\alpha$ - $Al_2O_3$  Particles, to *the Journal of Physical Chemistry C*, Oct 17, 2007

final morphology of the resultant particles. The growth habit of crystals is determined both by the internal structure factors of a given crystal and by the external conditions such as temperature, super-saturation, solution composition, etc [Adair *et al.*, 2001]. Early theoretical models attempting to predict crystal growth habits include the Bravais-Friedel theory, the morphological theory of Donnay and Harker, and of Hartman and Perdok (the so-called PBC theory) [Griedel, 1905; Donnay and Harker, 1937; Hartman and Oerdok, 1955]. However, these models put most of the emphasis on the internal structure factors of a given crystal and disregard the effects of external crystallization conditions. Therefore, the growth habits predicted by these theories are generally not in good agreement with experiment. The more recent Hartman-Bennema theory, developed in the eighties of the last century, incorporates the influences of super-saturation, crystallization mechanism and adsorbates by relating the growth habit of a crystal to the attachment energy of a particular habit plane, which is defined as the energy per molecule released when a layer of material crystallizes onto a crystal face [Harman and Bennema, 1980a]. They found that the relative growth rate of a crystal face always increase with increasing attachment energy. However, comparison between the prediction of their theory and the observed morphology of single  $\alpha$  -alumina crystals grown under hydrothermal conditions particles shows poor agreement. Hartman and Bennema attributed the discrepancy to the fact that other external factors (e.g. adsorption of solvent) were not taken into account in their model [Harman and Bennema, 1980b].

Recently, Li *et al.* presented new rules of the growth habit of metal oxide crystals based on the study of growth mechanism of such crystals in hydrothermal or

glycothermal conditions [Li *et al.*, 1999]. Their rules correlated the growth rates of various crystal faces to the element of which coordination polyhedron is present at the interface. Based upon their rules, they calculated the growth habit of  $\alpha$ -alumina and found that it is platy (001), and the ranking of the growth rates of different crystal faces are:  $V_{\langle 001 \rangle} < V_{\langle 113 \rangle} < V_{\langle 012 \rangle} < V_{\langle 110 \rangle}$  [Li *et al.*, 2000]. They concluded that the results are in good agreement with the observed results of hydrothermal experiments. However, effects of external conditions such as adsorption of solvent, stirring speed were not considered.

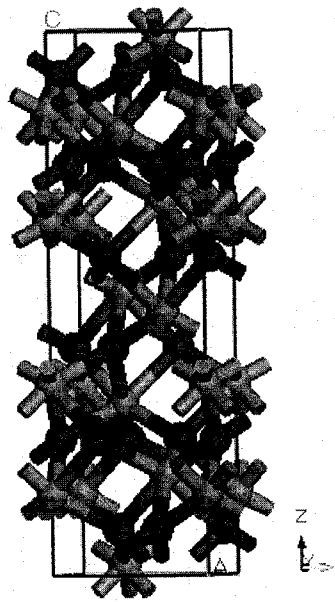
There exist some work in the literature that a few researchers focused on studying the influence of various external factors on the morphology of metal oxide particles under specific controlled experimental reaction conditions [Adair, *et al.*, 2001; Bell and Adair, 1999; Adair and Suvaci, 2000]. In a review of Adair *et al.*, effects of reaction conditions in glycothermal synthesis process of  $\alpha$ -alumina particles such as reaction time, stirring speed, solid loading, and the addition of methanol were discussed in detail [Adair *et al.*, 2001]. For example, it was shown that under the conditions of low stirring speed and without the presence of methanol, (001), (110) and (113) planes are three well developed crystal faces formed during the synthesis process. (012) and (102) crystal faces emerge at long reaction time or moderate and high stirring speeds.

It is generally recognized that interactions between crystal faces and adsorbates (i.e., solvent and other additives) play an important role in determining the morphology of  $\alpha$ - $Al_2O_3$  particles [Bell and Adair, 1999; Sohnle and Garside, 1993]. In particular, Kuznetsov utilized alkali mineralizers and high temperatures

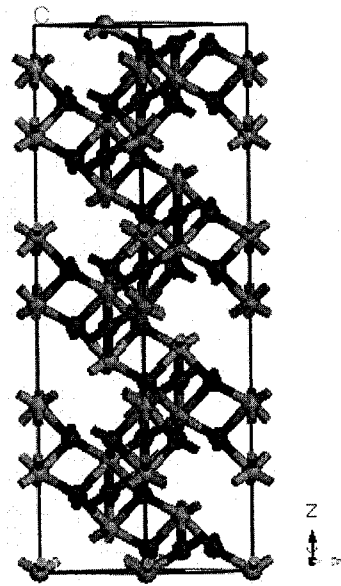
(600 °C ) to measure growth rates of  $\alpha$  -alumina particles [Kuznetsov, 1964; Kuznetsov, 1965; Kuznetsov, 1971]. They proposed that during the hydrothermal synthesis process, rate-limiting steps are linked to the surface chemical structure. And adsorption kinetics and the dehydration of crystal faces dominate the growth process. Bell and Adair investigated the effect of adsorbate on the morphology of glycothermally produced  $\alpha$  -alumina particles [Bell and Adair, 1999]. They concluded that in the absence of specific adsorbates, surfaces of alumina crystals must be dominated by the adsorption of the solvent used in the reaction. However, the authors did not carry out further work to quantitatively investigate the role of solvent during the synthesis process. To this end, we used a conventional method so-called MD simulation to study the interactions between adsorbed solvent molecules and various  $\alpha$  - alumina crystal faces quantitatively. The objective is to explore the correlation between the adsorption of solvent and the growth habit of  $\alpha$  -alumina particles synthesized in a 1, 4-butanediol solution.

## 6.2 Simulation models and methods

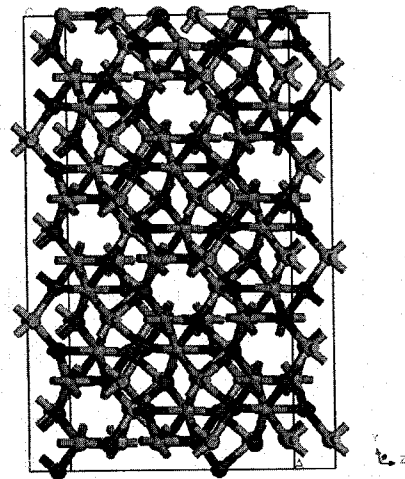
Figure 6-1(a) shows the bulk crystal structure of alumina, which was obtained from the model libraries of commercial software Material Studio [Ruberto *et al.*, 2003]. The crystal is composed of “sandwich” like non-polar layers of aluminium and oxygen atoms. Here, each electrically neutral layer contains three sub-layers in which a sub-layer of oxygen atoms is sandwiched by two sub-layers of aluminium atoms. Several alumina crystal faces of interest (i.e., (001), (010), (012), (102), (110), (111)



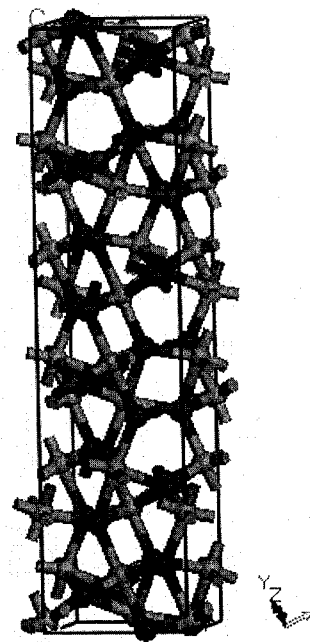
(a)



(b)



(c)



(d)

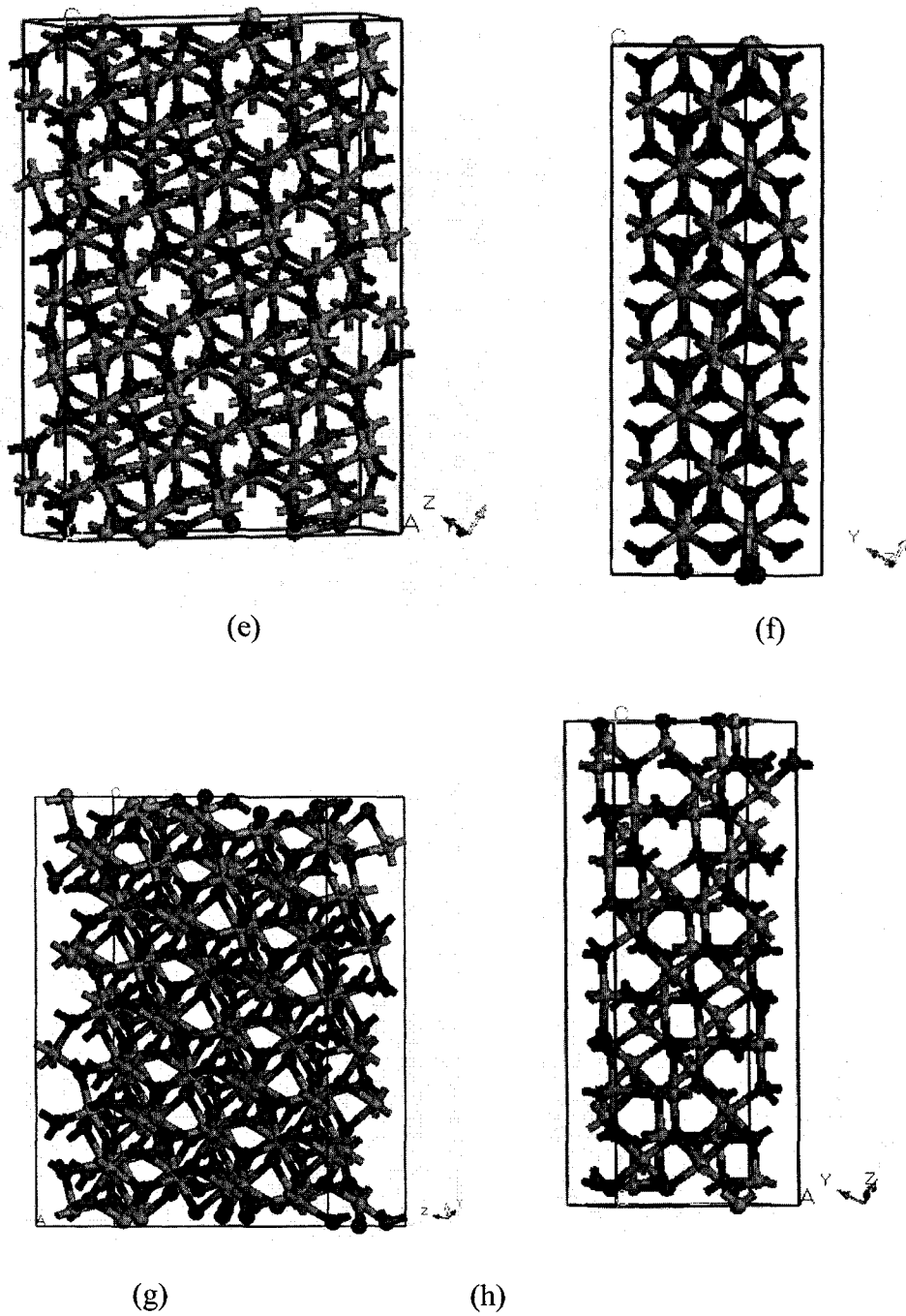


**Figure 6-1** Structure of bulk alumina crystal and slabs of cleaved  $\alpha$ -alumina crystal faces (a) bulk crystal; (b) (001) face; (c) (010) face; (d) (012) face; (e) (102) face; (f) (110) face; (g) (111) face; (h) (113) face

and (113)) were created by cleaving the aforementioned bulk structure through the corresponding planes and the resultant structures are depicted in Figures 6-1(b) to (h). Similar to the bulk crystal structure (no surfaces), these cleaved alumina crystal slabs (two free surfaces) were also subjected to three dimensional periodical boundary conditions. The thickness of each cleaved crystal slab was chosen such that its total charge of the slab should be zero and that when it is assembled with a thin film of 1, 4-butanediol molecules, the influence of 1, 4-butanediol molecules in the neighboring cells, especially those cells in the normal direction of the slab, is minimized. The thicknesses of  $\alpha - Al_2O_3$  slabs with two free surfaces are listed in the fourth column (i.e., cell parameter  $c$ ) in Table 6-1. It is worth noting that such cleaved surfaces were not subjected to any relaxation to correct the inter-layer spacings before they were assembled with the 1, 4-butanediol film. It is obvious that during the crystal face growth process, inter-layer spacings, especially those layers near the surface, would change as the next layer of growth unit is deposited onto them. Considering the fact that simulating such a dynamic process is computationally intensive (DFT calculations are needed) and that the inter-layer spacings might adopt the equilibrium values quickly, we feel justified to use the equilibrium crystal spacings for the surface atoms in the classical MD simulations. Nonetheless, the atomic charges of the aluminium and oxygen atoms in each slab were computed using the DFT based upon a procedure suggested by Roberto *et al.* and were determined to be 2.775 and -1.85  $e$ , respectively.

All MD simulations were carried out using the Discover module in Materials Studio along with the use of the COMPASS force field. The COMPASS



**Table 6-1** Unit cell parameters of  $\alpha$ -alumina slabs with two free surfaces generated by cleaving the  $\alpha$ -alumina crystal at various cleavage planes

<b>Crystal face</b>	$a$ $^{\circ}$ ( $\text{Å}$ )	$b$ $^{\circ}$ ( $\text{Å}$ )	$c$ $^{\circ}$ ( $\text{Å}$ )	$\alpha$ (degrees)	$\beta$ (degrees)	$\gamma$ (degrees)
(001)	4.759	4.759	21.167	90.000	90.000	60.000
(010)	12.991	4.759	20.494	90.000	90.000	90.000
(012)	4.759	5.128	19.530	90.000	90.000	90.000
(102)	15.385	4.759	21.780	90.000	90.000	90.000
(110)	6.996	5.128	20.687	90.000	90.000	95.844
(111)	8.243	13.835	20.174	90.000	90.000	107.331
(113)	8.243	5.128	21.663	90.000	90.000	105.538

force field is an *ab initio* force field optimized for condensed-phase applications. Previous simulation results of other researchers have shown that it can make accurate predictions of structural, conformational, cohesive and other physical properties for a broad range of molecules [Sun, 1998]. The functional forms used in this force field are presented in Table 5-1. The functions include two categories of energy terms – valence terms which include diagonal and off-diagonal cross-coupling terms, and non-bonded interaction terms. As can be seen from the table, a large quantity of parameters were used for different types of atoms involved in this research, and for clarity these parameters are not listed here. However, such parameters can be readily found from Sun’s article [Sun, 1998]. The COMPASS force field was validated by calculating the solubility parameter and self-diffusion coefficient of 1, 4-butanediol and comparing them with the corresponding experimental values. In this regard, three-dimensional periodic simulation cells with 100 1, 4-butanediol molecules were constructed to simulate the condensed states of the solvent. The simulation cells were subjected to the experimental density of 1, 4-butanediol at 25 °C [Sun, 1992]. Energy minimizations were performed on the systems before respective canonical (i.e., NVT) MD simulations were carried out at the same temperature for 1 nanosecond. The canonical MD trajectory was created using the velocity Verlet algorithm along with the Nose method with a time step of 1 femtosecond [Nose, 1984a].

A free standing thin film of 1, 4-butanediol containing 200 molecules was initially constructed with a bulk density value of  $0.7306 \text{ g/cm}^3$  at 4 MPa and 300 °C (conditions commonly used in the synthesis of  $\alpha - \text{Al}_2\text{O}_3$  particles). The density was

determined by using the Compostizo method [Compostizo *et al.*, 2005; Panayiotou and Sanchez, 1991]. The thin film had a nominal thickness of  $34.5 \text{ \AA}$ . Upon energy minimization using the COMPASS force field, the thin film and the alumina slab were assembled together. However, before the assembling process, dimensions of the alumina slabs and 1, 4-butanediol thin film were adjusted in such a manner that the lattice parameters of the two layers match with each other. The unit cell parameters of alumina slabs with different cleavage planes are presented in Table 6-1. The structure with the surface slab as the first layer and the 1, 4-butanediol molecules as the second layer was then constructed. The dimensions of the rearranged simulation cells ( $\alpha - Al_2O_3$  slab + solvent layer) are presented in Table 6-2. The total system was energy minimized again and then canonical MD simulations were carried out at 573.15 K for 100 picoseconds using the velocity Verlet algorithm and Nose thermostat. The table also shows the thickness of each simulation cell. MD simulations were also carried out for another set of rearranged cells with the same thickness of solvent layer ( $58 \text{ \AA}$ ) above various crystal faces. Table 6-3 depicts the parameters of these cells and the numbers of solvent molecules involved in each cell.

At the outset of the MD simulation of the systems shown in Tables 6-2 and 6-3, bonds between aluminium and oxygen atoms were removed manually due to the ionic nature of alumina crystal [Accelrys, 2004]. Therefore, interactions between aluminium and oxygen atoms and between  $\alpha - Al_2O_3$  surface atoms and solvent molecules are expressed as non-bonded energies. The van der Waals interaction was

**Table 6-2** Unit cell dimensions of the rearranged simulation cells ( $\alpha$ -alumina slab + solvent confined layer) and thicknesses of solvent layers with 200 1, 4-butanediol molecules sandwiched between  $\alpha$ -alumina free surfaces

<b>Crystal face</b>	$a$ ( $\text{\AA}$ )	$b$ ( $\text{\AA}$ )	$c$ ( $\text{\AA}$ )	$\alpha$ (degrees)	$\beta$ (degrees)	$\gamma$ (degrees)	<b>Thickness of solvent layers</b> ( $\text{\AA}$ )
(001)	28.554	28.554	77.124	90.000	90.000	60.000	58.00
(010)	25.982	23.792	83.748	90.000	90.000	90.000	63.25
(012)	28.554	25.642	68.528	90.000	90.000	90.000	55.93
(102)	30.771	23.795	69.735	90.000	90.000	90.000	55.93
(110)	27.985	25.642	75.833	90.000	90.000	95.844	57.37
(111)	24.729	27.671	81.586	90.000	90.000	107.331	62.70
(113)	24.728	25.642	85.844	90.000	90.000	105.538	67.04

**Table 6-3** Dimensions of the rearranged simulation cells (alumina surface + solvent confined layers) and the number of solvent molecules used in the solvent layer with a fixed thickness of  $58 \text{ \AA}$  for each system

<b>Crystal face</b>	$a$ ( $\text{\AA}$ )	$b$ ( $\text{\AA}$ )	$c$ ( $\text{\AA}$ )	$\alpha$ (degrees)	$\beta$ (degrees)	$\gamma$ (degrees)	<b>Number of solvent molecules</b>
(001)	28.554	28.554	77.124	90.000	90.000	60.000	200
(012)	28.554	25.642	70.598	90.000	90.000	90.000	207
(102)	30.771	23.795	71.805	90.000	90.000	90.000	207
(110)	27.985	25.642	76.463	90.000	90.000	95.844	202
(113)	24.728	25.642	76.804	90.000	90.000	105.538	231

calculated using atom-based summation with a cut-off distance of  $9.5 \text{ \AA}$  along with a spline width of  $1.00 \text{ \AA}$ , and a buffer width of  $0.50 \text{ \AA}$ . The Coulombic interaction was calculated using the Ewald summation method, with calculation accuracy of 0.01 kcal/mol, and an update width of  $1.00 \text{ \AA}$ . Partial atomic charges on each atom on 1, 4-butanediol were determined using the charge equilibration method [Rappé and Goddard, 1991]. Unlike other force fields, the COMPASS force field does not contain an explicit hydrogen bond term. The hydrogen bond interactions are included in the non-bonded Columbic term. To prevent the vaporization of solvent molecules, there is no vacuum above the solvent layer (as the simulation model in Chapter 5); therefore, one periodical image of the alumina substrate crystal face is directly positioned above the solvent layer.

The adsorption energy  $E_{ads}$  of 1, 4-butanediol solvent molecules on an  $\alpha - Al_2O_3$  crystal face is defined as the energy difference between the system with a thin film of 1, 4-butanediol molecules in close contact with the alumina surface ( $E_{solv+surf}$ ) and the individual isolated systems of 1, 4-butanediol molecules  $E_{solv}$ , and of a clean alumina surface  $E_{surf}$  [Lodziana *et al.*, 2004]:

$$E_{ads} = -E_{solv+surf} + E_{solv} + E_{surf} \quad (6-1)$$

For another set of systems, 20 methanol molecules were added to the system with 200 1, 4-butanediol solvent molecules to investigate the effects of the addition of methanol on the growth control of alumina crystals. Simulations for these systems

were also carried out at 573.15 K. Density of the solvent mixture were calculated to be  $0.7290 \text{ g/cm}^3$ , by simply using the linear combination of the densities of two pure substances under 573.15 K and 4 MPa.

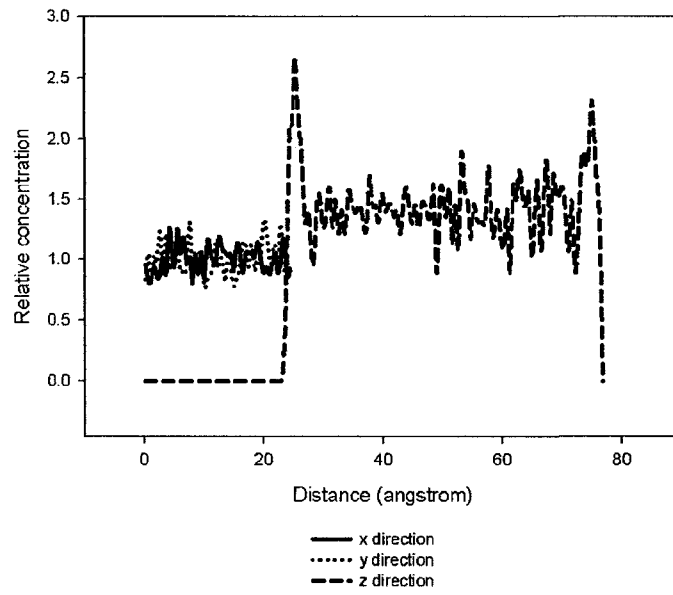
## **6.3 Results and discussion**

### **6.3.1 Validation of the COMPASS force field**

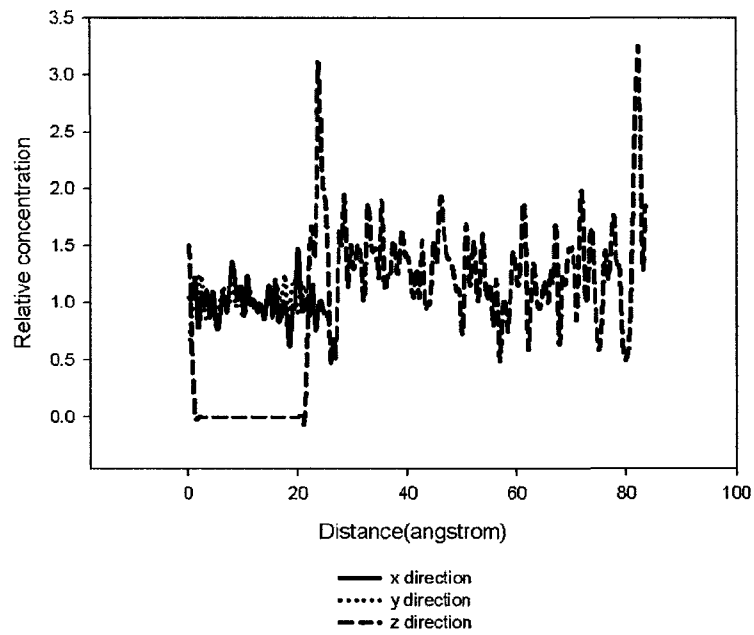
In the present work, the Hildebrand solubility parameter and self-diffusion coefficient of pure 1, 4-butanediol at  $25 \text{ }^\circ\text{C}$  were calculated to be  $30.1 \pm 0.2 (\text{J/cm}^3)^{1/2}$  and  $1.27 \times 10^{-11} \text{ m}^2/\text{s}$ , respectively. The computed Hildebrand solubility parameter is in good agreement with the reported range of the Hildebrand solubility parameter of 1, 4-butanediol ( $24.7 - 33.7 (\text{J/cm}^3)^{1/2}$ ) [Barton, 1991]. On the other hand, no experimental value for the self-diffusion coefficient of 1, 4-butanediol was available. However, it was reported that the diffusion coefficient of 1, 4-butanediol in an infinite diluted aqueous solution is  $9.05 \times 10^{-10} \text{ m}^2/\text{s}$ , and it decreases quickly with the increasing concentration of 1, 4-butanediol [Lyons and Sandquist, 1953; Yans, 1995], suggesting that our computed self diffusion coefficient may be comparable to the true value.

### **6.3.2 Adsorption of solvent molecules**

Figure 6-2 depicts the relative concentration profile (i.e., the ratio of the concentration of a given slice of 1, 4-butanediol molecules to that of the middle slice in the solvent layer) of 200 solvent molecules in  $x$ ,  $y$  and  $z$  directions on various alumina crystal faces after the 100 ps MD annealing. Note that some of the systems were reoriented

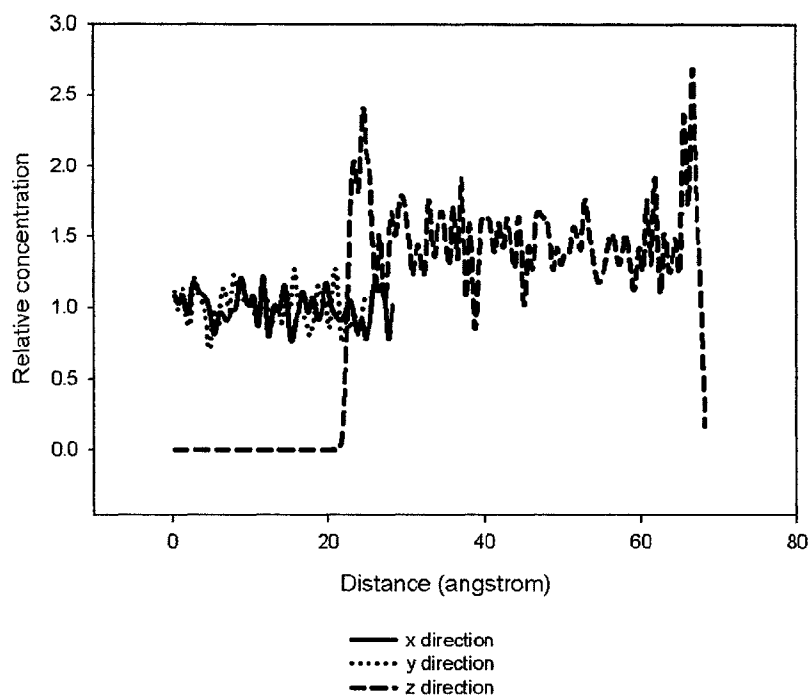


(a)

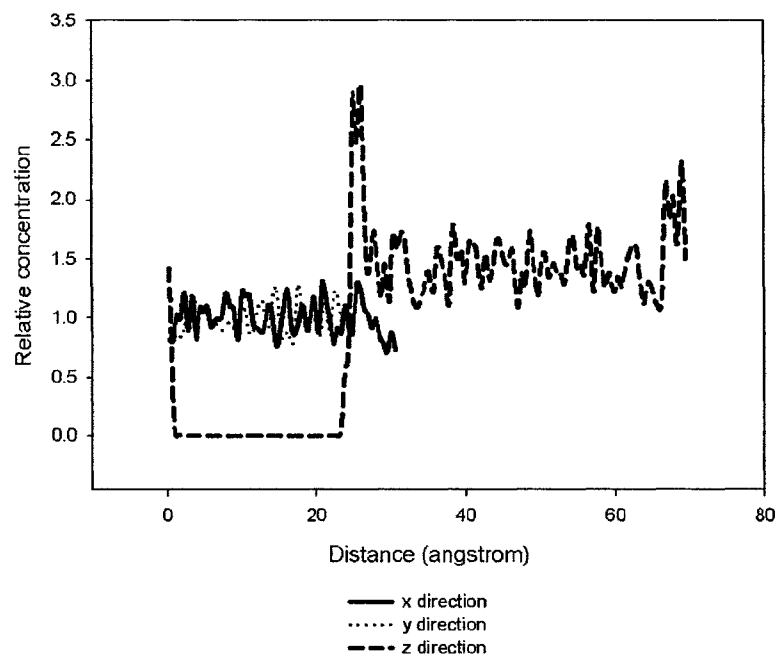


(b)

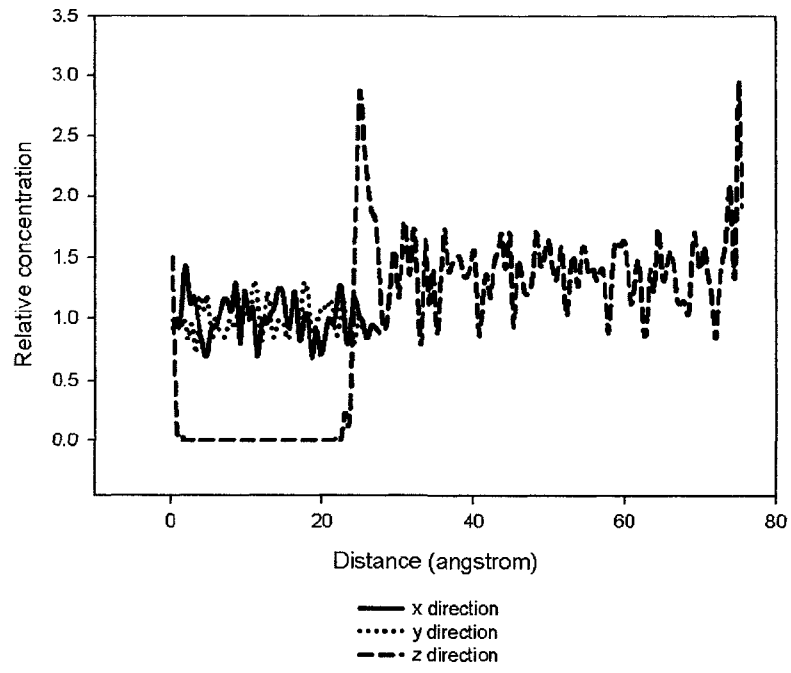




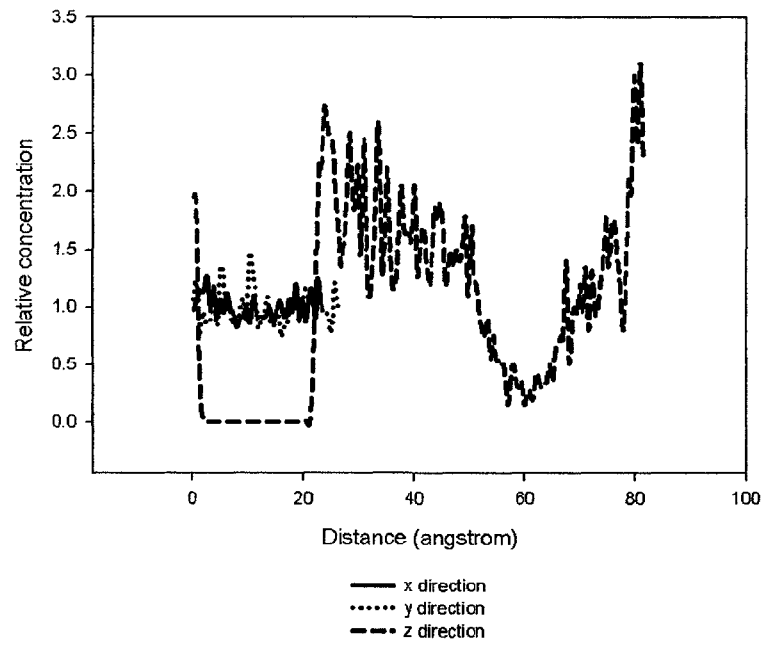
(c)



(d)



(e)



(f)

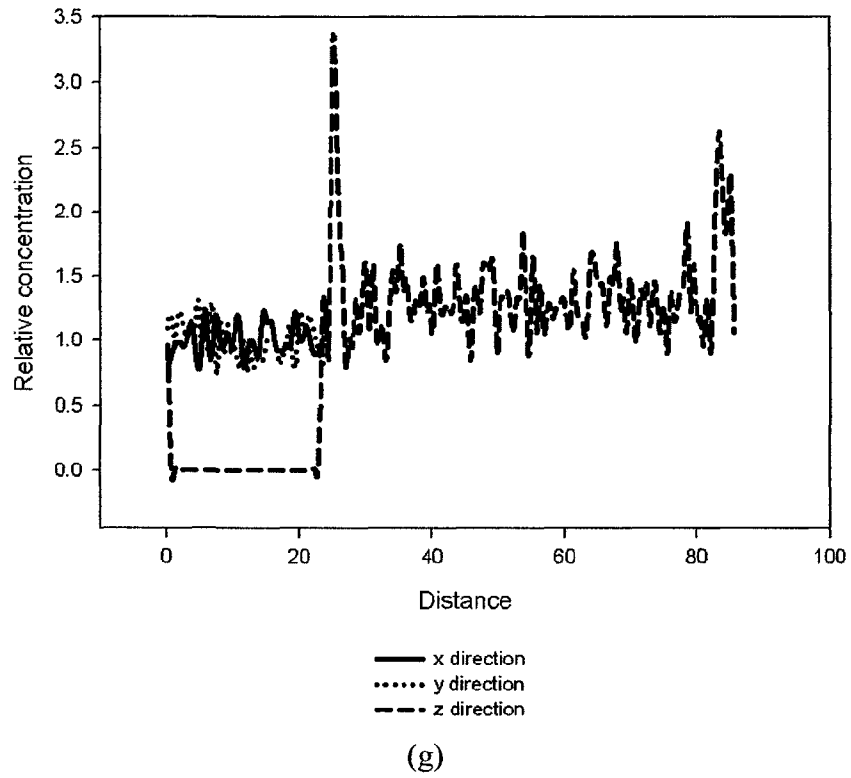
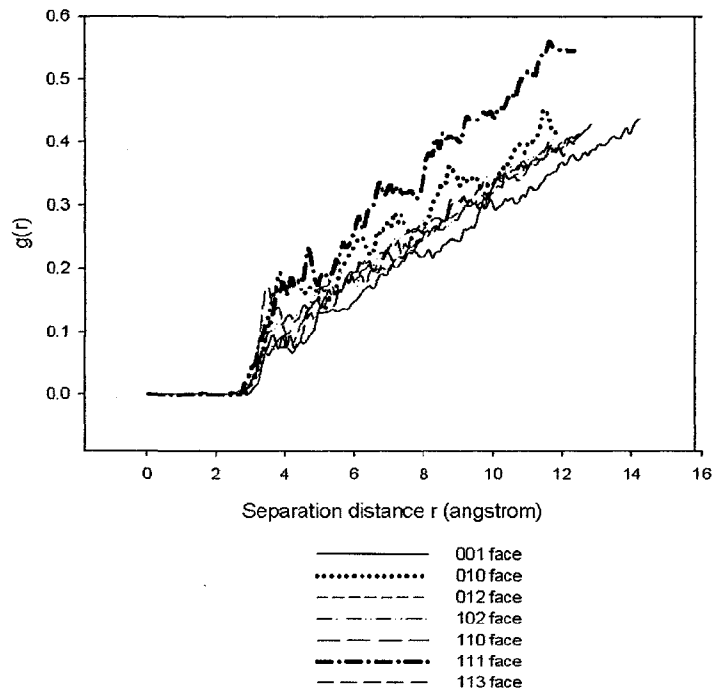


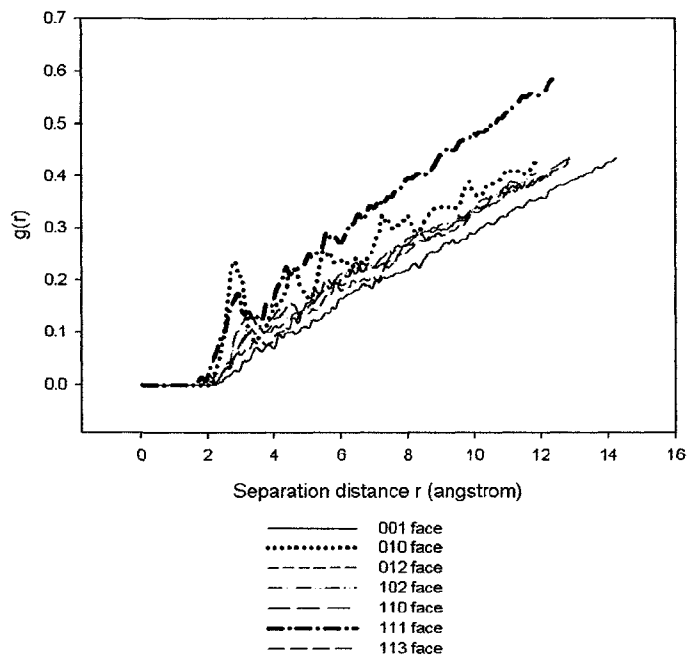
**Figure 6-2** Relative concentration profile of 1, 4-butanediol molecules near various alumina crystal faces: (a) (001) face; (b) (010) face; (c) (012) face; (d) (102) face; (e) (110) face; (f) (111) face; (g) (113) face

such that crystallographic  $c$  axis lies along the  $z$  direction and crystallographic  $b$  axis lies in the  $yz$  plane. All figures show similar concentration profiles in the sense that only one adsorption layer exists near the alumina surfaces with the exception of (111) surface. In the case of (111) surface, there exist multiple adsorption peaks and an extremely low concentration region, indicating that there are multiple adsorption layers near the surface. This means that the local packing of the solvent molecules is quite different from those on the other surfaces. We therefore examine the corresponding pair correlation functions, which are defined as the ratio of the local density to the average density of the chosen pair of atoms.

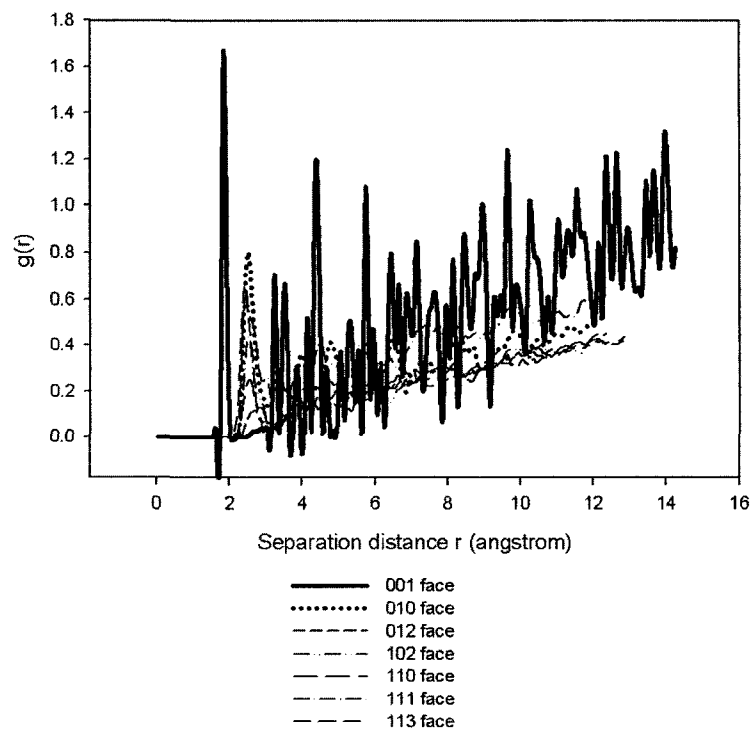
Figure 6-3 (a-f) depicts the pair correlation functions of surface atoms (Al and O) and solvent atoms (C, H, and O), respectively. It should be pointed out that all atoms of the same type in the  $\alpha$ -alumina slab and solvent layer were included in the calculation of the pair correlation functions. And each curve signifies an average pair correlation function over a simulation period of the last 10 ps of the 100 ps MD simulation. The figures show that the correlations ( $\alpha$ -alumina atom-solvent atom) of Al-C, Al-H, O-C, O-H, and O-O atoms on (010) and (111) faces are always stronger than those of the other crystal faces. In particular, the O-O correlations of such two faces contain multiple peaks. It is interesting to note that experiments show that (010) and (111) faces do not emerge in the final crystal morphology while the other five do. Given the above fact, it is speculated that the local structure formed by the solvent molecules, as quantified by the pair correlation functions, on the (010) and (111) surfaces would make those two surfaces more accessible to the incoming growth units (see discussion in section 6.3.3). It can be seen from all the figures that



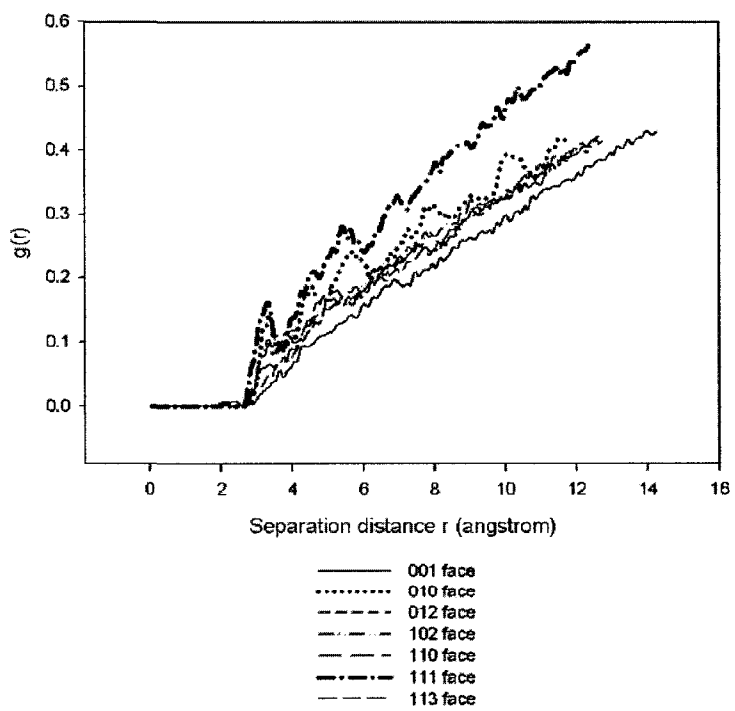
(a)



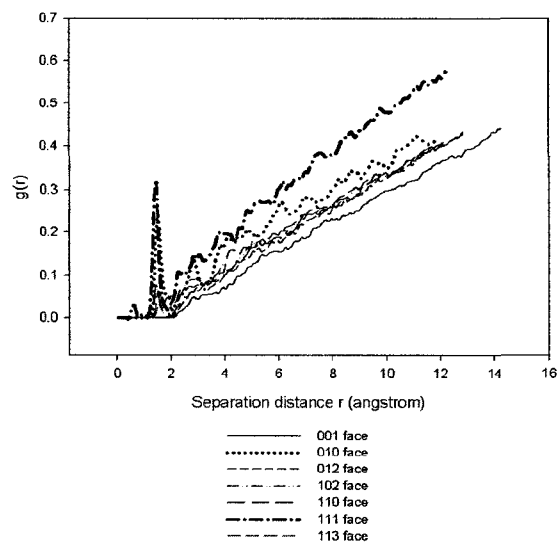
(b)



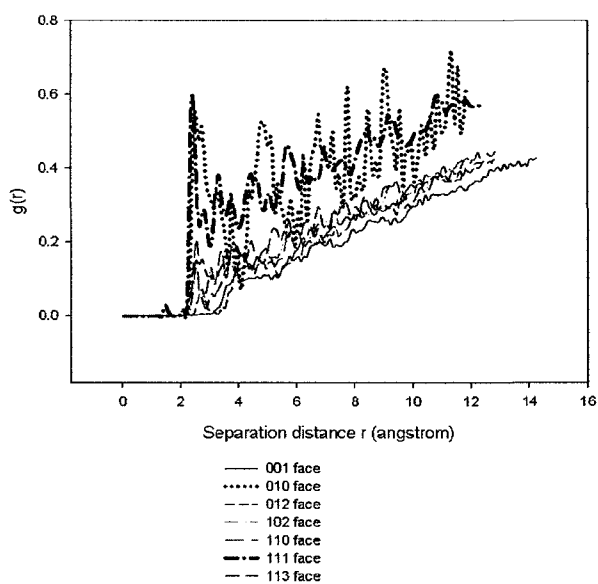
(c)



(d)



(e)



(f)

**Figure 6-3** Pair correlation functions of (a) Al-C; (b) Al-H; (c) Al-O; (d) O-C; (e) O-H; (f) O-O, where for each pair, the former atom represents those of the alumina slab while the latter those of 1, 4 - butanediol

all the correlations of the (001) face are the weakest. However, the Al-O correlation of the face shows rather different pattern from the other surfaces (Figure 6-3c). The reason for it is totally unclear.

The adsorption energy of 1, 4-butanediol solvent molecules on various crystal faces were calculated in terms of energy per mole of simulated system as well as per mole of solvent molecules by using Equation 6-1 and are presented in Table 6-4. Our simulation results are about one order of magnitude higher than the segmental adsorption energies for several polymers on inorganic solids reported by van der Beek, *et al.* [van der Beek *et al.*, 1991], where the structures of the monomers of these polymers are rather comparable to 1, 4-butanediol molecules (e.g., polytetrahydrofuran (PTHF), poly(butylmethacrylate) (PBMA), poly(methylmethacrylate) (PMMA), etc.). However, since our simulation can reproduce the segmental adsorption energy of alkane on  $\alpha - Al_2O_3(0001)$  crystal face very well [see Chapter 5], it is believed that even though the computed adsorption energy of 1, 4-butanediol molecules may deviate from the true values, the trend obtained for different crystal faces should be reliable. Here, our simulation results show that the adsorption energy of the solvents on different crystal faces could be compared in the following sequence:

$$E_{ads}(012) > E_{ads}(001) > E_{ads}(102) > E_{ads}(113) > E_{ads}(110) > E_{ads}(111) > E_{ads}(010)$$

Table 6-5 presents the computed adsorption energy of 1, 4-butanediol molecules at various crystal faces for the systems with a fixed thickness of  $58 \text{ \AA}$  rather than a fixed



**Table 6-4** Adsorption energy of 1, 4-butanediol at different alumina crystal faces for systems with 200 solvent molecules

Crystal face	Adsorption energy (kJ/mol)	
	Per mole of simulated system	Per mole of solvent molecules
(001)	$75702 \pm 213$	$379 \pm 1.1$
(010)	$7274 \pm 70$	$36.4 \pm 0.4$
(012)	$86297 \pm 209$	$432 \pm 1.1$
(102)	$46040 \pm 108$	$230 \pm 0.5$
(110)	$28604 \pm 85$	$143 \pm 0.4$
(111)	$23110 \pm 190$	$116 \pm 1.0$
(113)	$32483 \pm 88$	$162 \pm 0.5$

**Table 6-5** Adsorption energy of 1, 4-butanediol molecules at different alumina crystal faces for systems with a fixed thickness of  $58 \text{ \AA}$

Crystal face	Adsorption energy (kJ/mol)	
	Per mole of simulated system	Per mole of solvent molecules
(001)	$75702 \pm 213$	$379 \pm 1.1$
(012)	$77288 \pm 174$	$373 \pm 0.9$
(102)	$42580 \pm 140$	$206 \pm 0.7$
(110)	$28520 \pm 88$	$141 \pm 0.5$
(113)	$41653 \pm 139$	$180 \pm 0.6$

number of solvent molecules. As shown, the adsorption energy of the solvent molecules follows a slightly different sequence:

$$E_{ads}(001) > E_{ads}(012) > E_{ads}(102) > E_{ads}(113) > E_{ads}(110)$$

Here, to save computational times, we did not perform the calculations on (111) and (010) faces as experiments show that they do not emerge in the final morphology of  $\alpha$ -alumina crystal, as mentioned before. It should be pointed out that for a given surface, the adsorption energy value of the second sequence is slightly different from that of the first sequence as the numbers of solvent molecules used in two sequences are different. Obviously, the system that contains more solvent molecules would yield lower adsorption energy. This is because adsorption energy is calculated with the inclusion of all the solvent molecules in the system, as shown in Equation 6-1.

Nevertheless, thickness of a solvent layer used in the periodic unit cell could be thought as the distance between the surfaces of two  $\alpha$ -alumina particles. And such a distance is related to the concentration of  $\alpha$ -alumina particles synthesized in a solution. According to the solid loading amounts of aluminum hydrous oxide precursors presented by Adair *et al.*, the distance between two  $Al^{3+}$  ions in their solutions was estimated to be 13.0 - 23.1  $\text{\AA}$  (5 - 30 g of  $Al(OH)_3$  precursors [Prodromou and Pavlatou-Ve, 1995], while the distance between the surfaces of two  $Al_2O_3$  particles with a diameter of 2  $\mu m$  was about 6.1 - 12.7  $\mu m$  (assuming that they are approximately spherical). Therefore, thicknesses of solvent layers used in the present work correspond to the early stage of the synthesis process. In other

words, our results represent the growth habit of nano-sized  $\alpha - Al_2O_3$  particles. As a result, we also carried out further simulations to check if there is any effect of solvent layer thickness on adsorption energy of 1, 4-butanediol on the (001), (012), (102), (110), and (113) crystal faces and the results are depicted in Figure 6-4. The (010) and (111) surfaces were not studied for the reason mentioned before. The adsorption energy values for all the above five crystal faces decrease with the increasing solvent layer thickness, probably due to the dilution effect as discussed earlier. According to Figure 6-4, it seems that regardless of the thickness of solvent, the adsorption energy more or less follows the following sequence:

$$E_{ads}(001) > E_{ads}(012) > E_{ads}(102) > E_{ads}(113) > E_{ads}(110)$$

Here, the above ranking of adsorption energy is slightly different from the one that 200 solvent molecules were used (i.e.,  $E_{ads}(012) > E_{ads}(001)$ ). This seems to be related to the difference in the thickness dependence of adsorption energy of (001) and (012) surfaces (see Figure 6-4).

### 6.3.3 Effect of solvent adsorption on crystal growth

It is generally believed that adsorption of solvent molecules on a particular crystal face would inhibit its growth [Yin and Alivisatos, 2005]. One possible explanation is that large quantities of solvent molecules near such a crystal face may occupy the bonding sites, thus preventing the incorporation of growth units into the crystal lattice. According to our simulation results, the substantially lower adsorption energy

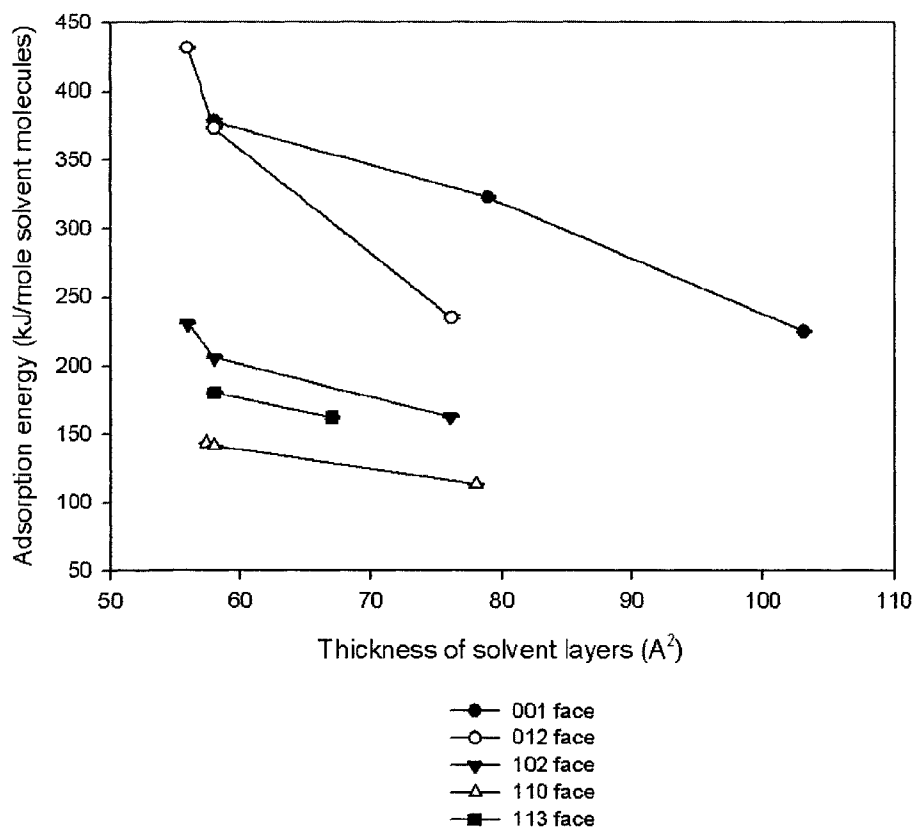


**Figure 6-4** Effect of solvent layer thickness on the computed adsorption energy for 1, 4- butanediol on (001), (012), (102), (110), and (113) alumina crystal faces

of 1, 4-butanediol molecules on the two  $\alpha$ -alumina crystal faces (111) and (010) seem to be consistent with the above viewpoint. This is because low adsorption energy implies high solvent mobility. It is worth noting that crystal faces that grow without difficulty are the ones that do not emerge in the final morphology of the crystal (see discussion below).

As reported in Adair *et al.*'s article, the  $\alpha$ -alumina crystals tend to grow as polyhedra with 20 faces under no stirring conditions [Adair *et al.*, 2001]. In particular, (001), (110) and (113) crystal faces are dominant for this morphological form. With increases in the precursor loading amounts, stirring speed and reaction time, other crystal faces such as (012) and (102) emerge, and the final morphology of the  $\alpha$ -alumina particles are modified on the edges, and therefore other shapes of crystals form. These authors also applied crystal structure modeling programs to predict the relative center-to-face distances of various equilibrium shapes of  $\alpha$ -alumina particles under different reaction conditions. The center-to-face distance refers to the perpendicular distance from the center of the crystal to the faces of the corresponding form. It is believed that the greater the distance, the smaller the area of the faces of that form in the final crystal shape. Therefore, it is also a measurement of relative growth velocities among various crystal faces. The authors presented the central-to-face distance of polyhedron with 20 faces as 1.0 for (001) face, 0.8 for (113) face, and 0.6 for (110) face, respectively. That is, the relative growth rates of those three crystal faces are  $V(110) > V(113) > V(001)$ . On the other hand, with the change of precursor concentrations, completely different relative growth rates of the three crystal faces were obtained (for instance:  $V(001) > V(113) > V(110)$  for

hexagonal prism with habit modifications of (113) and (113) on the edges, and  $V(110) > V(001) > V(113)$  for elongated hexagonal prism with habit modification of (113) and (113) on the edges).

In this research, it was found that (001), (110) and (113) are the three faces with the high adsorption energy values. The sequence of adsorption energy of them could be compared as follows:  $E_{ads}(001) > E_{ads}(113) > E_{ads}(110)$ . Therefore, the growth rates of these three crystal faces could be compared as:  $V(110) > V(113) > V(001)$ . This result suggests that the thicknesses of the solvent layer used in our simulations are probably comparable to the precursor concentration used in the corresponding experiment that shows polyhedron with 20 faces. Li *et al.* calculated the relationship between the number of corners per unit area present at the above crystal faces:  $N(110) > N(113) > N(001)$  [Li *et al.*, 2000]. They claimed that (110) face has the strongest force to bond with the growth units; while (001) face where every  $AlO_6$  octahedral has a face occurring at the interface has the weakest force to bond with the growth units. Therefore, our adsorption energy comparison implies that the solvent molecules prefer to adsorb onto the crystal faces which have a larger number of octahedral faces per unit area.

#### **6.3.4 Diffusivity of 1, 4-butandiol**

As shown before, the adsorption energy of (012) and (102) crystal faces is relatively high, even higher than that of (113) and (110) surfaces. According to the experimental observation, (012) and (102) crystal faces only emerge under moderate stirring rate or long reaction time conditions. Therefore, it suggests that in addition to

the adsorption energy, diffusivity of the solvent molecules might also play a role in the growth of various crystal faces.

Self-diffusion coefficients ( $D$ ) of the 1, 4-butanediol molecules above various alumina crystal faces were calculated using the well-known Einstein's diffusion equation. According to this equation, the three-dimensional diffusion coefficient of a molecule can be evaluated as the derivative of its mean square displacement with respect to time as given by [Allen and Tildesley, 1987]

$$D = \frac{1}{6} \lim_{t \rightarrow \infty} \frac{d \langle |r(t) - r(0)|^2 \rangle}{dt} \quad (6-2)$$

The total mean square displacement of all solvent molecules on various alumina surfaces are depicted in Figure 6-5. The corresponding diffusion coefficients in  $x$ ,  $y$ , and  $z$  directions were calculated and are presented in Table 6-6. As mentioned above,  $z$  is the direction perpendicular to various  $\alpha$ -alumina surfaces, while  $x$  and  $y$  are the two directions tangential to the  $\alpha$ -alumina surface. The computed diffusion coefficients of 1, 4-butanediol molecules towards the (012) and (102) faces are by far the lowest comparing with those of the solvent molecules towards other crystal faces. This may explain the experimental observation that (012) and (102) faces do not emerge unless moderate stirring rate is applied. Obviously, with no stirring or under low stirring rate conditions, it would reduce the number of solvent molecules move to the (012) and (102) crystal faces, thereby decreasing the ability of such molecules blocking the reaction sites.



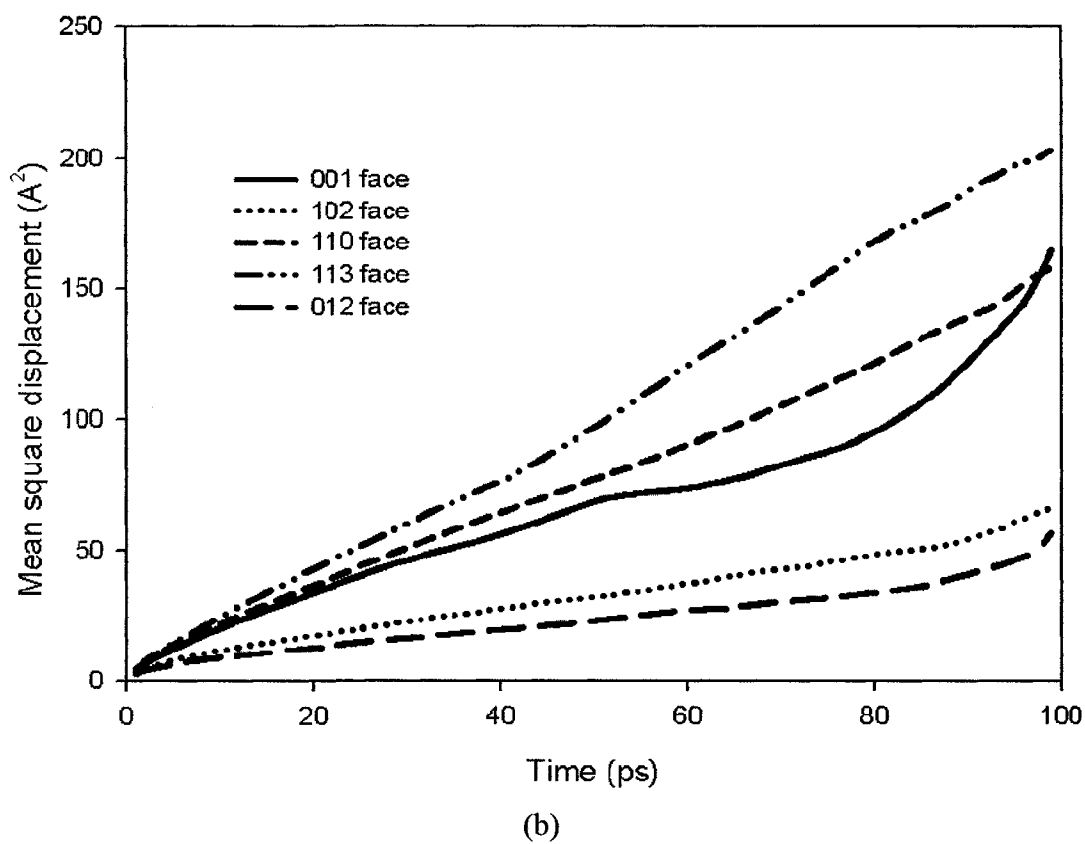


**Figure 6-5** Time dependence of mean square displacement of 1, 4-butanediol above various  $\alpha$ -alumina crystal faces

**Table 6-6** Computed diffusion coefficients of 1, 4-butanediol near different alumina crystal faces for systems containing the same number of solvent molecules

Crystal face	Self diffusion coefficient ( $\text{\AA}^2 / ps$ )			
	<i>x</i> direction	<i>y</i> direction	<i>z</i> direction	Total
(001)	0.31	0.72	0.21	1.24
(012)	0.15	0.16	0.09	0.41
(102)	0.25	0.16	0.14	0.55
(110)	0.54	0.53	0.39	1.46
(113)	0.80	0.92	0.32	2.05

### 6.3.5 Addition of methanol molecules

Owing to the success of using molecular modeling techniques for predicting  $\alpha$ -alumina crystal growth habits, we furthered the techniques to study solvent mixture effects. It has been reported that the addition of methanol also has significant effects on the morphology control of  $\alpha$ -alumina particles synthesized in 1, 4-butanediol solution (Adair *et al.*, 2001). In particular, the methanol addition to the synthesis processes causes the (001) basal planes to be modified and the formation of new, low symmetry (1012) planes. In addition, the (110) and (1012) planes become dominant. Effects of methanol addition were also investigated in this research. Table 6-7 presents the dimension of such simulation cell (alumina surface + solvent confined layer) and thicknesses of solvent layers with 200 1, 4-butanediol molecules and 20 methanol molecules above each crystal face. Our simulation results show that the adsorption energies of solvent molecules on various crystal faces follow the sequences:

$$E_{ads}(012) > E_{ads}(001) > E_{ads}(102) > E_{ads}(113) > E_{ads}(110) > E_{ads}(1012)$$

The values of those adsorption energies are listed in Table 6-8. It is not surprising that the absolute adsorption energies change with the addition of methanol molecules. However, the sequence of the energies on various crystal faces does not change comparing with those systems containing no methanol molecules. Besides, the interactions between solvent molecules and (1012) crystal face are by far the weakest

**Table 6-7** Dimension of the rearranged simulation cell (alumina surface + solvent confined layer) and thicknesses of solvent layers with 200 1, 4-butanediol molecules and 20 methanol molecules above each crystal face

<b>Crystal face</b>	$a$ ° (Å)	$b$ ° (Å)	$c$ ° (Å)	$\alpha$ (degrees)	$\beta$ (degrees)	$\gamma$ (degrees)	<b>Thickness of solvent layers</b> ° (Å)
(001)	28.554	28.554	79.314	90.000	90.000	60.000	60.19
(012)	28.554	25.642	70.618	90.000	90.000	90.000	58.02
(102)	30.771	23.795	71.855	90.000	90.000	90.000	58.05
(110)	27.985	25.642	77.973	90.000	90.000	95.844	59.51
(113)	24.728	25.642	88.344	90.000	90.000	105.538	69.54
(1012)	51.135	14.277	75.929	90.000	90.000	90.000	54.67

**Table 6-8** Adsorption energy of 1, 4-butanediol molecules at different crystal faces for systems with 200 1, 4-butandiol molecules and 20 methanol molecules

Crystal face	Adsorption energy (kJ/mol)	
	Per mole of simulated system	Per mole of solvent molecules
(001)	81005 ± 164	405 ± 0.84
(012)	85627 ± 207	428 ± 1.05
(102)	43341 ± 123	217 ± 0.63
(110)	31593 ± 96.5	158 ± 0.50
(113)	36153 ± 127	181 ± 0.63
(1012)	20472 ± 139	102 ± 0.71

comparing with other systems, indicating that (1012) face should not dominate in the final morphology.

On the other hand, diffusion coefficients of methanol + 1, 4-butanediol molecules on most crystal faces do show different sequences comparing with those of the pure 1, 4-butanediol systems, as depicted in Figure 6-6 and Table 6-9. It was observed that solvent molecules diffuse rather rapidly on (102) and (1012) crystal faces. Combining the adsorption energy and diffusivity results, our simulation shows that (1012) crystal face should not be present in the final morphology of  $\alpha$ -alumina particles prepared in the glycothermal process. This is obviously not consistent with the experimental findings. The reason for the discrepancy is totally unclear. It may be due to the model we used to represent the solvent mixture is not representative.

#### 6.4 Concluding remarks

MD simulation was carried out to study the interactions between various  $\alpha$ -alumina crystal faces and 1, 4-butanediol solvent molecules. Simulation results show that the adsorption energies of solvent molecules (200 of them) on different crystal faces are in the following sequence:

$$E_{ads}(012) > E_{ads}(001) > E_{ads}(102) > E_{ads}(113) > E_{ads}(110) > E_{ads}(111) > E_{ads}(010)$$

When constant thickness of solvent molecules was used, the sequence is slightly different with  $E_{ads}(001) > E_{ads}(012)$ . Weaker adsorption was found for the two

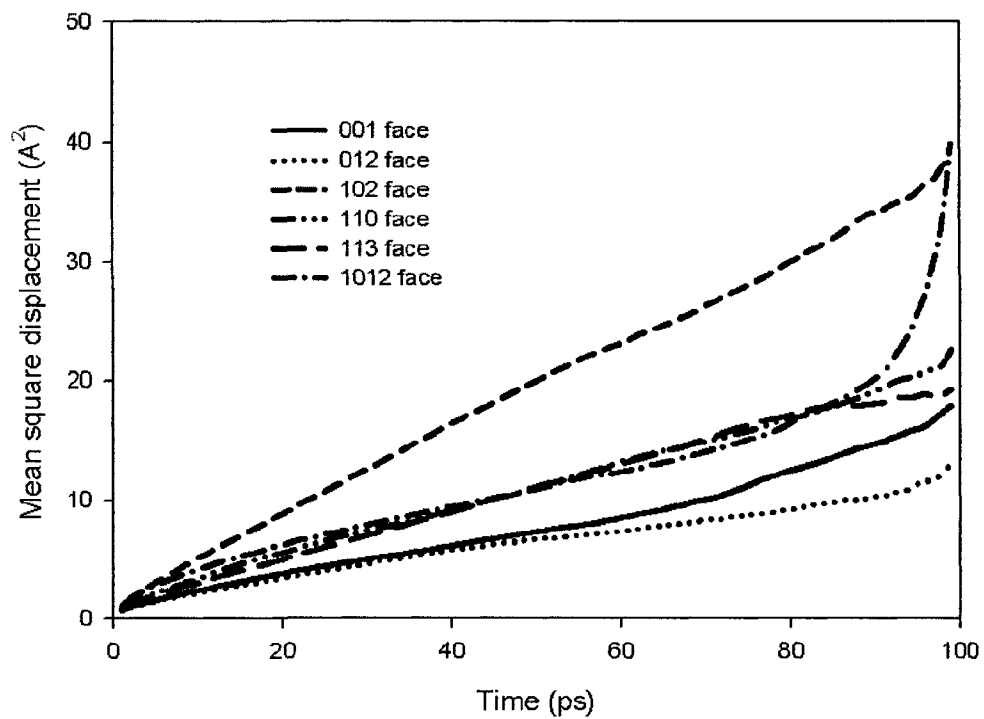


**Figure 6-6** Total self diffusion coefficients of solvent molecules above various crystal faces with methanol molecules added to the systems

**Table 6-9** Diffusion coefficients of 1, 4-butanediols at different crystal faces for systems with methanol molecules added

Crystal face	Self diffusion coefficient ( $\text{\AA}^2 / ps$ )			
	<i>x</i> direction	<i>y</i> direction	<i>z</i> direction	Total
(001)	0.37	0.23	0.15	0.76
(012)	0.19	0.21	0.10	0.50
(102)	0.63	0.63	0.36	1.63
(110)	0.18	0.29	0.20	0.67
(113)	0.29	0.32	0.19	0.80
(1012)	0.28	0.67	0.22	1.17



crystal faces (111) and (010) and they are the ones that do not emerge in the glycothermal synthesis process. Compared the adsorption energy results of the three dominant crystal faces ((001), (110), and (113) faces) with the corresponding results under low stirring rates or without stirring, it is concluded that adsorption of solvent molecules does have effects on the growth rates of different crystal faces. In addition to the adsorption energy, it seems that diffusivity of solvent also plays a role in the crystal growth process. In particular, the substantially lower self-diffusion coefficients of 1, 4-butanediol above the (012) and (102) faces may explain the experimental observation that those two crystal faces only becomes dominant as moderate or high stirring rates are applied.

# Chapter 7 Stability of Water/Toluene Interfaces Saturated With Adsorbed Naphthenic Acids

## 7.1 Introduction

Increasingly high contents of naphthenic acids in crude oils are encountered in the production of petroleum reserves [Goldszal *et al.*, 2002; Rousseau *et al.*, 2002]. They are a class of organic monoacids with the general formula of RCOOH, where R is a cycloaliphatic moiety. Frequently the polar and hydrophilic carboxylic acid head group and the hydrophobic cycloaliphatic segment are bridged by a short linear carbon chain. These amphiphilic species display natural tendency of self-organization, and can accumulate at the water/oil interfaces to form monolayers, liquid crystalline films, and other colloidal structures, thus stabilizing water-in-oil emulsions [Hsu *et al.*, 2000; Acevedo *et al.*, 1999]. The interfacial organization of these unique molecules involves a number of intertwining factors, and the elucidation of the mechanism(s) responsible for such organization constitutes one of the most fascinating challenges, both theoretically and experimentally, in the studies of emulsions. In the petroleum industry, emulsions are generally undesirable as it contributes to high pumping costs, reduced throughput, and special handling requirements. Thus, understanding of emulsion stabilization, and probably more

---

Another version of this chapter has been published as **Chunli Li**, Zhiying Li, and Phillip Choi, Stability of Water/Toluene Interfaces Saturated with Adsorbed Naphthenic Acids – A molecular Dynamics Study, *Chemical Engineering Science*, 2007, 62, 6709

importantly, identifying solutions for emulsion destabilization based on such understanding, bears significant ramifications.

Not surprisingly, considerable efforts have been devoted to the study of the interfacial activities of these important species, from which critical information has been obtained regarding their association and micellization behaviors [Urdao and Sjöblom, 1995; Schildberg *et al.*, 1995; Saeter *et al.*, 1999; Mouraille *et al.*, 1998; Friiso *et al.*, 1998; Gundersen *et al.*, 1999; Havre *et al.*, 2003A; Havre *et al.*, 2003B; Häger *et al.*, 2005], phase equilibrium [Horvath-Szabo *et al.*, 2001A; Horvath-Szabo *et al.*, 2001B; Horvath-Szabo *et al.*, 2002; Häger *et al.*, 2006A; Häger *et al.*, 2006B), formation of liquid crystalline phases [Friberg *et al.*, 1969; Friberg *et al.*, 1971; Friberg *et al.*, 1970; Friberg *et al.*, 1976; Friberg *et al.*, 1986], amongst other properties. Most notable is the profound stabilization of emulsion observed by a lamellar lyotropic liquid crystalline phase present at the water/oil interfaces. Phase diagrams of certain model binary (surfactant and water) and ternary (surfactant, water, and oil) solutions have been constructed, from which the formation of the liquid crystalline phases is clearly revealed [Horvath-Szabo *et al.*, 2001A; Horvath-Szabo *et al.*, 2001B; Horvath-Szabo *et al.*, 2002]. Critical surfactant concentrations for the formation of mesophases have also been suggested [Horvath-Szabo *et al.*, 2001A; Horvath-Szabo *et al.*, 2001B; Horvath-Szabo *et al.*, 2002]. It is believed that such a mesophase not only provides a physical barrier between emulsion droplets, it also reduces the mobility of the interface, thus retarding the water droplets coalescence process.

Extensive theoretical studies have also been carried out toward a general understanding of the stabilizing role(s) played by surfactants. However, most of these efforts deal with systems featuring surfactant molecules at flat interfaces as opposed to dispersed emulsion droplets with adsorbed surfactants; the latter is a more accurate modeling of the experimental systems [Dominguez, 2002]. In other work, not all phases are modeled at the same atomic level. As such, the techniques employed cannot offer a detailed molecular stabilization mechanism [Urbina-Villalba *et al.*, 2000].

Our efforts in this vein utilize a molecular dynamics approach to first simulate the coalescence of nanometer-sized water droplets in both vacuum and *n*-heptane [Zhao *et al.*, 2004] in order to gain insights into the pathway(s) by which the droplets coalesce. It has been found that in the absence of any stabilizing surfactants, the water droplets undergo coalescence by first forming a common water bridge, through which water molecules of the individual droplets merge and eventually form one larger and unified water droplet. It appears that the initial contact of water molecules from the droplets involved is the key step toward the formation of a bridge. As such, it is understandable, and as confirmed by our molecular dynamics simulations, that when *n*-heptane molecules are present, the coalescence is significantly slowed down as compared with the results obtained under a vacuum setting. In other words, the dissociation of the water surface-bound *n*-heptane molecules may be viewed as a rate limiting step. Indeed, once the common water bridge is formed, the time required for the formation of a single final water droplet is essentially independent of the initial chemical environment of the individual water droplets [Zhao *et al.*, 2004].

The above initial efforts provide significant mechanistic insights into the coalescence of water-in-oil droplets. Nevertheless, the scenario is too simplified to reflect the situation typically encountered in crude oils production where surface-active molecules such as naphthenic acids or asphaltenes or stabilizing inorganic solids are normally adsorbed onto the water/oil interfaces. We therefore in a more recent study extended our efforts to the investigation of the coalescence of water droplets with the interfacial presence of naphthenic acids [Li *et al.*, 2005]. The chemical structure of the naphthenic acids we employed is 6-methyl-2-naphthathenepropionic acid, as shown in Figure 7-1. Our goal was to understand by computational means the stabilizing roles played by the amphiphilic molecules. Our simulation revealed that the presence of naphthenic acids at the water/*n*-heptane interface of one of the two coalescing droplets considerably slows down the initialization of the water-bridge formation, but the time needed to complete the coalescence was about the same as when naphthenic acids were absent. In the case where two water droplets were both totally covered by naphthenic acids, the initialization of water bridge formation is slowed down dramatically, and the overall coalescence process is also retarded significantly. This is understandable as a higher energy barrier has to be overcome for the water molecules from different droplets to be in contact. Our simulations indicate that the departure of the naphthenic acids from the water/*n*-heptane interface is an essential step in this “activation” process [Li *et al.*, 2005]. Therefore, we proposed to use the mobility of naphthenic acids, which can be quantified by their diffusion coefficients ( $D$ ), to characterize the stability of the water/*n*-heptane interfaces.

In general,  $D$  is a parameter dependent on the following factors: The naphthenic acid-water interactions, the intermolecular interactions involving naphthenic acid molecules themselves, the naphthenic acid-oil phase interactions, and temperature. The naphthenic acid-water interactions are primarily hydrogen bonding in nature, involving the polar carboxylic acid group of naphthenic acids. Such interactions are responsible for the observed reduced mobility of droplet-confined water molecules, especially in the initial stage of the water-bridge formation. They are rather localized and therefore, should only be slightly affected by the nature of the oil phase, if at all. The interactions present between naphthenic acid molecules are twofold: first being hydrogen bonding between the carboxylic acid groups and the second being hydrophobic interactions involving the cycloaliphatic segments and the carbon chain in between. When a critical concentration of naphthenic acid is reached, its self-organization due to the aforementioned, synergetic interactions leads to the experimentally observed and theoretically corroborated liquid crystalline phase, a situation similar to the formation of a self-assembled monolayer on a metal surface. By forming the mesophase, the mobility of naphthenic acid molecules is reduced, and water droplets are stabilized. The structure of the hydrophobic segment of a naphthenic acid is critically important as it affects its packing effectiveness, and therefore, the eventual stability of the mesophase, if formed. As for the third type of interaction, alluded to above as naphthenic acid-oil phase interaction, its significance becomes clear once the naphthenic acid utilized is specified. Here, the oil-phase molecules (referred to as “solvent molecules” thereafter) can solvate the naphthenic acid molecules by penetrating into the hydrophobic regions of the liquid crystalline

structure; such interactions, by reducing the compactness of naphthenic acid organization in the mesophase, are expected to be destructive. The overall stability of the mesophase is thus reduced if a strongly naphthenic acid-interacting solvent system is employed.

With the forgoing recognitions and on the basis of our previous work in which the solvent used was *n*-heptane, we carried out the present comparative study using toluene as the solvent. The primary objective of our efforts is to demonstrate how the nature of the solvent affects the stability of water/oil phase interface, thereby the coalescence behavior of emulsified water droplets. Such comparative studies are worthwhile as they may suggest means of stabilizing or destabilizing water-in-oil emulsions, and thus providing guidelines for practical improvement in petroleum industry and food processing, among many other applications.

## 7.2 Simulation details

A software package so-called Materials Studio from Accelrys Inc. was used for all the calculations reported here except the simulation of 2, 2-dimethyl pentane. However, in our previous work [Zhao *et al.*, 2004; Li *et al.*, 2005], a different software package (Cerius<sup>2</sup>) from the same vendor was used in which a generic force field DREIDING 2.21 was adopted [Mayo *et al.*, 1990]. However, instead of using the default Lennard Jones (LJ) parameters for the CH<sub>2</sub> and CH<sub>3</sub> groups in *n*-heptane, LJ parameters of Ryckaert and Bellemans were used [Ryckaert *et al.*, 1975]. It was found that the modified DREIDING 2.21 yielded fairly accurate predictions of the heat of vaporization ( $\Delta H_v$ ) and self-diffusion coefficient ( $D$ ) for *n*-heptane and therefore was employed to describe interactions encountered in the interfacial models involving *n*-

heptane. However, owing to the complexity of the aromatic structure of toluene molecules, calculations based on such a generic force field becomes inadequate. Instead, the COMPASS force field [Sun, 1998] was used in the present work to investigate interactions involving toluene. COMPASS is an *ab initio* force field optimized for condensed-phase applications. Simulation results have shown that it can make accurate predictions of structural, conformational, cohesive and other physical properties for a wide range of substances. Energy expressions of this force field are presented in Table 5-1. Interested reader should refer to the original article for the coefficients used in the expressions [Sun, 1998].

The COMPASS force field was validated using an approach similar to what was used before; that is, the heat of vaporization and self-diffusion coefficient of toluene were determined and compared with experiments. Since the force field was also used for describing water molecules, validation was also performed on water as well. To simulate the condensed states of toluene and water, three-dimensional periodic simulation boxes with 66 toluene and 210 water molecules were constructed and they were subjected to the corresponding experimental density at 25 °C. The systems were then subjected to energy minimization before respective molecular dynamics simulations were carried out at the same temperature. For each condensed state model, one nanosecond canonical (i.e., NVT) molecular dynamics trajectory at 25 °C was created using the Nose method with a time step of 1 femtosecond [Nose, 1984a]. The heats of vaporization were calculated using the procedure described elsewhere [Choi *et al.*, 1992]. The self-diffusion coefficient of toluene was calculated



using the well-known Einstein equation and the procedure summarized in reference [Allen and Tildesley, 1987]

$$D = \frac{1}{6} \lim_{t \rightarrow \infty} \frac{d \langle |r(t) - r(0)|^2 \rangle}{dt} \quad (7-1)$$

Unlike the previous work, all the pure condensed state as well as interfacial models used consisted of explicit hydrogens. The van der Waals interactions were calculated using a cut off distance of  $9.5 \text{ \AA}$  with a spline width of  $1.00 \text{ \AA}$  and a buffer width of  $0.50 \text{ \AA}$ . The coulombic interactions involved in the systems were calculated using the Ewald summation method [Allen and Tildesley, 1987]. Partial atomic charges were assigned to each atom by performing the charge equilibration method [Rappe and Goddard, 1991]. This included the estimation of the partial atomic charges on the water molecules as well. Unlike other force fields, the COMPASS force field does not contain an explicit hydrogen bond term. The hydrogen bond interactions are included in the nonbond coulombic term.

The models that were constructed in the present work to describe the toluene/water interfaces saturated with adsorbed naphthenic acids are similar to those used in the previous work in which *n*-heptane was used as the solvent. However, only flat interface models were used in the present work. As the previous work showed, the mobility of naphthenic acids at the interface is independent of the curvature of the interface [Li *et al.*, 2005]. In addition, water droplets encountered in practice usually have sizes on the order of micron; therefore, the effect of curvature

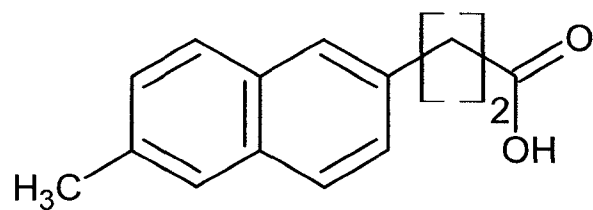
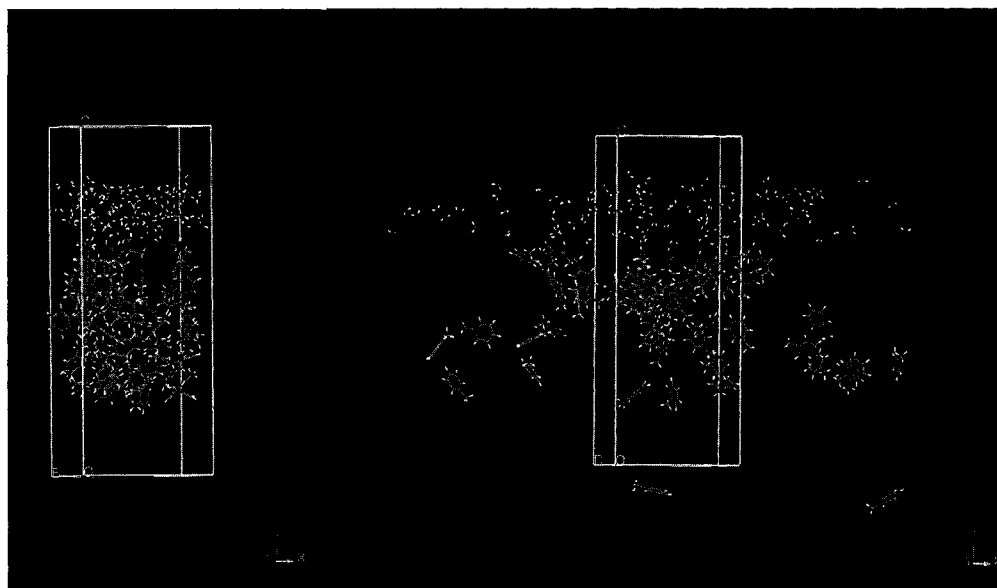


**Figure 7-1** Chemical structure of 6-methyl-2-naphthalenepropionic acid

should be minimal. In the flat interface models, 100 water molecules and 30 toluene molecules were used. The rationale for the choice of the numbers of molecules used in the models was given in reference [Li *et al.*, 2005]. The carbon atom numbers of the short carbon chain connecting the carboxylic and cycloaliphatic groups on the naphthenic acid also varied from 2 to 6. Figure 7-1 depicts the chemical structure of 6-methyl-2-naphthatepropionic acid used in the present work. The hydrophilic part of naphthenic acids was modeled as two charge carrying moieties C=O and OH. The dissociation of the COOH group into COO<sup>-</sup> and H<sup>+</sup> was ignored to reduce the computational times. Besides, the initial structures of the interface models were constructed in such a manner that the naphthenic acid molecules were inserted into the interfaces with the hydrophilic head oriented towards the water phase and hydrophobic part oriented to the toluene phase. This would significantly reduce the equilibration time of the simulated system. Therefore, only 1000 picoseconds of simulation time were used for each model. Eight naphthenic acid molecules were used for each model. The number of naphthenic acid molecules was chosen based on the experimental results of Havre and Sjoblom [Havre *et al.*, 2003] and would saturate the interface. Figure 7-2(a) depicts an initial structure set up for the modeled systems. All the models were energy minimized before the canonical molecular dynamics simulations were carried out at 25 °C. One snapshot at 1000 picosecond is also shown in Figure 7-2(b). To explore the effect of the geometry of solvent molecule, one molecular dynamics simulation using 2, 2-dimethyl pentane as the solvent was also carried out using the modified DREIDING force field that was used in our previous work. In this simulation, naphthenic acid with a carbon chain with 2



(a)

(b)

**Figure 7-2** Snapshots for the simulated system (a) Initial structure; (b) 1000 picoseconds

carbons was used. It should be noted that all of *n*-heptane, toluene and 2, 2-dimethyl pentane contain 7 carbons but their shapes differ significantly.

### **7.3 Results and discussion**

#### **7.3.1 Validation of the COMPASS force field**

Apparently, two different force fields were employed for toluene and *n*-heptane systems respectively, which may make the intention to compare the dynamics of the two systems questionable. Here, so long as the COMPASS force field yielded heat of vaporization and self-diffusion coefficient of pure toluene comparable to the experimental values, we consider the force field to be adequate for describing the models. In the present work, the calculated heats of vaporization for pure toluene and pure water were  $34.5 \pm 0.55$  and  $42.3 \pm 0.32$  *kJ/mole*, respectively, compared reasonably well with respective experimental values of 33.5 and 40.0 *kJ/mole* [Zhao, *et al.*, 2004; Yaws, 1992]. Also, the computed self-diffusion coefficients at 25 °C are  $1.84 \times 10^{-9}$  and  $3.20 \times 10^{-9}$  *m<sup>2</sup>/s* which are in fairly good agreement with the corresponding experimental value of  $1.68 \times 10^{-9}$  and  $2.60 \times 10^{-9}$  *m<sup>2</sup>/s*, respectively (Antalek *et al.*, 1996; Angell *et al.*, 1976). Although the values for water are not as accurate as those of toluene, we feel justified to use the force field as the interactions between toluene and naphthenic acids as well as those between toluene itself are of the main interest in this work.

#### **7.3.2 Diffusion coefficients of naphthenic acids**

Diffusion coefficients of naphthenic acids adsorbed at flat water/*n*-heptane interfaces were used in our previous studies to quantitatively evaluate their mobility. A direct

comparison of the computed diffusion coefficients obtained in the present work with those from our previous study on *n*-heptane clearly indicates that mobility of naphthenic acid molecules is drastically reduced when the solvent is toluene. As summarized in Table 7-1, mobility of naphthenic acids is reduced by 10 to 50 times depending on the length of the carbon chain. As a whole, these reduced diffusion coefficients predict that coalescence of the water droplets in toluene would be much more sluggish. This implies that at room temperature, water droplets are more stable in toluene than in *n*-heptane when naphthenic acids are present at the interface. Here, experimental verification is needed.

As the solvent is the only difference, the observed difference in the mobility of naphthenic acids should be rationalized in terms of the interactions involving the solvents, including the interactions between the solvents and the naphthenic acids and those between the solvent molecules themselves. The former may be viewed as the “solvation” of naphthenic acids involving primarily the hydrophobic segment (the cycloaliphatic moiety and the linking group). The extent of this interaction depends not only on the electronic and structural similarities of the species involved, but also the interactions within the individual species (both naphthenic acid and toluene). In other words, naphthenic acid and the solvent interact at the expense of both the solvent-solvent and naphthenic acid-naphthenic acid interactions. Generally speaking, a weakly self-interacting solvent system should be more propitious to solvent-naphthenic acid interactions than a more strongly self-interacting solvent. Toluene, an aromatic compound, can participate in aromatic-aromatic interactions. Although such non-covalent interactions are relatively weak and largely manifested in the solid

**Table 7-1** Average diffusion coefficients of naphthenic acids obtained from the calculations with water/*n*-heptane and water/toluene flat interfaces at 25 °C . A drastically reduced mobility of naphthenic acid molecules is observed in the case of the simulation with water/toluene interface. The mobility of the naphthenic acid is reduced by 10 to 50 times depending on the length of its linking group. As a whole, these reduced diffusion coefficients directly reflect the much more sluggish coalescence of the water droplets in toluene

<b>Number of Carbons in the Linking Group</b>	<b><math>D</math> (<i>n</i>-Heptane), <math>m^2/s \times 10^{11}</math></b>	<b><math>D</math> Value (Toluene), <math>m^2/s \times 10^{11}</math></b>
2	8.98	0.88
3	8.78	0.38
4	8.38	0.41
5	6.88	0.00013
6	6.08	0.00015

state, they may be significant if one considers the net effect. As compared with a purely aliphatic system such as *n*-heptane, inter-solvent interactions of toluene are considerably stronger, resulting in a higher kinetic barrier than in the case of alkanes for its interaction with the interfacial naphthenic acids. The computed and experimental heats of vaporization of *n*-heptane and toluene (experimental values are 31.7 and 33.5 kJ/mol, respectively) seem to support such an argument. One possible counter argument is that the solubility parameters of the naphthenic acids may be closer to that of *n*-heptane ( $15.1 (MPa)^{1/2}$ ) than that of toluene ( $18.2 (MPa)^{1/2}$ ) so that mobility of naphthenic acids is prone to leave the interface. However, this is not likely the case as the structure of naphthenic acids is somewhat similar to that of fatty acids that generally have solubility parameters with a minimum value of  $22 (MPa)^{1/2}$ . In addition, comparing solubility parameters of naphthenic acids with those of *n*-heptane and toluene is not sensible as only the hydrophobic tails of the acids interact with the solvents.

Equally important, if not more, is the steric effects of the solvent molecules in influencing their interactions with the naphthenic acids. Such interactions are primarily through the “solvation” of the hydrophobic segment of the naphthenic acids with solvent molecules penetrating into the aggregation of the naphthenic acid liquid crystalline mesophase. Smaller molecules can disperse throughout the compact mesophase more rapidly than their bulkier relatives, causing a more profound disruption of the otherwise stable liquid crystalline structure. This disruption would enhance the mobility of the naphthenic acids resulting larger diffusion coefficients. To confirm this idea, a simulation with the use of 2, 2-dimethyl pentane as the solvent



was carried out. Same temperature and numbers of molecules were used expecting that the modified DREIDING 2.21 force field [Li *et al.*, 2005] was used as this was the force field we used for *n*-heptane. As mentioned, 2, 2-dimethyl pentane also contains 7 carbons and can be viewed as a branched heptane and the naphthenic acid used contained 2 carbon atoms in the carbon chain. Simulation result showed that the diffusion coefficient is  $3.6 \pm 0.5 \times 10^{-11} \text{ m}^2 / \text{s}$  which is about 2 – 3 times lower than that of *n*-heptane ( $9.0 \pm 1.0 \times 10^{-11} \text{ m}^2 / \text{s}$ ). The comparison showed that the geometry of the solvent molecules does play a role in determining the mobility of the naphthenic acid. Comparing *n*-heptane with toluene, the linear chain structure of the former is probably more effective for its molecules to penetrate into the aggregate structure of the adsorbed naphthenic acid. The above arguments based on the electronic and steric structures of the solvent both point to weaker solvent-naphthenic acid interactions in the water/toluene system than the water/*n*-heptane system. Our simulation studies indeed suggest that departure of the naphthenic acid molecules from the interface is a low probability event, making such emulsion systems more stable.

Experimental evidence indicates that emulsion stability is weakly dependent on the molecular weight of the adsorbed naphthenic acids, with naphthenic acid of higher molecular weight having slightly better stabilizing effects. Our previous studies have also resulted in supporting evidence for these experimental observations. Specifically, increasing the length of the linking groups seems to cause a reduction in the mobility of the naphthenic acid molecules, but only with moderate magnitude. This may be understood in terms of the effects of the relative steric bulk of the

cycloaliphatic segment with respect to the linking group on the organization of the naphthenic acid molecules. The bulky cycloaliphatic group prevents sterically a close packing of naphthenic acid molecules. Increasing the chain length of the linking group in effect attenuates or “dilutes” the steric bulk of the cycloaliphatic moiety. In turn, this leads to a better “bundling” of the linear linking group. A corollary is that a more compact structure is achieved, and the mobility of the component naphthenic acid molecules is reduced. The influence of the linking group length on the mobility of the naphthenic acid molecules is again revealed in the present work if only the overall trend is considered (see Figure 7-3). An abrupt decrease in diffusion coefficient is observed when the linking group is elongated from an ethylene linkage to propylene, followed by an irregular and less dramatic change of  $D$ . The reason for the observed irregularity in the change of  $D$  is unclear, which invites further studies in the future. However, the magnitude in the decrease in  $D$  is close to one order of magnitude which means that the molecular weight dependence of the mobility of naphthenic acid for the case of toluene is significantly stronger than that of  $n$ -heptane, indicating that when the side chain of naphthenic acid is long enough, toluene molecules would find it more difficult to destabilize the mesophase. Along the same line of reasoning, the previous puzzling observation of the naphthenic acid with an ethylene linking group having comparable diffusion coefficients when adsorbed on a flat and a highly curved interface may now be better understood. That is, when a short linking group is utilized, the mesophase formed is relatively loose as a result of an ineffective packing of the naphthenic acid molecules, and the relative significance of the curvature of the interface is diminished. Simulations of systems containing

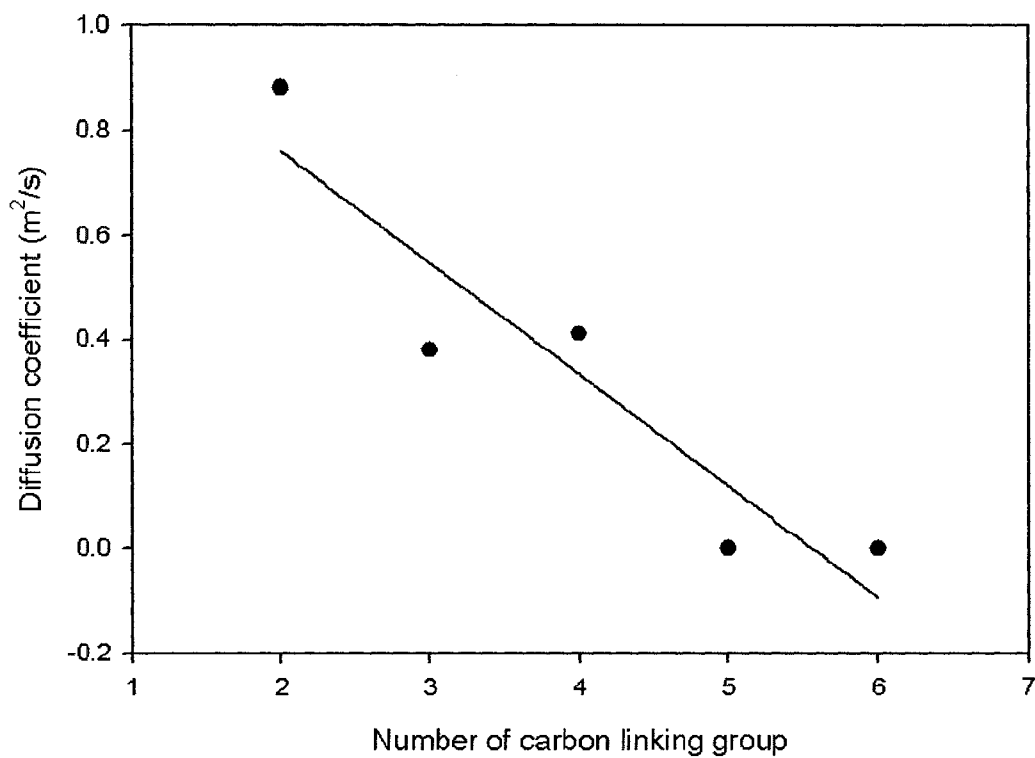


**Figure 7-3** The influence of the linking group chain length on the mobility of the naphthenic acid molecules.

water droplets stabilized by longer naphthenic acids would provide the answer. However, the computational times required for such simulations are prohibitively high at the time being.

#### **7.4 Concluding remarks**

Molecular dynamics simulations were carried out to study the stabilization of water in toluene emulsion by naphthenic acids. Simulation results showed that comparing with the water/*n*-heptane system, naphthenic acids exhibited a much lower mobility at the water/toluene interfaces saturated by naphthenic acids, suggesting that water droplets are more stable in toluene than in *n*-heptane with the interface. Such computational results require experimental verification. It is believed that toluene molecules are strongly self-interacting, compared to *n*-heptane, which causes weaker interactions between toluene and naphthenic acids. In addition, geometry of toluene molecules may also contribute to unfavorable interactions between toluene and naphthenic acids and therefore help stabilize the water/toluene emulsion. It was also observed that with the increasing linking group chain length, mobility of the naphthenic acids was reduced considerably. It seems that the nature of the solvent plays an important role in determining the stability of water-in-oil emulsions.

## Chapter 8 Summary and Suggestions for Future Work

### 8.1 Surface tensions of chain molecules

In this thesis, a novel molecular dynamics (MD) simulation strategy has been proposed to estimate the surface tensions ( $\gamma$ ) of normal alkanes and methyl methacrylate (MMA) oligomers with various molecular weights in the low molecular weight range. With the use of a generic force field, the experimentally observed molecular weight dependence ( $M_n^{-2/3}$ ) of  $\gamma$  was reproduced for both series of oligomers. On the other hand, however, it was also found that comparing with normal alkanes, the calculated numerical values of surface tensions of MMA oligomers deviate significantly from the experimental measurements. One possible reason is that the DREIDING force field may not be able to correctly deal with the electrostatic interactions in those MMA oligomers. Different combinations of force field parameters were also tested to calculate the electrostatic interactions, and but unfortunately, even the combination of Ewald summation method and COMPASS force field can not do a significantly better job. The other reason may be attributed to the use of constant density for all the MMA models with different chain lengths.

Therefore, the future work will include the continuing search of a suitable force fields to accurately take into account the electrostatic interactions involved in the MMA oligomers. On the other hand, the MD approach developed in this research also needs to be verified by estimating surface tensions of other various oligomer series. Besides, it is well known that the surface tension of polymers follows a  $M_n^{-1}$  dependence with moderate to high molecular weights [Sauer and Dee, 1991; Sauer

and Dee, 1994; Dee and Sauer, 1993; Jalbert *et al.*, 1993]. Due to the limitations of computational ability, coarse grain methods are usually used to simulate long chain polymers with high molecular weights. Therefore, it would be a valuable work to verify whether the MD strategy developed here could be applied to the coarse grain methods and reproduce the  $M_n^{-1}$  dependence of surface tensions of these polymers.

## 8.2 Adsorption behavior of chain molecules at solid surface

In this work, density functional theory (DFT) and molecular dynamics (MD) simulation techniques were combined together to investigate the adsorption behavior of two normal alkanes ( $C_{11}$  and  $C_{200}$ ) on a relaxed  $\alpha - Al_2O_3(0001)$  crystal face. DFT calculations were firstly carried out to relax the alumina (0001) crystal face. And then the positions of all the atoms in the alumina surface were fixed during the following MD simulations, since the vibration frequency of the aluminum-oxygen bond is much faster than that of the relaxations of the alkane chains [Kodziana and Norskov, 2003; Goo, 2002].

As a matter of fact, behaviors of MMA oligomers near alumina crystal face were also expected to be investigated since they have so many applications in various industries [Colletii, *et al.*, 1987; Leidheiser and Deck, 1988]. Besides, experimental measurements on properties of MMA oligomers related to the adsorption behavior have also been reported [Konstadinidis *et al.*, 1992]. However, our simulation results were not prosperous, and the COMPASS force field was also blamed for this. Therefore, a suitable force field still need to be found in the future to apply the strategy developed here. And the problems discussed here may also be able to be

extended to other species of chain molecules, and even other crystal faces of various types of inorganic substrates.

As to the morphology control of alumina particles, firstly, the simulated numerical values of adsorption energy of solvent molecules on various alumina crystal faces are about 1 order of magnitude higher than the reported experiment results. The reason for this discrepancy is not quite clear yet. Secondly, due to the limitation of computer resources, thickness of solvent layers used in this work only corresponds to the early stage of the synthesis process. It is worthy to explore how thickness of solvents affects the adsorption energy, and therefore the growth mechanism of the particles. Besides, the simulation results for systems with the addition of methanol molecules seem not quite consistent with the experimental observations, which also need more exploration in the future. Similarly, the growth habit of other crystals and particles may also be explored by using this simulation strategy in the future.

### **8.3 Stability of water/oil interfaces**

Stability of water/toluene interfaces saturated with adsorbed naphthenic acids with various sizes at room temperature was also studied by MD simulation. In direct comparison with our recent results on similar systems involving *n*-heptane as the oil phase, it has been found that toluene significantly enhances the stability of the water/oil interface, as suggested by the considerably reduced diffusion coefficients of the interface-bound naphthenic acids. Consistent with our previous studies, mobility of naphthenic acid has been found to be dependent on its size, with naphthenic acid featuring a longer carbon chain in between the carboxylic and cycloaliphatic groups

showing lower mobility, leading to a more stable interface. However, such size dependence is much more pronounced for the water/toluene than the water/*n*-heptane interface. This may be understood in terms of the structural influence of toluene on the compactness of the liquid crystalline mesophase formed by naphthenic acids adsorbed at the interface. Our computational results require experimental verification in the future.



## Bibliography

- Abrams, C. F.; Kremer, K., *Macromolecules*, **2003**, *36*, 260
- Abrams, C. F., *Computational Soft Matter: From Synthetic Polymers to Proteins*, NIC series, **2004**, *23*, 275
- Accelrys, *Materials Studio user manual*, **2004**
- Acevedo, S.; Escobar, G.; Ranaudo, M. A.; Khazen, J.; Borges, B.; Pereira, J. C.; Mendez, B., *Energy Fuels*, **1999**, *13*, 333
- Adair, J. H.; Cho, S. B.; Bell, N. S.; Perrotta, A. J., *J. Dispersion Science and Technology*, **2001**, *22*, 143
- Adair, J. H.; Suvaci, E., *Current Opinion in Colloid & Interface Science*, **2000**, *5*, 160
- Ahn J.; Rabalais, J. W., *ibid.* **1997**, *388*, 121
- Allen, G.; Gee, G.; Wilson, G., *J. Polymer*. **1960**, *1*, 456
- Allen M. P.; Tildesley, D. J., *Computer Simulation of Liquids*, Oxford University Press, Oxford. **1987**
- Allinger, N. L.; Chem, K. S.; Katzenellenbogen, J. A.; Wilson, S. R.; Anstead, G. M., *J. Comput. Chem.*, **1996**, *17*, 747
- Andersen, H. C., *J. Chem. Phys.*, **1980**, *72*, 2384
- Angell, C. A.; Finch, E. D.; Woolf, L. A.; Bach, P., *J. Chem. Phys.*, **1976**, *65*, 3063
- Antalek, B.; Williams, A. J.; Texter, J., *Phys. Rev. E*, **1996**, *54*, R5913
- Askadskii, A. A., *Computational Materials Science of Polymers*, Cambridge International Science, Cambridge, **2003**
- Askin, A.; Inel, O. *Separation Science and Technology*, **2001**, *36*, 381
- Aubouy, M.; Manghi, M.; Raphael, E., *Phys. Rev. Lett.* **2000**, *84*, 4858

Bader, R. F., *Atoms in Molecules*, Oxford, New York, **1990**

Baerends, E. J.; Gritsenko, O. V., *Phys. Chem. A*, **1997**, *101*, 5383

Barton, A. T. M., Ed. *CRC Handbook of Solubility Parameters and Other Cohesion Parameters*, CRC Press: Boca Raton, FL, **1991**, 4<sup>th</sup> ed

Baschnagel, J.; Meyer, H.; Varnik, F.; Metzger, S.; Aichele, M.; Muller, M.; Binder, K., *Interface Science* **2003**, *11*, 159

Becher, P., *Encyclopedia of Emulsion Technology*. **1983**, 17

Becke, A. D., *Phys. Rev. A*, **1988**, *38*, 3098

Becke, A. D., *J. Chem. Phys.*, **1992**, *97*, 9173

Becke, A. D.; Roussel, M. R., *Phys. Rev. A*, **1989**, *39*, 3761

Bell, N. S.; Adair, J. H., *J. Crystal Growth.*, **1999**, *203*, 213

Bennett, C. H., *J. Comput. Phys.* **1976**, *22*, 245

Bethe, H. A., *Intermediate Quantum Mechanics*, Benjamin, New York, **1964**

Berendsen, H. J. C.; Van Gunsteren, W. F., *Proceedings of the Enrico Fermi Summer School. Varenna, Soc. Italiana di Fisica, Bologna.*, **1986**, 43

Berger, L. L.; Sauer, B. B., *Macromolecules*, **1991**, *24*, 2096

Binder, K., *Phys. Rev. A*. **1982**, *25*, 1699

Born, M.; Oppenheimer, J. R., *Ann. Physik.*, **1927**, *84*, 457

Brostow, W.; Cassidy, P. E.; Macossay, J.; Pietkiewicz.; Venumbaka, S., *Polymer Int.* **2003**, *52*, 1498

Brown, H. R.; Kramer, E. J., *Journal of Macromolecular Science. Physics*, **1981**, *B19*, 487

Buff, F. P.; Lovett, R. A.; Stillinger Jr., F. H., *Phys. Rev. Lett.* **1965**, *15*, 621

- Carre, A.; Vial, J., *J. Adhesion*, **1993**, *42*, 265
- Ceperley D. M.; Alder, B. J., *Phys. Rev. Lett.*, 1980, *45*, 566
- Cho, S. B.; Venigalla, S.; Adair, J. H., *J. Am. Ceram. Soc.*, **1996**, *79*, 88
- Choi, P. T.; Kavassalis, A.; Rudin, A., *J. Colloid Interf. Sci.*, **1992**, *150*, 386
- Chretien, S.; Salahub, D. R., *Les Houches Summer School, Course 4: Density Functional Theory, Methods, Techniques, and Applications*, Springer Berlin/Heidelberg, **2001**
- Claire, P. de Sainte; Hass, K. C.; Schneider, W. F.; Hase, W. L., *J. Chem. Phys.*, **1997**, *106*, 7331
- Colbourn, E. A., *Computer Simulation of Polymers*, Longman, London, **1994**
- Colletti, R. F.; Gold, H. S.; Dybowski, C., *Appl. Spectrosc.* **1987**, *41*, 1185
- Compostizo, A.; Pascual, A.; Colin, A. C.; Rubio, R. G., *J. Chem. Eng. Data.*, **2005**, *50*, 591
- Connolly, M. L., *J. Am. Chem. Soc.* **1985**, *107*, 1118
- Cornell, W. D.; Cieplak, P.; Bayly, C. I.; Gould, I. R.; Merz, K. M.; Ferguson, D. M.; Spellmeyer, D. C.; Fox, T.; Caldwell, J. W.; Kollman, P. A., *J. Am. Chem. Soc.*, **1995**, *117*, 5179
- Cornell, W. D.; Cieplak, P.; Bayly, C. I.; Gould, I. R.; Merz, K. M.; Ferguson, D. M.; Spellmeyer, D. C.; Fox, T.; Caldwell, J. W.; Kollman, P. A., *J. Am. Chem. Soc.*, **1996**, *118*, 2309
- Dee, G. T.; Sauer, B. B., *J. Colloid and Interface Sci.*, **1992**, *152*, 85
- Dee, G. T.; Sauer, B. B. *Macromolecules*, **1993**, *26*, 2771
- Dee, G. T.; Sauer, B. B., *Advances in Physics*, **1998**, *2*, 161

De Gennes, D. G., *Scaling Concepts in Polymer Physics*, **1979**

Delle Site, L.; Abrams, C. F.; Alavi, A.; Kremer, K., *Phys. Rev. Lett.*, **2002**, *89*, 156103-1

Delle Site, L.; Kremer K., *International Journal of Quantum Chemistry*, **2005**, *101*, 733

Dkhissi, A.; Esteve, A.; Jeloica, L.; Esteve, D.; Djafari Rouhani, M., *J. Am. Chem. Soc.*, **2005**, *127*, 9776

Dominguez, H., *J. Phys. Chem. B.*, **2002**, *106*, 5915

Donnary, J. D. H.; Harker, D., *Amer. Min.*, **1937**, *22*, 446

Doolittle, A. K., *J. Chem. Eng. Data*. **1964**, *2*, 275

Dreizler, R. M.; Gross, E. K. U., *Density Functional Theory*, Springer, Berlin, **1990**

Eastwood, J. W.; Hockney, R. W.; Lawrence, D., *Comput. Phys. Commun.*, **1980**, *19*, 215

Eichkorn, K; Treutler, O; Öhm, H; Häser, M; Ahlrichs, R., *Chem. Phys. Lett.*, **1995**, *242*, 652

Elman, J. F.; Johs, B. D.; Long, T. E.; Koberstein, J. T., *Macromolecules*, **1994**, *27*, 5341

Escobedo, J.; Mansoori, G. A., *AICHE Journal*, **1996**, *42*, 1425

Everhart, D. S.; Reilley, C. N., *Surf. Interface Anal.*, **1981**, *3*, 126

Ewald, P., *Ann. Phys.*, **1921**, *64*, 253

Flory, P. J., *The Statistics of Chain Molecules*, Hanser Publishers, New York, **1988**

Flour, C. S.; Paplrer, E., *Ind. Eng. Chem. Prod. Res. Dev.* **1982**, *21*, 337

Frenkel, D.; Smit, B., *Understanding Molecular Simulation* 2<sup>nd</sup> Ed., Academic Press, San Diego, CA, **2002**

Friberg, S.; Mandell, L.; Larsson, M. J., *J. Colloid Interf. Sci.*, **1969**, 29, 155

Friberg, S.; Mandell, L., *J. Pharm. Sci.*, **1970**, 59, 1001

Friberg, S., *J. Colloid Interf. Sci.*, **1971**, 37, 291

Friberg, S.; Jansson, P. O.; Cederberg, E., *J. Colloid Interf. Sci.*, **1976**, 55, 614

Friberg, S.; Solans, C., *Langmuir*, **1986**, 2, 121

Friiso, T.; Schildberg, Y.; Rambeau, O.; Tjomsland, T.; Forderal, H.; Sjöblom, J., *J. Dispersion Sci. Technol.*, **1998**, 19, 93

Garbassi F.; Morra, M.; Occhiello E., *Polymer Surfaces: From Physics to Technology*. John Wiley and Sons, Chichester, **1994**

Gear, C. W., *Numerical Initial Value Problems in Ordinary Differential Equations*, Prentice-Hall, Englewood Cliffs, NJ. **1971**

Gillan, M. J., in *Computer Simulation in Materials Science*, Meyer, M.; Pontikis, V. Dordrecht, Kluwer, Ed. **1991**

Gloor, G. J.; Jackson, G., *J. Chem. Phys.*, **2005**, 123, 134703

Goldszal, A.; Hurtevent, C.; Rousseau, G., *SPE Oilfield Scale Symposium*, (Aberdeen, UK, SPE74661), 2002.

Goo, G. H., *Bull. Korean. Chem. Soc.*, **2002**, 23, 1595

Goudeau, S.; Galy, J.; Gerard, J. F.; Gulchiron, R.; Barrat, J. L., *Materials Research Society Symposium*. **2000**, FF9.2.1

Gray, C. G.; Gubbins, K. E., *Theory of Molecular Liquids*, Clarendon Press, Oxford, **1984**

- Griedel, G., *Bull. Soc. Granc. Min.*, **1905**, 28, 6
- Gundersen, S. A.; Sjöblom, J., *Colloid Polym. Sci.*, **1999**, 277, 462
- Gupta, S.; Koopman, D.C.; Westermann-Clark, G.B.; Bitsanis, I.A., *J. Chem. Phys.* **1994**, 100, 8444
- Häger, M.; Ese, M. H.; Sjöblom, J., *J. Dispersion Sci. Technol.*, **2005**, 26, 673
- Häger, M.; Sjöblom, J., *J. Dispersion Sci. Technol.*, **2006A.**, 27, 399
- Häger, M., Sjöblom, J., *J. Dispersion Sci. Technol.*, **2006B**, 27, 643
- Haile, J., *Molecular Dynamics Simulation: Elementary Methods*, Wiley-Interscience Publication, New York, **1992**
- Halgren, T. A., *J. Comput. Chem.*, **1996**, 17, 490
- Hapke, T.; Patzold, G.; Heermann, D. W., *J. Chem. Phys.*, **1998**, 109, 10075
- Hariharan, A.; Kumar, S. K.; Russel, T. P., *Macromolecules*, **1990**, 23, 3584
- Hartman, P.; Perdok, W. G., *Acta Cryst.*, **1955**, 8, 49
- Harman, P.; Bennema, J. *Cryst. Growth*, **1980a**, 49, 145
- Harman, P.; Bennema, J. *Cryst. Growth*, **1980b**, 49, 166
- Hass, K. C.; Schneider, W. F.; Curioni, A.; Andreoni, W., *Science*, **1998**, 282, 265
- Havre, T. E.; Sjöblom, J., *Colloids and Surfaces A.*, **2003A**, 228, 131
- Havre, T. E.; Sjöblom, J.; Vindstad, J. E., *J. Dispersion Sci. Technol.*, **2003B**, 24, 789
- He, D; Reneker, D. H.; Mattice, W. L., *Comp. and Theor. Polymer Science.* **1997**, 1, 19
- Hedin, L.; Kundqvist, S., in *Solid State Physics*, Vol. 23, Seitz, F.; Turnbull, D.; Ehrenreich, H., Eds., *Effects of Electron-Electron and Electron-Phonon Interactions on the One-Electron States of Solids*, Academic Press, New York, **1969**

Heyes, D. M., *J. Chem. Phys.*, **1981**, *74*, 1924

Hildebrand, J. H.; Scott, R. L., *The Solubility of Nonelectrolytes.*, Dover Publications: New York, **1964**

Hill, T.L., *An Introduction to Statistical Thermodynamics.*, Dover Publications: New York, **1986**

Hockney, R. W., *Methods Comput. Phys.*, **1970**, *9*, 136

Hohenberg, P.; Kohn, W., *Phys. Rev.*, **1964**, *136*, B864

Hong, K. M.; Noolandi, J., *Macromolecules*, **1981**, *14*, 1223

Hoover, W. G., *Phys. Rev. Lett.*, **1982**, *48*, 1818

Hoover, W. G., *Phys. Rev. A*, **1985**, *31*, 1695

Horvath-Szabo, G.; Czarnecki, J.; Masliyah, J., *J. Colloid Interf. Sci.*, **2001A**, 236, 233

Horvath-Szabo, G.; Masliyah, J.; Czarnecki, J., *J. Colloid Interf. Sci.*, **2001B**, 242, 247

Horvath-Szabo, G.; Czarnecki, J.; Masliyah, J., *J. Colloid Interf. Sci.*, **2002**, 253, 427

Hsu, C. S.; Dechert, G. J.; Robbins, W. K.; Fukuda, E. K., *Energy Fuels*, **2000**, *14*, 217

Hung, F. R.; Gubbins, K. E.; Franzen, S., *Chemical Engineering Education*, **2004**, 242

Hwang, M. J.; Stockfisch, T. P.; Hagler, A. T., *J. Am. Chem. Soc.*, **1994**, *116*, 2515

Inoue, M., *J. Phys.: Condens. Matter.*, **2004**, *16*, S1291

Jalbert, C.; Kobersten, J. T.; Yilgor, I.; Gallagher, P.; Krukoniš, V., *Macromolecules.*, **1993**, *26*, 3069

Jenkel, E.; Rumbach, B. Z., *Electrochem*, **1951**, *55*, 612

Jensen, F., *Introduction to Computational Chemistry*, John Wiley and Sons, Chichester, **1999**

Jorgensen, W. L.; Maxwell, D. S.; Tiradorives, I., *J. Am. Chem. Soc.*, **1996**, *118*, 11225

Joubert, D., *Density Functionals: Theory and Applications*, Springer, **1997**

Kambour R. P., *Journal of Polymer Science*, **1964**, *2*, 4165

Kempton V., *Surf. Sci.*, **1997**, *370*, 190

Kim, W. K.; Mattice, W. L., *Langmuir*, **1998**, *14*, 6588

Kirkwood, J. E.; Buff, F. P., *J. Chem. Phys.*, **1949**, *17*, 338

Koch, W.; Holthausen M. C., *A Chemist's Guide to Density-functional Theory*, **2001**

Kohn, W.; Sham, L.J., *Phys. Rev.*, **1965**, *140*, A1133

Konstadinidis, K.; Thakkar, B.; Chakraborty, A.; Potts, L. W.; Tannenbaum, R.; Tirrell, M.; Evans, J. F., *Langmuir*, **1992**, *8*, 1307

Krishnamoorti, R.; Graessley, W. W.; de, G. T.; Walsh, D. J.; Fetters, L. J.; Lohse, D. J., *Macromolecules*. **1996**, *29*, 367

Kumagai, M.; Messing, G. L., *J. Am. Ceram. Soc.*, **1985**, *68*, 500

Kuznetsov, V. A., *Kristallografiya*, **1964**, *9*, 123

Kuznetsov, V. A., *Kristallografiya*, **1965**, *10*, 663

Kuznetsov, V. A., in: Lobachev, A. N., *Hydrothermal Synthesis of Crystals*, **1971**

Ladd, A. J. C., *Molecular Physics*, **1977**, *33*, 1039

Ladd, A. J. C., *Molecular Physics*, **1978**, *36*, 463

LeGrand, D. G.; Gaines, G. L. Jr., *J. Colloid Interface Sci.* **1969**, *31*, 162



Leidheiser, J. R.; Deck, P. D. *Science*, **1988**, *241*, 1176

Levine, *Quantum Chemistry*, 4<sup>th</sup> edition, Prentice Hall, Engelwood Cliffs, New Jersey, **2000**

Levy, M., in Seminario, J. M. Ed. *Recent Developments and Applications of Modern Density Functional Theory*, Elsevier, Amsterdam, **1996**

Lewars, E., *Computational Chemistry: Introduction to the Theory and Applications of Molecular and Quantum Mechanics*, **2003**

Li, W. J.; Shi, E. W.; Zhong, W. Z.; Yin, Z. W., *J. Crystal Growth*, **1999**, *203*, 186

Li, W. J.; Shi, E. W.; Yin, Z. W., *J. Crystal Growth*, **2000**, *208*, 546

Li, Z.; Cranston, B.; Zhao, L.; Choi, P., *J. Phys. Chem. B*, **2005**, *109*, 20929

Lii, J. H.; Allinger, N. L., *J. Am. Chem. Soc.*, **1989**, *111*, 8576

Lodziana, Z.; Norskov, J. K., *J. Chem. Phys.*, **2003**, *118*, 11179

Lodziana, Z.; Topsoe, N. Y.; Norskov, J. K., *Natural Materials*, **2004**, *3*, 289

Lyons, P., Sandquist, C. L. *J. Am. Chem. Soc.*, **1953**, *75*, 3896

Mackerell, A. D.; Wiorkiewicz-Kuczera, J.; Karplus, M., *J. Am. Chem. Soc.*, **1995**, *117*, 11946

Mansfield, K. F.; Theodorou, D. N., *Macromolecules*, **1990**, *23*, 4430

Mansfield, K. F.; Theodorou, D. N., *Macromolecules*, **1991**, *24*, 6283

MaQuarrie, D. A., *Statistical Mechanics*, University Science Books, Sausalito, **2000**

Maranas, J. K.; Mondello, M.; Grest, G. S.; Kumar, S. K.; Gebenedetti, P. G.; Graessley, W. W., *Macromolecules*, **1998**, *31*, 6991

March, N. H., *Self-Consistent Fields in Atoms*, Pergaman Press, Oxford, **1975**

Mattice, W. L.; Suter, U. W., *Conformational Theory of Large Molecules. The Rotational Isomeric State Model in Macromolecular Systems*, Wiley, New York, **1994**

Mayo, S. L.; Olafson, B. D.; Goddard III, W. A., *J. Phys. Chem.* **1990**, *94*, 8897

Mazo, R. M., *Brownian Motion*, Clarendon Press, Oxford, **2002**

McArdle, J. L.; Messing, G. L., *J. Am. Ceram. Soc.*, **1986**, *69*, 51

McArdle, J. L.; Messing, J. L., *J. Am. Ceram. Soc.*, **1987**, *72*, 864

McArdle, J. L.; Messing, G. L., *Adv. Ceram. Matls.*, **1988**, *3*, 387

Misra, S.; Fleming III, P. D.; Mattice, W. L., *J. Computer-Aided Materials Design.* **1995**, *2*, 101

Mouraille, O.; Skodvin, T.; Sjöblom, J.; Peytavy, J. L., *J. Dispersion Sci. Technol.*, **1998**, *19*, 339

Norde, I. in *Surface and Interfacial Aspects of Biomedical Applications*, **1995**

Nose, S., *J. Chem. Phys.*, **1984a**, *81*, 511

Nose, S. *Molecular Physics*, **1984b**, *52*, 255

Onsager, L., *J. Am. Chem. Soc.*, **1936**, *58*, 1486

Panayiotou. C.; Sanchez, I. C., *J. Phys. Chem.*, **1991**, *95*, 10090

Park, D., *Introduction to the Quantum Theory*, McGraw-Hill, New York, **1974**

Parr, R. G.; Yang, W., *Density Functional Theory of Atoms and Molecules*, Oxford University Press, New York, **1989**

Patterson, D.; Siow, K. S., *Macromolecules*, **1970**, *4*, 26

Patterson, D.; Rastogi, A. K., *J. Phys. Chem.*, **1970**, *74*, 1067

Pennings, J. F. M.; Bosman, B., *Colloidal Polymer Science*, **1979**, *257*, 720

Perdew, J. P.; Zunger, A., *Phys. Rev.*, **1981**, *B23*, 5048

Perdew, J., *Phys. Rev. Lett.*, **1985**, *55*, 1665

Perdew, J. P.; Yue, W., *Phys. Rev. B*, **1986**, *33*, 8800

Perdew, J. P., *Phys. Rev. B*, **1986a**, *33*, 8822

Perdew, J. P., *Phys. Rev. B*, **1986b**, *34*, 7406E

Perdew, J. P., Chevary, J. A.; Vosko, S. H.; Jackson, K. A.; Pederson, M. R.; Singh, D. J.; Fiolhais, C., *Phys. Rev. B*, **1992**, *46*, 6671

Perdew, J. P., Chevary, J. A.; Vosko, S. H.; Jackson, K. A.; Pederson, M. R.; Singh, D. J.; Fiolhais, C., *Phys. Rev. B*, **1993**, *48*, 4978E

Perdew, J. P.; Burke, K.; Yang, Y., *Phys. Rev. B*, **1996**, *54*, 16533

Prodromou, K. P., Pavlatou-Ve, A. S., *Clays and Clay Minerals*, **1995**, *43*, 111

Puchin, V. E.; Gale, J. D.; Shluger, A. L.; Kotomin, E. A.; Günster, J.; Brause, M.;

Rabe, J. P.; Buchholz, S., *Science*, **1991**, *253*, 424

Rabin, Y. J., *Polym. Sci., Polym. Lett. Edn.*, **1984**, *22*, 335

Rapaport, D., *The Art of Molecular Dynamics Simulation*, Cambridge University Press, **2004**

Rappé, A. K.; Goddard III, W. A., *J. Phys. Chem.*, **1991**, *95*, 3358

Rappé, A. K.; Casewit, C. J.; Colwell, K. S.; Goddard, W. A.; Skiff, W. M., *J. Am. Chem. Soc.*, **1992**, *114*, 10024

Rodgers, P. A., *J. Appli. Polymer Science*, **1993**, *48*, 1061

Rousseau, G.; Zhou, H.; Hurtevent, C., *SPE Oilfield Scale Symposium* (Aberdeen, UK, SPE68307), **2002**

Rowlinson, J. S.; Widom, B., *Molecular Theory of Capillarity*. Clarendon, Oxford, **1982**

Ruberto, C.; Yourdshahyan, Y.; Lundqvist, B. I., *Phys. Rev. B*, **2003**, 67, 195412

Russell, T. P., *Mater Sci Rep.*, **1990**, 5, 171

Rychaert, J. P.; Bellemans, A., *Chem. Phys. Lett.* **1975**, 30, 123

Saeter, O.; Sjöblom, J., *Colloid Polym. Sci.*, **1999**, 277, 541

Sauer, B. B.; Dee, G. T., *Macromolecules*, **1991**, 24, 2124

Sauer, B. B.; Dee, G. T., *J. Colloid Interface Sci.*, **1994**, 162, 25

Schildberg, W.; Sjöblom, J.; Christy, A. A., *J. Dispersion Sci. Technol.*, **1995**, 16, 575

E. Schrödinger, *Ann. Phys.*, (Leipzig) **1926A**, 489, 79

E. Schrödinger, *Phys. Rev.*, **1926B**, 28, 1049

Shusterman, G. P.; Shusterman, A. J., *J. Chem. Educ.*, **1997**, 74, 771

Siow, K. S.; Patterson, D., *Macromolecules*, **1971**, 4, 26

Sohnel, O.; Garside, J., *Precipitation Basic Principles and Industrial Crystallization*, **1993**

Stanton, D. T.; Jurs, P. C., *J. Chem. Inf. Comput. Sci.*, **1992**, 32, 109

Sun, H., *J. Phys. Chem. B*, **1998**, 102, 7338

Sun, J.; Stirner, T.; Hagston, W. E.; Leyland, A.; Matthews, A., *Journal of Crystal Growth*. **2006**, 290, 235

Sun, T. F., *J. Chem. Eng. Data.*, **1992**, 37, 246

Sun H., *J. Phys. Chem. B*, **1998**, 102, 7338

Szabo, A.; Ostlund, N. S., *Modern Quantum Chemistry-Introduction to Advanced Electronic Structure*, McGraw-Hill, New York, **1989**

Theodorou, D. N., *Macromolecules*, **1988**, *21*, 1400

Theodorou, D. N.; Suter, U. V., *Macromolecules*, **1985**, *18*, 1467

Thomas, L. H., *The Calculation of Atomic Fields, Proc. Camb. Phil. Soc.*, **1927**, *23*, 542

Urbina-Villalba, G.; Garcia-Sucre, M., *Langmuir*, **2000**, *16*, 7975

Urdao, O.; Sjöblom, J., *J. Dispersion Sci. Technol.*, **1995**, *16*, 557

Van Damme, H. S., Hogt, A. H., Feijen, J., *J. Colloid Interface Sci.*, **1986**, *114*, 167

van der Beek, G. P., Cohen Stuart, M. A., Fleer, G. J., Hoffman, J. E., *Macromolecules*, **1991**, *24*, 6600

Van Voorhis, T.; Scuseria, G. E., *J. Chem. Phys.*, **1998**, *109*, 400

Verlet, L., *Phys. Rev.*, **1967**, *159*, 98

Vial, J.; Carre, A., *Int. J. Adhesion and Adhesives*, **1991**, *11*, 140

Wu, S., *J. Phys. Chem.*, **1970**, *74*, 632

Wu, S., *Polymer Interface and Adhesion*, **1982**

Yang, A. C. M.; Kramer, E. J., *Journal of Polymer Science. Polymer Physics*, **1985**, *23*, 1353

Yans, C. L., *Handbook of Transport Property Data*, **1995**

Yaws, C. L., *Thermodynamic and Physical Property Data (Gulf, Houston)*, **1992**

Yin, Y.; Alivisatos, A. P., *Nature*, **2005**, *437*, 664

Yourdshahyan, Y.; Ruberto, C.; Halvarsson, M.; Bengtsson, L.; Langer, V.; Lundqvist, B.; Rупpi, S.; Rolander, U., *J. Am. Ceram. Soc.*, **1999**, *82*, 1365

Zhao, L.; Choi, P., *J. Chem. Phys.*, **2004**, *120*, 1935

Ziegler, T., *Chem. Rev.*, **1991**, *91*, 651

Zwanzig, R., *Nonequilibrium Statistical Mechanics*, Oxford University Press, New York, **2001**